October 2018

Equilibrium Partitioning of Binary Polymer Mixtures into Biological Nanopores

Mehmet Alphan Aksoyoglu
University of Massachusetts Amherst

EQUILIBRIUM PARTITIONING OF BINARY POLYMER MIXTURES INTO BIOLOGICAL NANOPORES

A Dissertation Presented

by

MEHMET ALPHAN AKSOYOĞLU

Submitted to the Graduate School of the
University of Massachusetts Amherst in partial fulfillment
of the requirements for the degree of

DOCTOR OF PHILOSOPHY

September 2018

Physics

EQUILIBRIUM PARTITIONING OF BINARY POLYMER MIXTURES INTO BIOLOGICAL NANOPORES

A Dissertation Presented

by

MEHMET ALPHAN AKSOYOĞLU

Approved as to style and content by:

V. Adrian Parsegian, Chair

Rudolf Podgornik, Member

Murugappan Muthukumar, Member

Jennifer Ross, Member

Anthony Dinsmore, Member

Rory Miskimen, Department Chair
Physics

DEDICATION

This thesis is dedicated to my mother, father, and brother, whose love and support had made this work a reality.

ACKNOWLEDGMENTS

First and foremost I would like to thank Professor Rudolf Podgornik, Dr. Sergey Bezrukov, and Dr. Philip Gurnev, all of whom have made invaluable contributions to this project, and have provided invaluable scientific assistance throughout this project, as well as for their contributions in my professional development. Dr. Philip Gurnev, especially for being a friend and mentor, and Dr. Sergey Bezrukov and Professor Podgornik for their mentorship and guidance.

I would like to thank Professor Carlo Dallapiccola for their invaluable guidance and assistance throughout graduate school as the graduate program director, for their friendship and willingness to resolve any situation without hesitation, and with determination.

I would like to thank Professors Anthony Dinsmore, Jennifer Ross, and Murugappan Muthukumar for being on my committee and for their assistance throughout the course of this work.

I would like to thank Walter Pollard and Rick Miastkowski, for their help and assistance in the machine shop, and for them designing, and making exceptionally well made components for many equipment we have used in the laboratory.

I would like to thank, Jane Knapp, and Ingrid Pollard of the Physics Department for their excellent administrative support.

Last but not the least I would like to thank my advisor Professor V. Adrian Parsegian for the many pleasant discussions, and for their financial support.

ABSTRACT

EQUILIBRIUM PARTITIONING OF BINARY POLYMER MIXTURES INTO BIOLOGICAL NANOPORES

SEPTEMBER 2018

MEHMET ALPHAN AKSOYOĞLU

B.Sc., BOĞAZİÇİ UNIVERSITY, TURKEY

Ph.D., UNIVERSITY OF MASSACHUSETTS AMHERST

Directed by: Professor V. Adrian Parsegian

The cell interior, enclosed by membrane barriers, is a condensed solution of inorganic ions, polymers, carbohydrates, polynucleotides, and a large number of other organic molecules. Within cells, transport of metabolites and biopolymers, such as polynucleotides and proteins, occurs partly through specific transmembrane pores (mesoscopic ion channels) spanning cellular compartments. Examples of such functions are translocation of matrix RNA molecules from cell nucleus through nuclear pore complexes, ejection of viral genome from bacterial virus capsids into host bacterial cells, and translocation of protein factors across toxin channels in biological membranes. All these processes, that occur in the cellular milieu, are mediated by complex membrane structures and must be affected by molecular crowding. However, the effects of crowding are insufficiently addressed. Particular effects of certain types of molecular "crowders" have only begun to be understood. Partially they stem

from the dramatic complexity of the cellular translocation machinery, which makes direct observation of crowding phenomena extremely challenging. In addressing pore-assisted metabolite transport, a simplified experimental system with isolated protein channels in artificial membranes has been a useful model to probe and to assess crowding effects of such transport. In the experimental scheme employed here, a single pore is spontaneously assembled into an artificial bilayer separating two voltage-clamped electrolyte compartments. As the electric field is applied across the pore, the resulting ion current can be detected with high precision; interference of channel-passing or channel-excluded polymers with the ion flow gives a sensitive report on the studied phenomena of molecular crowding. In the absence of a field, polymers partition "passively" into the pores, a direct result of the "osmotic stress" induced by the polymers (crowders) themselves.

Here, we study partitioning of polymers from a non-ideal binary mixture composed of polymers of different molecular weights going into structurally different ion channels. This is based on the assumption that in a two-component polymer mixture, one component that is preferentially excluded from the channel cavity will "actively" force the other component into the channel cavity. In order to assess the extent to which our results are useful in understanding concrete examples of ion-conducting aqueous pores and size-dependent forced partitioning into these pores. We,

(i) Describe the equation of state of a polymer mixture by its osmotic pressure,

(ii) Study the effects of polymer crowding on electrolyte solutions,

(iii) Investigate the partitioning of polymers from such mixtures into structurally different ion channels.

TABLE OF CONTENTS

LIST OF TABLES

Table **Page**

LIST OF FIGURES

Figure **Page**

INTRODUCTION

The effects of molecular crowding on equilibrium and dynamic phenomena in biophysical, biochemical, and physiological sciences (*e.g.,* solution equilibria, reaction rates and transport of solutes) are well known [1]. The addition of high concentrations of natural and synthetic macromolecules (*e.g.,* PEGs) in buffers enables crowding to be mimicked *in vitro* [2]. Macromolecules used as such not only act as steric crowding agents but also act as osmotic agents via exclusion. This osmotic push is a standard scenario defining the "osmotic stress" technique, proposed originally to probe inter- and intramolecular forces but also used successfully to probe changes in the size of nano-cavities of some proteins [3, 4]. Partitioning of polymers into nanosize cavities is a direct result of this osmotic action [5] and has broad relevance [6]. In particular, this is seen in single-molecule sensing and characterization based on the variation of current through an ion-conducting aqueous pore [7, 8, 9, 10]. Alpha-Hemolysin from *Staphylococcus aureus* has been studied in the presence of neutral polymers such as poly(ethylene glycol) (PEG) [11, 12, 13, 14, 15, 5] and has been shown to exhibit pronounced size-sensitivity with resolution in the monomer range [16]. Recently other aqueous pores, such as aerolysin from *Aeromonas hydrophila*, were also shown to discriminate polymer sizes with very high resolution [17].

This type of passive size-dependent partitioning and size discrimination can be manipulated to actively force polymers into nanosize pores [5]. Forcing polymers into nanosize cavities is particularly relevant to recent studies of controlled ejection of viral genomes from capsids [18], where osmotic stress is applied to push a DNA molecule into or to allow its partial release from the viral capsid by the action of PEG dissolved in the ambient solution [19]. In contrast to "passive" size-dependent partitioning, the

identities of the polymer forced into the nano-cavity (DNA) and the polymer pushing it (PEG) differ.

In this work we propose to study an "active" type of polymer partitioning in the context of binary polymer mixtures, where a preferentially excluded large polymer component (PEG3400) will be used to push another, easily penetrating small polymer component (PEG200), into the channel cavity. Reaching a quantitative description of partitioning performed in this manner requires several problems to be addressed.

The first is the osmotic pressure of a mixture of polymers. The osmotic pressure of a polymer solution, defining the equation of state, is the primary parameter to be addressed. Although the osmotic pressure of monodisperse polymer solutions has been quantitatively described [20], introducing a single parameter defining a transition between Van't Hoff and Des Cloizeaux regimes, in many cases the polydispersity of osmoticants such as PEG is seen as a drawback to accurately selecting the desired osmotic pressure of a polymer solution. Here we will perform osmotic pressure measurements of PEG mixtures and will provide a quantitative description of the osmotic pressures of these mixtures.

The second problem is the study of polymer solutions crowded with electrolytes, particularly studying the effect of polymers on conductivity of these solutions and their effect on ion activity. The primary method to infer the amount of polymer that has partitioned into an ion channel is to examine the effect of polymer on channel conductance [7, 5], along with several assumptions on channel conductance itself [7]. The state of the electrolyte solution, primarily its conductance and the ion activity in the solution have direct consequences regarding channel conductance analysis [21, 12, 5]. To address these questions, we performed measurements on the conductivities of polymer solutions, as well as ion selectivity measurements using ion selective electrodes (ISE) on these solutions.

The third problem is the experimental determination of channel conductance itself, in the presence of polymer solutions, in order to determine the partition coefficients of these polymers. We will be performing measurements on three structurally different ion channels: voltage-dependent anion channel from outer mitochondrial membrane (VDAC), bacterial outer membrane protein C (OmpC), and bacterial channel-forming toxin Alpha-Hemolysin. We will be using a single-channel recording apparatus to record the conductance of a single ion channel at varying polymer concentrations and mixtures, our methodology is described in detail in section 5.1.3.

Overall we strive to determine an equation of state of a polymer mixture (osmotic pressure as a function of composition) which will in turn be used in conjunction with our findings on polymer effects on electrolyte solution and single channel experiments to interpret the polymer partitioning coefficient. Alpha-Hemolysin, which has been extensively used in these settings, is expected to be a strong benchmark for our results, while VDAC is chosen for its almost cylindrical geometry [22, 23], and OmpC for its three-porin structure. Testing structurally different channels will allow us to comment on the effects of channel geometry such as effects of constriction zones, varying channel radii, and their implications on channel access resistance. Introducing these variances will help us to assess the extent to which the measured partitioning conforms to the theoretically expected equilibrium partitioning and to discuss the efficiency of several approaches [5, 24, 25].

CHAPTER 1

BACKGROUND

1.1 Polymer Partitioning is Size and Concentration Dependent

The size dependence of polymer partitioning has been previously studied [26, 27]. Since then it has been used a tool primarily to determine ion channel radii [22] in conjunction with channel access resistance measurements [28]. A quantitative description of the size dependence of polymer partitioning has been worked out [5]. A single alpha-hemolysin channel is probed, for example, with PEGs of different sizes, PEG200, PEG1500, PEG2000, and PEG3400. It has been observed that partitioning is both size dependent and concentration dependent. The result of this work is presented in Fig. 1.1A.

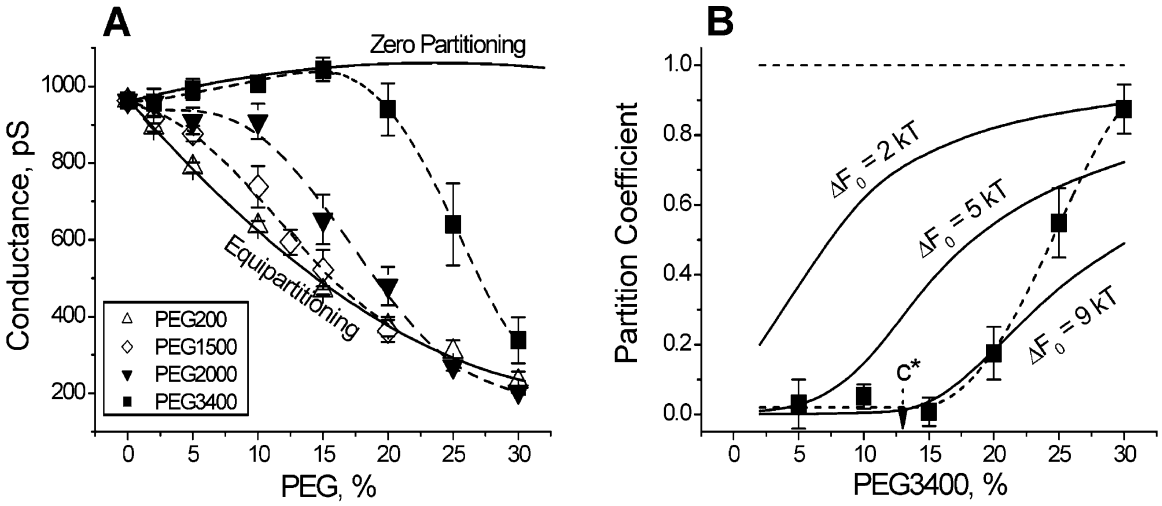

Figure 1.1: A)Partitioning of Different-Size PEGs into Alpha-Hemolysin Channel B) Measured and Calculated Partition Coefficients of PEG3400[1]

It is seen here that although small polymers (PEG200), whose size is small compared with the channel radii ($R_g < R_c$), partition relatively easily into the channel interior; large polymers (PEG3400) do not penetrate the channel up to a certain concentration, then show a sharp increase in their partitioning beyond this concentration. This behavior is rationalized in the sense that as polymer concentration is increased in the bath beyond the polymer overlap concentration (c^*), the solution becomes non-ideal, impacting both polymer radii (R_g) and the osmotic pressure (Π), causing a previously non-partitioning polymer to enter the channel pore.

1.2 A Quantitative Description Based on Solution Non-Ideality

As mentioned before, the quantitative description of partitioning is rationalized based on solution non-ideality. Details of this calculation are explained in section 5.2.1.

It is seen from Figure 1.1B that this calculation fails to describe the partitioning of PEG3400, which will be discussed in detail in section 5.2. Regardless, this work forms the basis of our approach to partitioning of binary mixtures. These basic principles will hold under equilibrium conditions:

- The chemical potential of the polymer in the pore and in the bulk should be the same, offset by a free energy of confinement (ΔF_{conf}),

$$\mu_s^{bulk}(\phi_s^{bulk}, \phi_b^{bulk}) = \mu_s^{pore}(\phi_s^{pore}) + \Delta F_{conf}. \tag{1.1}$$

- The chemical potential of the solvent (*e.g.,* Osmotic Pressure) in the pore and in the bulk should be the same,

[1]Reprinted with permission from Krasilnikov O V., Bezrukov SM (2004) Polymer Partitioning from Nonideal Solutions into Protein Voids. Macromolecules 37(7):26502657. Copyright (2004) American Chemical Society.

$$\mu_w^{bulk}(\phi_s, \phi_b) = \mu_w^{pore}(\phi_s). \tag{1.2}$$

When the chosen binary mixture consists of a small easily partitioning polymer (PEG200) along with a polymer that is preferentially excluded from the pore interior (PEG3400) this will allow us to rationalize the idea of "forced" partitioning. In other words, the increased chemical potential of the small polymer in the bulk by the presence of large polymer $\uparrow$ $(\phi_b^{bulk}) \Rightarrow \uparrow$ (μ_s^{bulk}) will be offset by an increase in the concentration of small polymer in the pore $\uparrow$ $(\phi_s^{pore}) \Rightarrow \uparrow$ (μ_s^{pore}), effectively causing the large polymer (PEG3400) to push the small polymer (PEG200) into the channel interior.

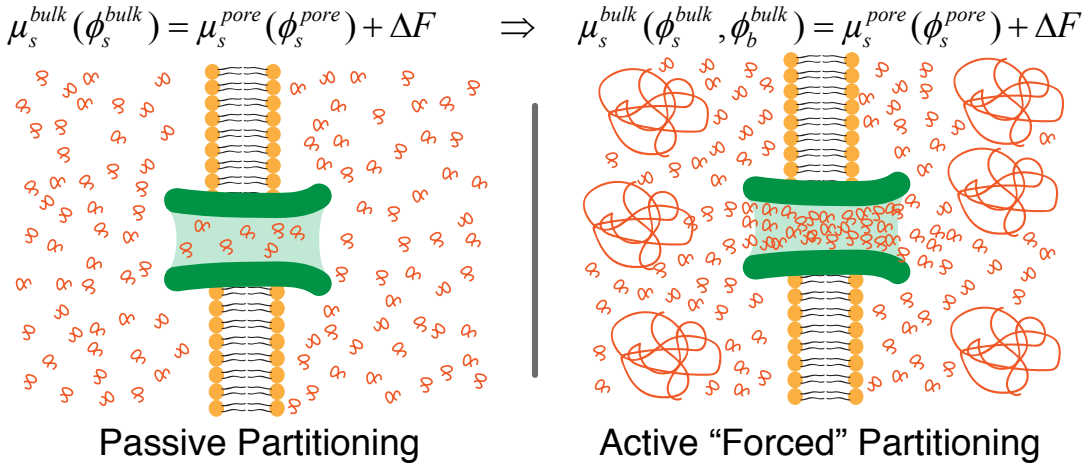

Figure 1.2: Passive and "Forced"" Partitioning of PEG200 into an Ion Channel

CHAPTER 2

BASIC POLYMER THEORY

Throughout this work, we are going to be interested in polymers confined to nano-size ion channels ($\approx 20 - 50$Å diameter). The theory of polymers in solutions is vast. It applies a wide range of mathematical, theoretical and experimental approaches [29, 30, 31, 6] where the scope is well beyond this document. We will, however, be concerned with several aspects of polymers in solution. We are interested in the size of a polymer molecule in solution. This comes in various forms ,*e.g.,* mean end-to-end distance (R_F) and the radius of gyration (R_g). We are going to show how these properties are calculated in a lattice model and their equivalence with a Gaussian chain (in Section 2.1). We will also discuss volume exclusion, which sets a difference between ideal and real chains. In section 2.2 we are going to look at how polymer behavior varies in dilute and semi-dilute concentrations. Another relevant dimension enters the picture, the "correlation length" (ξ), or the "blob size". In section 2.3 we make a brief statement about Flory-Huggins mean field theory of polymer solutions which yields a free energy of mixing (ΔF_{mix}) of a polymer solution and what it yields for the osmotic pressure of a polymer solution (Π_{osm}). It will also be seen in chapter 3 that this theory needs to be extended to provide a better description of polymer osmotic pressure. In section 2.4 we are going to look at scaling laws which yield a free energy of confinement of a polymer (ΔF_{conf}) in a tube and expected polymer osmotic pressure at high concentrations.

The basic concepts covered here and their expansion in chapter 3 will provide us with a complete set of tools to interpret our measurements. We will provide a brief description and demonstration of the concepts.

2.1 Polymer Chains, Relevant Dimensions and Concentrations

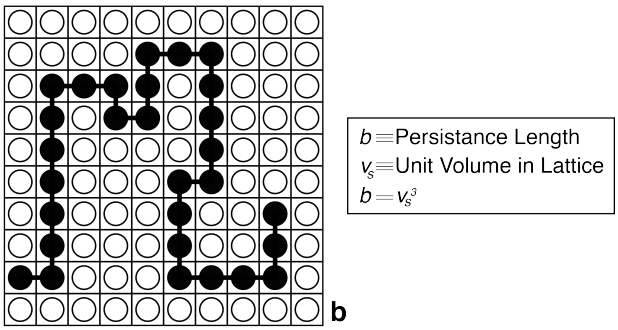

Figure 2.1: A polymer chain on a square lattice

Perhaps one of the most simple and intuitive ways to look at a polymer in solution is to place it in a square lattice, as in Figure 2.1. Here the areas of the lattice not occupied by the polymer are occupied by the solvent molecules. The lattice constant becomes the polymer persistence length (b), and a unit volume (ν_s) on the lattice is simply $\nu_s = b^3$. We will see more of the lattice model in section 2.3. Here we are interested in the size of the polymer chain.

2.1.1 Random Walks

Random Walk in 1-D: We can model a linear flexible chain, like a polymer on a square lattice, as a random walk. In 1-D, constrained to the x dimension, the chain is allowed to take a step to $-x$ or the $+x$ direction with a step size of b (which is the persistence length) with probabilities p and q respectively. Since the chain has no preference between these two directions we take $p = q = \frac{1}{2}$. We assign n as

the number of steps taken in the $+x$ direction in a total of N steps (which is the total number of monomers on the polymer chain). This 1-D random walk is simply a binomial distribution. We can write the probability of taking a total of n steps in the $+x$ direction among a total of N steps as,

$$P_n = \frac{N!}{n!(N-n)!} p^n q^{(N-n)}. \tag{2.1}$$

We are interested in the mean square displacement of the chain in the x direction. The displacement of a random walker in N steps is $\Delta x = x - \langle x \rangle$. The mean square displacement is $\langle \Delta x^2 \rangle$. Given that $x = b(2n-N)$, we can calculate all these quantities from $\langle n \rangle$ and $\langle n^2 \rangle$ so that the expectation value of any function of n can be calculated from

$$\langle f(n) \rangle = \sum_{n=0}^{N} f(n) P_n. \tag{2.2}$$

From here on it is easy to demonstrate that $\langle x \rangle = 0$ and $\langle \Delta x^2 \rangle = bN^2$, making use of the binomial expansion setting $p = q = 1$

$$(p+q)^N = \sum_{n=0}^{N} \frac{N!}{n!(N-n)!} p^n q^{(N-n)} \tag{2.3}$$

$$2^N = \sum_{n=0}^{N} \frac{N!}{n!(N-n)!} \tag{2.4}$$

However there is a neater way to think about this that is easily applied to higher dimensions, and processes not strictly related to square lattices. Let us consider the displacement at the n^{th} step, which is Δx_n. Since the different steps are not correlated, it is straightforward that $\langle \Delta x_n \rangle = 0$ and $\langle \Delta x_n^2 \rangle = b^2$. That is

$$\langle \Delta x_n \Delta x_m \rangle = b^2 \delta_{nm}. \tag{2.5}$$

Then one can calculate $\langle \Delta x \rangle$ and $\langle \Delta x^2 \rangle$ as follows:

$$\langle \Delta x \rangle = \left\langle \sum_{n=1}^{N} \Delta x_n \right\rangle = \sum_{n=1}^{N} \langle \Delta x_n \rangle = 0 \tag{2.6}$$

$$\langle \Delta x^2 \rangle = \left\langle \sum_{n=1}^{N} \Delta x_n \sum_{m=1}^{N} \Delta x_m \right\rangle = \sum_{n=1}^{N} \langle \Delta x_n^2 \rangle = Nb^2 \tag{2.7}$$

Random Walk in Continuous Space. Now let us consider a random walk that is not limited to a lattice. We consider a random walker that starts in position $\mathbf{r}_0$ and takes N random steps in any orientation of length b of $\Delta \mathbf{r}_i$ to arrive at the coordinate $\mathbf{r}_N$. The exact same statistics for Δx applies in this case too, since each step is uncorrelated. Thus

$$\langle \Delta \mathbf{r}_i \rangle = 0, \quad \langle \Delta \mathbf{r}_i \cdot \Delta \mathbf{r}_j \rangle = b^2 \delta_{ij} \tag{2.8}$$

And, in a total of N steps since $\langle \Delta \mathbf{r}^2 \rangle = \langle (\mathbf{r} - \langle \Delta \mathbf{r} \rangle)^2 \rangle$ and $\langle \Delta \mathbf{r} \rangle = 0$, we have $\langle \mathbf{r}^2 \rangle = Nb^2$. Since a part of the random chain is also a random walking chain, the mean square distance between the i^{th} and j^{th} monomers can be expressed as

$$\langle (\mathbf{r}_i - \mathbf{r}_j)^2 \rangle = b^2 |i - j|. \tag{2.9}$$

2.1.2 Mean end-to-end distance and Radius of Gyration

Mean end-to-end distance. Among many other ways to think about polymer dimensions, we are going to define the mean end-to-end distance (R_F) and the radius of gyration (R_g), which are most relevant to this work. The two dimensions are demonstrated in Fig 2.2 The mean end-to-end distance (R_F) is simply the square

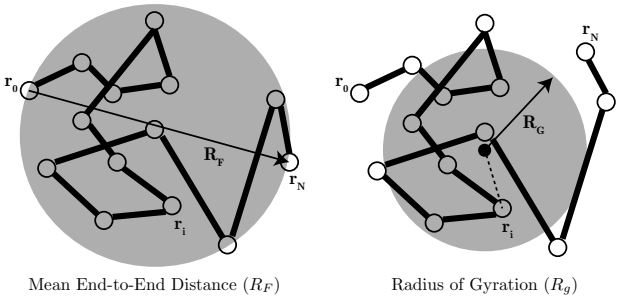

Figure 2.2: Mean end-to-end distance and the radius of gyration

root of the mean square end-to-end distance, which is easily obtained by setting $|i-j|$ in Eq 2.9 to N

$$R_F^2 = \langle (\mathbf{r}_N - \mathbf{r}_0)^2 \rangle = Nb^2 \tag{2.10}$$

Radius of Gyration. The radius of gyration is defined as the square root of the mean square of the distance between monomers (beads) and the center of mass of the polymer. The center of mass of the chain given that all units of the chain have the same mass m can be expressed as

$$\mathbf{r}_{cm} = \frac{1}{N+1} \sum_{i=0}^{N} \mathbf{r}_i. \tag{2.11}$$

Then we can express R_g^2 as,

$$R_g^2 = \left\langle \frac{1}{N+1} \sum_{i=0}^{N} (\mathbf{r}_i - \mathbf{r}_{cm})^2 \right\rangle \tag{2.12}$$

using the following identity,

$$\sum_{i,j=0}^{N} (\mathbf{r}_i - \mathbf{r}_j)^2 = \sum_{i,j=0}^{N} [(\mathbf{r}_i - \mathbf{r}_{cm}) - (\mathbf{r}_j - \mathbf{r}_{cm})]^2 = 2(N+1) \sum_{i=0}^{N} ((\mathbf{r}_i - \mathbf{r}_{cm})^2). \tag{2.13}$$

We end up with,

$$R_g^2 = \frac{1}{2(N+1)^2} \sum_{i,j=0}^{N} \langle (\mathbf{r}_i - \mathbf{r}_j)^2 \rangle. \tag{2.14}$$

Finally plugging Eq. 2.9 into Eq. 2.14, we end up with $R_g = \frac{1}{6} N b^2$. For a random walking freely jointed ideal chain where there is no correlation between its bond, we end up with the following dimensions,

$$R_F^2 = N b^2, \quad R_g^2 = \frac{1}{6} N b^2. \tag{2.15}$$

2.1.3 Gaussian Chain, Bead-Spring Model, Volume Exclusion, and Real Chains

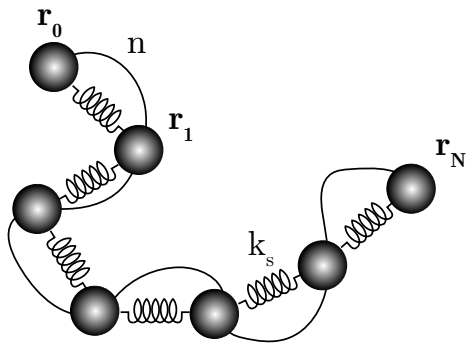

A bead and spring chain
wrapped in a gaussian chain

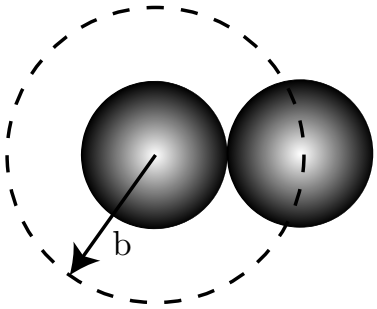

Volume exclusion

Figure 2.3: Bead-Spring Model and Volume Exclusion

Real polymer chains are different from ideal polymer chains in the sense that ideal polymer chains can overlap each other and interactions are not taken into account. As we have mentioned, the methods and literature on this subject is quite vast on its own. However, we will attempt to show in a simple manner how to obtain the so called "Flory Exponent" ν which distinguishes the dimensions of real chains from those of ideal ones. The physical realization of a Gaussian chain in a bead spring model is useful in that sense.

Gaussian Chain In the limit ($N \to \infty$) the binomial distribution (Eq. 2.1) approaches the Gaussian distribution. We can define a Gaussian chain by extending the ideality of the chain to smaller parts of the chain such that any two points on the chain $\mathbf{r}_1$ and $\mathbf{r}_2$ follow a Gaussian distribution. Here each segment on the chain consists of n segments of length b,

$$G(\mathbf{r}_1, \mathbf{r}_2; n) = (2\pi n b^2/3)^{-3/2} \exp\left(-\frac{3(\mathbf{r}_1 - \mathbf{r}_2)^2}{2nb^2}\right). \tag{2.16}$$

By virtue of the Gaussian distribution, the Gaussian chain has the property that any part of a Gaussian chain is also a Gaussian chain, and a combination of Gaussian chains also forms a Gaussian chain

$$\int G(\mathbf{r}_1, \mathbf{r}; n_1) G(\mathbf{r}, \mathbf{r}_2; n_2) dr = G(\mathbf{r}_1, \mathbf{r}_2; n_1 + n_2) \tag{2.17}$$

Bead Spring Chain

One can consider the short-range interactions in a polymer chain as caused by springs of spring constant k_s between the monomers, as seen in Figure 2.3. If one is to model the chain as such, then the potential energy U_{ch} of the chain can be expressed as,

$$U_{ch} = \frac{1}{2} k_s \sum_{n=1}^{N} (\mathbf{r}_n - \mathbf{r}_{n-1})^2 \tag{2.18}$$

If we look at the Boltzmann distribution of this chain, without the normalization constant, we have

$$e^{-U_{ch}/kT} = \prod_{n=1}^{N} e^{-\frac{k_s}{2kT}(\mathbf{r}_n - \mathbf{r}_{n-1})^2} \tag{2.19}$$

Here is where the Gaussian chain plays a role. Each factor in the distribution is identical to the Gaussian distribution of a single chain if one sets the spring constant k_s as

$$b^2 = \frac{3kT}{k_s} \tag{2.20}$$

Here, b^2 is the mean square length of a segment of $n = 1$. In fact, due to the property of a Gaussian chain as described by Eq. 2.17, one can model the entire chain of N units by a single spring constant,

$$k_s = \frac{3kT}{Nb^2} = \frac{3kT}{R_F^2}. \tag{2.21}$$

We can thus calculate the entropy of a Gaussian chain in terms of its separation $(\mathbf{r} - \mathbf{r}')$ as,

$$S = kln(G) = -\frac{3k}{2R_F^2}(\mathbf{r} - \mathbf{r}')^2 \tag{2.22}$$

Volume Exclusion. Consider the two hard spheres in Figure 2.3. When overlapping is not allowed, there are excluded volume effects. The presence of one of the spheres prevents the center of the other sphere accessing a volume of ν_e. The change of the configurational entropy of a sphere can be expressed as

$$\Delta S = kln\left(\frac{V - \nu_e}{V}\right) \cong -kln\left(\frac{\nu_e}{V}\right), \tag{2.23}$$

and the change in the free energy is $\Delta A/kT = \nu_e/V$. For a polymer consisting of N spheres there are $N^2/2$ such interactions thus the total change in free energy is

$$\frac{\Delta A}{kT} = (N^2/2)\frac{\nu_e}{V} \tag{2.24}$$

Real Chain Dimension and Flory Exponent We can estimate the dimension of a real chain by considering the changes in the free energy of the chain due to bead-spring interactions (Eq. 2.22) and due to volume exclusion (Eq. 2.24). Denote $(\mathbf{r} - \mathbf{r}') = R^3$ as the chain dimension. Getting rid of any numerical coefficients, the

excluded volume can be expressed as $\nu_e \cong b^3$, the volume occupied by the chain is $V \cong R^3$. Then we can express the free energy of the chain as,

$$\frac{A}{kT} = \frac{R^2}{Nb^2} + \frac{b^3N^2}{R^3}. \tag{2.25}$$

We are interested in the value of R that minimizes this free energy $\frac{\partial A}{\partial R} = 0$, which yields,

$$R = bN^{3/5}. \tag{2.26}$$

The change in the exponent of N from (1/2) to (3/5) accounts for the swelling of polymer chains in solution. The exponent, however, is approximately (3/5) and only in good solvents. The dimension of a polymer chain is usually expressed as $R = bN^{\nu}$ where ν is the Flory Exponent. The exponent ν has different values for different dimensions and for different solvents. The actual calculations can be found in [29]. For the purposes of our study here, we are going to assume the chains to have a dimension as in Eq. 2.26.

2.1.4 Polymer Concentrations

It will be useful from this point on to mention that there are many ways to express the concentration of polymers in solution. They are used indiscriminately in lab procedures and in literature. Some have the virtue of making calculations easier, and some have experimental benefits. Although there is not really a direct method of converting these concentrations to one another, it can be done via measurements of densities and specific volumes. In Table 2.1 we provide the relevant concentration units used in this work as well as their symbols which will be used consistently throughout. A table of conversions and relevant values for polymers and solvents used in this work is also provided in Appendix A.

Table 2.1: Polymer Concentration Types

Symbol	Definition	Units
ϕ	Monomer Fraction	-
Φ	Volume Fraction	-
c_w	Weight(Mass) Fraction	-
p	Monomer Density	#(Monomer) /V
c_m	Weight(Mass)Density	(M/V) usually g/ml
c	Polymer Density	#(Polymer) /V

2.2 Dilute Concentrations, Semi-Dilute Concentrations, and Blobs

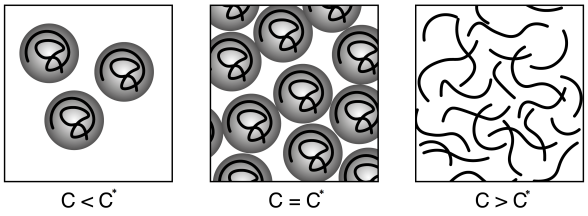

Figure 2.4: Overlap Concentration

Overlap Concentration Polymer solutions show different behavior depending on their concentration. Approximately in dilute solutions a polymer is expected to occupy a sphere of volume (R^3). As the polymer concentration is increased the spheres are expected to start interacting with each other. As the concentration is increased further, polymer spheres become indistinguishable. One is expected to have an entangled soup of polymers. This change in concentrations is demonstrated in Figure 2.4.

Here it is useful to define the quantity "overlap concentration". The overlap concentration is defined as the concentration when the concentration within a polymer sphere is the same as the concentration in the overall polymer solution. This concentration can be defined for different concentration types. In terms of volume fractions,

we can estimate that a monomer occupies a volume of (b^3) inside a sphere. For N such monomers we have for the volume fraction

$$\Phi^* \cong \frac{Nb^3}{R^3} \cong \frac{Nb^3}{(bN^\nu)^3} = N^{1-3\nu}. \tag{2.27}$$

The overlap concentration plays an important role in scaling arguments and in rationalizing polymer partitioning. When solution concentration reaches concentrations beyond the overlap concentration, we are not going to think of polymer sizes in terms of (R) but in terms of the blob size (or correlation length) (ξ).

Blob Size

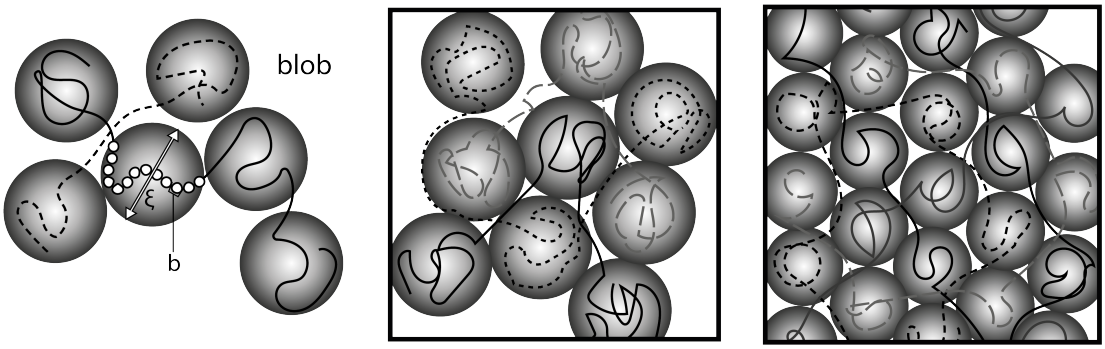

Figure 2.5: Blob Size and Variance with Concentration

At a highly concentrated and entangled polymer concentration, one can surmise that a portion of the chain caught between two entanglement points still claims its own territory. Let us consider a polymer solution at overlap concentration. In terms of monomer densities the overlap concentration can be expressed as

$$\rho^* = \frac{N}{R^3} = b^{-3}N^{1-3\nu} \quad \rho^* = b^{-3}N^{-4/5} \tag{2.28}$$

At the overlap concentration the blob size is equal to the size of the polymer sphere $\xi = R$. As the solution concentration increases, we can determine the blob

size by making two assumptions on polymer behavior. Assuming that there are (N_b) monomers in a blob, the first assumption is that the density of monomers in a blob will be the same as the density of monomers in the whole solution $\rho = N_b/\xi^3$. The second assumption is that the blobs behave like isolated polymer chains of dimension (ξ), that is $bN_b^{3/5} = \xi$. Using these two assumptions and Eq. 2.28, we can express the blob size of the polymer in a concentrated solution in terms of its size in dilute solution (R_0) and the overlap concentration (ρ^*) as,

$$\xi = R_0(\rho/\rho^*)^{-3/4}. \tag{2.29}$$

2.3 Flory-Huggins Theory, Entropy of Mixing and Osmotic Pressure

In this section we are going to introduce the Flory-Huggins mean field theory [32, 33] to look at thermodynamic properties of a polymer solution. Namely this is the free energy of mixing ΔF and the osmotic pressure Π_{osm} derived from this theory. This theory is going to form a basis for thinking about polymer solutions. In Chapter 3 we are going to introduce an important correction to Flory-Huggins mean field theory which arises due to monomer density fluctuations [34]. We will discuss the effects of these corrections, which ultimately result in establishing a model for partitioning of polymers from binary mixtures into ion channels.

Flory-Huggins mean field theory makes use of a lattice model to describe the thermodynamics of a polymer solution, n_p polymers composed of N monomers are laid out on a lattice consisting of n_t total sites and ν_s is the volume per site.

Entropy of Mixing

In this model calculating the entropy of mixing is to compare the number of possible arrangements of n_p chains on the lattice compared with that of their arrangement in

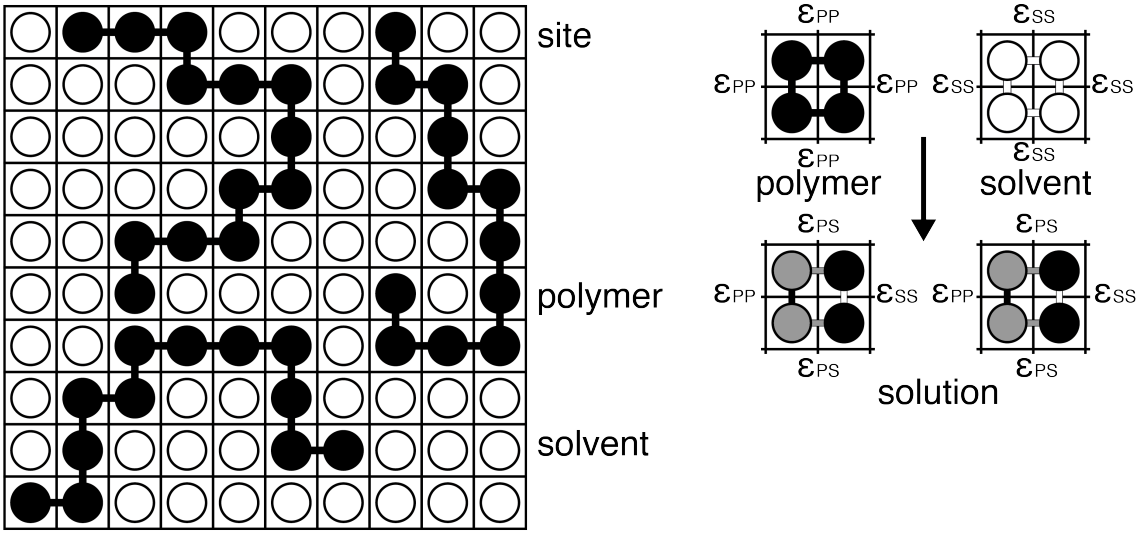

Figure 2.6: Flory Lattice Model

a lattice of $n_p N$ sites (which is an ideal polymer melt). When one proceeds with this calculation, one obtains for the entropy of mixing per lattice site as,

$$\frac{-\Delta S_{mix}}{n_t k} = \frac{\Phi}{N} ln(\Phi) + (1-\Phi) ln(1-\Phi) \tag{2.30}$$

Here the volume fraction of the polymer Φ is related to n_p as $n_p = n_t \Phi / N$. And the number of solvent molecules is $n_s = n_t(1-\Phi)$.

Interaction Energy of Mixing

In order to describe the interaction energy change upon mixing, one first defines three interaction terms $\varepsilon_{PP}, \varepsilon_{SS}$ and ε_{PS}, these are the interactions governing polymer-polymer, solvent-solvent, and polymer-solvent interactions, these interactions are short term interactions assumed to be between two lattice sites, Figure 2.6 shows a depiction of this scheme. Assuming a mixing scheme depicted in Figure 2.6, the change in interaction energy of these 8 bonds upon mixing is $4(\varepsilon_{PP} + \varepsilon_{SS}) \rightarrow 4\varepsilon_{PS} + 2(\varepsilon_{PP} + \varepsilon_{SS})$. That is per newly created P-S bond the energy change is $\varepsilon_{PS} - (\varepsilon_{PP} + \varepsilon_{SS})/2$. Here the Flory-Huggins χ Parameter is defined as,

$$\chi = \frac{z}{kT}(\varepsilon_{PS} - (\varepsilon_{PP} + \varepsilon_{SS})/2) \tag{2.31}$$

The χ parameter basically describes whether P-S contacts or P-P and S-S contacts are favored in a solution; z here denotes the nearest number of neighbors of a lattice site, and the total number of bonds per site is $z/2$. Here in this model one mixes Nn_p number of unconnected monomers and n_s solvent molecules. In this mixing the probability of seeing a particular contact is given in Table 2.2

Table 2.2: Polymer Contacts

Contact	Probability
P-P	Φ^2
P-S	$2\Phi(1-\Phi)$
S-S	$(1-\Phi)^2$

Thus the change in the interaction free energy ΔU_{mix} can be expressed as,

$$\Delta U_{mix} = \frac{zN_t}{2}(\varepsilon_{PS} - (\varepsilon_{PP} + \varepsilon_{SS})/2) \cdot 2\Phi(1-\Phi), \tag{2.32}$$

and the change per site is,

$$\frac{\Delta U_{mix}}{n_t kT} = \chi\Phi(1-\Phi). \tag{2.33}$$

Free Energy, Osmotic Pressure, and Osmotic Pressure of a Dilute Solution

Equipped with equations 2.30 and 2.33, we can express the free energy change upon mixing per site $\Delta G_{mix} = \Delta U_{mix} - T\Delta S_{mix}$ as,

$$\frac{\Delta G_{mix}}{n_t kT} = \frac{\Phi}{N} ln(\Phi) + (1-\Phi) ln(1-\Phi) + \chi\Phi(1-\Phi), \tag{2.34}$$

which for a total of n_t sites is,

$$\frac{\Delta G_{mix}}{kT} = n_p ln(\Phi) + n_s ln(1-\Phi) + \chi n_s \Phi. \tag{2.35}$$

The osmotic pressure of the solution is related to the chemical potential of the solvent $\Delta\mu_s = -\Pi\nu_s$, the molecular volume of water ν_s is the same as the volume of a site in this model $\nu_s = \nu_{site}$. The change in the chemical potential of the solvent is found via,

$$\frac{\Delta\mu_s}{kt} = \left(\frac{\partial}{\partial n_s}\frac{\Delta G_{mix}}{kT}\right)_{T,P,n_p}. \tag{2.36}$$

Using $\left(\frac{\partial\Phi}{\partial n_s}\right)_{n_p} = -(1/Nn_p)\Phi^2$, and expressing the total volume as $V = \nu_{site}n_t$, we obtain the osmotic pressure as,

$$\frac{\Pi V}{n_t kT} = \frac{\Phi}{N} - ln(1-\Phi) - \Phi - \chi\Phi^2 \tag{2.37}$$

in a dilute solution where $\Phi \ll 1$, the osmotic pressure is, via the expansion of the $ln(1-\Phi)$ term,

$$\frac{\Pi V}{n_t kT} = \frac{\Phi}{N} + \left(\frac{1}{2} - \chi\right)\Phi^2 + \frac{1}{3}\Phi^3, \tag{2.38}$$

and finally in an ideal solution the osmotic pressure reduces to the Van't Hoff osmotic pressure

$$\Pi_{VH} = \frac{n_t\Phi}{NV}kT \quad \Pi_{VH} = RTc_{molar}. \tag{2.39}$$

Where R is the gas constant and c_{molar} is the polymer molar concentration, $c_{molar} = c/M_p = \frac{1}{M_p}\frac{M_p\Phi}{N_A N\nu_{site}}$, where M_p is the polymer molar mass.

The Flory-Huggins theory is tremendously successful in its qualitative and quantitative predictions [34]. However we cannot utilize it in describing a binary polymer

mixture. As will be seen in Chapter 5 our solutions are composed of polymer mixtures, and our solutions cover an entire range from dilute to semi-dilute polymer solutions. In concentrated solutions, the form of the osmotic pressure differs as we will demonstrate in Section 2.4 and in Section 3.1 and the Flory-Huggins Osmotic Pressure does not capture the whole behavior.

2.4 Scaling Laws for Confinement and the DesCloizeaux Osmotic Pressure

The scaling arguments we are going to consider here use physical arguments where in certain conditions the solution properties should not depend on the degree of polymerization of the polymer N. They provide good estimates for the osmotic pressure of a semi-dilute polymer solution, and a confinement energy for when a polymer partitions into a confined space.

DesCloizeaux Osmotic Pressure

An important quantity when thinking about semi-dilute polymer solutions is the overlap concentration Φ^* introduced in Section 2.2 which has the form in Equation 2.27. For all practical purposes using the expansion presented in Section 2.3 in Equation 2.38 can be expressed as,

$$\frac{\Pi}{kT} = \frac{\Phi}{N\nu_s ite} f_\Pi \left(\frac{\Phi}{\Phi^*} \right). \tag{2.40}$$

We impose two conditions on the behavior of f_Π. (i) in the dilute regime, f_Π should behave like $f_\Pi = 1 + A + \frac{\Phi}{\Phi^*} \cdots$. (ii) At semidilute concentrations $\Phi^* \ll \Phi \ll 1$, the thermodynamic properties of the solution should be independent of N but only to the polymer concentration Φ, as in the semidilute concentrations any polymer mix acts like a "soup" of polymers where the total monomer content is the major player, since individual polymers in the solution are indistinguishable. This suggests that f_Π should behave like a power function of its arguments

$$\lim_{\Phi \to \inf} f_{\Pi} \left(\frac{\Phi}{\Phi^*} \right) = A \left(\frac{\Phi}{\Phi^*} \right)^m . \tag{2.41}$$

Using Equation 2.27 and the second condition we impose on the behaviour of the osmotic pressure, we find that m should be $m = 5/4$. Thus for semi-dilute solutions we end up with the expression,

$$\frac{\Pi_{dC} \nu_{site}}{kT} = A\Phi^{(9/4)} \tag{2.42}$$

This is the des Coizeaux Osmotic Pressure. As we shall see in Section 3.1 the des Cloizeaux osmotic pressure describes the osmotic pressures at concentrations in the regime $\Phi^* \ll \Phi \ll 1$ sufficiently. However it should be noted that the Flory description of the osmotic pressure, Equation 2.37 cannot be reduced to this form.

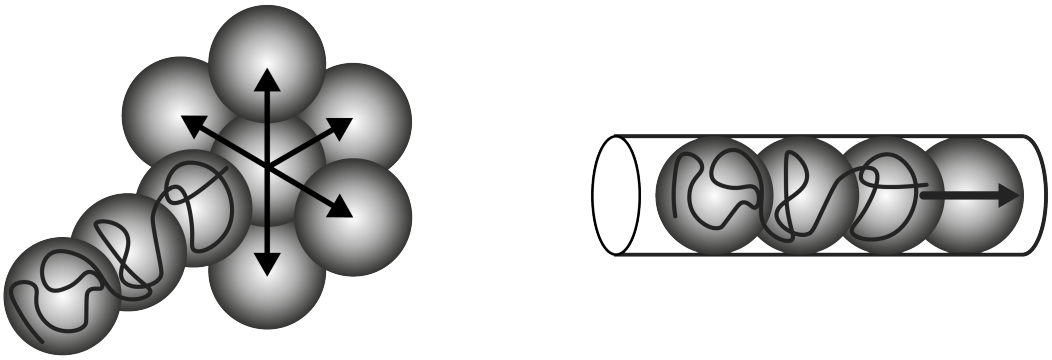

Figure 2.7: Confinement of Blobs

Free Energy of Polymer Confinement We have been discussing the behavior of polymer solutions, yet we have not made a statement about polymer confinement. When thinking about polymer confinement, or confinement energy ΔF_{conf}, we are concerned with the entropy change of confinement ΔS_{conf} through this work. As we shall see further down the line, investigating polymer partitioning into channels requires many assumptions and simplifications on our part. The assumption that when

polymers are confined in tubes (ion channels), the free energy change depends only to the entropy of confinement is one of them. Thus we are ignoring any interactions between polymers and ion channels.

If one considers the blob picture, we can picture the polymer confinement as the polymer, confining to a tube of diameter D in the form of blobs of diameter D. This picture, as in Figure 2.7, provides a very intuitive answer for polymer confinement. We consider the number of possible arrangement of blobs of diameter D w.r.t that of blobs arranged in a tube. In this case the size of the blobs are $D = bN_b^{3/5}$ as in the blob picture. We are considering the arrangement of N/N_b blobs in a three dimensional space. The total number of arrangements for such spheres is roughly $5^{N/N_b}$, and the total number of arrangement of spheres in the tube is precisely 1. The ratio of possible arrangements p is then,

$$p = \frac{1}{5^{N/N_b}} \tag{2.43}$$

This ratio is related to the entropy as $p = e^{-\Delta S_{conf}/k}$. Thus we find the entropy of confinement and the free energy of confinement (ΔF_{conf}) as,

$$\frac{\Delta F_{conf}}{kT} = \frac{-\Delta Sconf}{k} = \left(\frac{R}{d}\right)^{5/3}. \tag{2.44}$$

Here R is the radius of the polymer as defined in Section 2.1.3 Equation 2.26.

CHAPTER 3

BINARY POLYMER MIXTURES

In the preceding chapter, we presented the size of a flexible polymer in solution (2.1.3), how the size of the polymer varies with concentration (2.2) and how it influences the free energy of partitioning (2.4). We demonstrated the Flory-Huggins Theory as a thermodynamic approach to describe polymers in solution, and the osmotic pressure of a polymer solution (2.3). Before considering binary polymer mixtures however, we need to revisit the osmotic pressure of a polymer solution. In this chapter we are going to present osmotic pressure measurements performed on PEG in water and PAMS in Toulene [20] and talk about the Van't Hoff and Des Cloizeaux behavior in these measurements (Section 3.1). As mentioned in section 2.3, the Flory-Huggins theory does not account for the des Cloizeaux regimes of osmotic pressure. In Section 3.2 we are going to introduce a correction to the Flory-Huggins theory, which arises due to monomer density fluctuations [34], which is an important correction that makes the theory account for the osmotic pressure measurements. And finally in Section 3.3 we are going to extend the formulation presented in Section 3.2 to binary mixtures [25] and calculate the osmotic pressure and partitioning coefficients of binary polymer mixtures.

3.1 Osmotic Pressure Revisited

We have stated that the osmotic pressure of a polymer solution is expected to behave differently depending on the concentration of the solution. Namely, in the dilute regime one expects Van't Hoff 2.39 behavior; and in semi-dilute concentrations des Cloizeaux 2.42 behavior is expected. In Ref. [20], the authors have measured the osmotic pressures of PEGs in Water and PAMSs in Toulene for a wide range of molecular weights and concentrations. Their results are summarized in Figure 3.1.

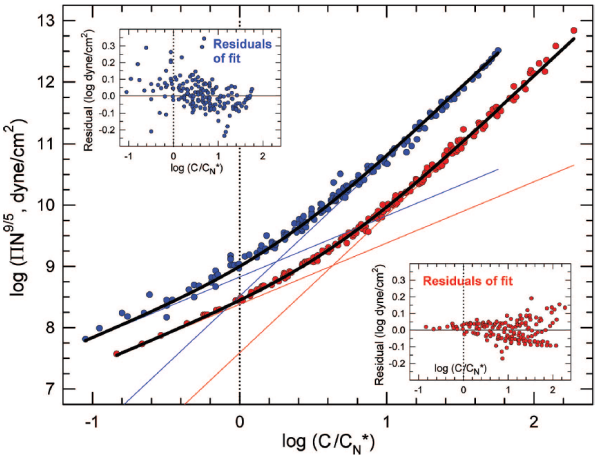

Figure 3.1: Osmotic Pressures of PEGs in Water and PAMSs in Toulene[1]

The behavior of the osmotic pressure agrees remarkably with the Van't Hoff and des Cloizeaux pressure in their relevant concentration regimes. To describe the entire data, they envision an osmotic pressure function of the form $\Pi = \Pi_{VH} \rightarrow \Pi_{dC}$, smoothly varying from one region to another linked by a single parameter α. Formally

$$\Pi N^{9/5} = \frac{RT}{M_m \bar{V}} \left[\left(\frac{c}{c^*} \right) \rightarrow \alpha \left(\frac{c}{c^*} \right)^{9/4} \right] \tag{3.1}$$

[1]Reprinted with permission from Cohen J A., Podgornik R, Hansen PL, Parsegian V A. (2009) A phenomenological one-parameter equation of state for osmotic pressures of PEG and other neutral flexible polymers in good solvents. J Phys Chem B 113(12):37093714. Copyright (2009) American Chemical Society.

Here $\bar{V}$ is the partial specific volume of polymer and M_m is the mass of one monomer. And the smooth transition is accomplished by,

$$\Pi N^{9/5} = \frac{RT}{M_m \bar{V}} \left[\left(\frac{c}{c^*} \right) + \alpha \left(\frac{c}{c^*} \right)^{9/4} \right] \tag{3.2}$$

As Figure 3.1 shows the agreement of the measurements with this result is remarkable. The important aspect of this work we need to observe is the behavior along the crossover regime, i.e. $c \sim c^*$. The crossover region is small, behavior here is smooth and the measurements does not vary greatly from the Van't Hoff, or des Cloizeaux behavior (1 and (9/4) slopes are indicated in Figure 3.1). This is an important observation for an assumption to come in Section 3.3

3.2 Flory-Huggins is not Sufficient

Before getting into the discussion of polymer partitioning, we need an equation of state that describes the properties of the polymer solution. Due to the nature of our experiments, we need this description to be valid in dilute and semi-dilute regimes of polymer concentration. The free energy (ΔF) of a polymer solution is not a measurable quantity, the osmotic pressure (Π_{osm}) of a polymer solution, however, is a measurable quantity and is an equation of state of the polymer solution.

Discussions of polymer theory are beyond the scope and purpose of this document. However Flory-Huggins theory is essentially a theory of dilute solutions and other shortcomings of the theory are addressed clearly in Ref [34] as,

"Nevertheless, the mean field theory clearly fails under the conditions where the density fluctuations are dominant such as dilute and semidilute solutions. It is well known, e.g., that the Flory Huggins theory predicts erroneous molecular weight dependencies for the second virial coefficient [29] and the critical concentration for the phase separation in polymer solutions [35, 36, 37, 38]. Furthermore, the density correlations are such that the failure to account for these correlations leads to the experimentally

observed apparent "composition-dependent χ parameter." The density fluctuations in polymer solutions are of two types. The first is the composition fluctuation which is the same as that encountered in simple (low-molecular weight) binary mixtures. These fluctuations grow tremendously as the system approaches criticality and playa significant role in such phenomena as the dynamics of spinodal decomposition, etc. [38, 39] The second type of density fluctuations is specific to polymers and arises from the monomer density correlations. The manner in which two monomers belonging to the same chain are spatially correlated is described by the monomer density correlations [40, 41]. Thus the characteristic wavelength of the composition fluctuations is typically much larger than that of monomer density fluctuations which in turn is larger than the Kuhn length (l) but shorter than or comparable to the size of the polymer chain. Any refinement of the Flory-Huggins theory should account for both of these fluctuations."

The author, M. Muthukumar, of this work [34], refines the Flory-Huggins theory by taking into account the density fluctuations and two-, three-body interactions in polymer solutions. We are going to use a form of this equation which ignores the three-body interactions. In this form the free energy of a polymer solution (per site) becomes (we are going to use $n_0 = n_t$ to indicate the total number of sites),

$$\frac{\Delta F(\Phi)}{n_0 kT} = \frac{\Phi}{N} ln\Phi + (1-\Phi) ln(1-\Phi) + \chi\Phi - \frac{1}{2}\Phi^2 + \alpha(\frac{1}{2} - \chi)^{3/4}\Phi^{9/4}. \tag{3.3}$$

Equation 3.3 is going to form the basis of our analysis of binary polymer solutions in this work. It is important to note the $\Phi^{9/4}$ term here. This is a crucial term making this equation consistent with the phenomenological result for the osmotic pressure 3.2. The parameter α is derived in Ref [34] as $\alpha = 1.872$.

3.3 Binary Mixtures and the Polymers Pushing Polymers Framework

3.3.1 Polymers Pushing Polymers Framework

Free Energy of Mixing of a Polymer Mixture In Section 3.2 we introduced a correction to the well known Flory-Huggins mean field theory, which arises due to monomer density fluctuations. Now we are going to apply this free energy to binary mixtures of polymer solutions. A quantitative description of the free energy of binary mixtures, osmotic pressures and partition coefficients of polymers has been worked out in [25]. In this section we are going to follow reference [25] and describe binary mixtures of polymer solutions.

As we have seen in Section 3.2, the free energy of a polymer solution is given by:

$$\frac{\Delta F(\phi)}{kT} = n_0 \left(\frac{\phi}{N} ln\phi + (1-\phi) ln(1-\phi) + \chi\phi - \frac{1}{2}\phi^2 + \alpha(\frac{1}{2} - \chi)^{3/4}\phi^{9/4} \right). \quad (3.4)$$

Here $n_0 = n_w + n_p$ is the total number of monomers (water and polymer), χ is the Flory-Huggins parameter and $\alpha = 1.87$ is a constant evaluated in Ref. [34]. $(\frac{1}{2} - \chi)$ is the second virial coefficient for the osmotic pressure. We are slightly modifying Eq. 3.3 and converting volume fractions (Φ) to monomer fractions (ϕ). This is essentially a simplification regarding the volume occupancy of polymer and water molecules (ν_p, ν_w), setting them equal to 1 and getting rid of the volume dimension. It is possible to convert measurements done in physical concentrations (e.g., c_w, Φ) to monomer fractions using experimental quantities such as solution densities, and specific volumes of PEG and waters ($\bar{\nu}_p, \bar{\nu}_w$). Please refer to Appendix A for these conversions.

Now, Ref, [25] assumes that each of the two components (a small and a big polymer indicated by (s) and (b) respectively) separately conforms to the limits of validity of

the above formula, that is $\phi \rightarrow (\phi_s + \phi_b)$, and obtains the Free Energy of Mixing of a binary polymer mixture as,

$$\begin{aligned} \frac{\Delta F(n_w, n_s, n_b)}{kT} &= n_w ln\phi_w + n_s ln\phi_s + n_b ln\phi_b + \chi n_0(\phi_s + \phi_b) \\ &\quad -\tfrac{1}{2} n_0(\phi_s + \phi_b)^2 + \alpha n_0(\tfrac{1}{2} - \chi)^{3/4}(\phi_s + \phi_b)^{9/4}. \end{aligned} \tag{3.5}$$

The results of Ref. [20] that we have discussed in Section 3.1 are important for validating this assumption. We stated three major results in Section 3.1

(i) The Osmotic Pressure of polymer solutions in the dilute limit conforms to the Van't Hoff Osmotic Pressure.

(ii) The Osmotic Pressure of polymer solutions in the sem-dilute limit conforms to the des Cloizeaux Osmotic Pressure.

(iii) The crossover region from the Van't Hoff to des Cloizeaux regimes is small, and the variance of the experimental data from both regimes is small.

Now, the Van't Hoff regime is linear in polymer concentrations ($\Pi_{VH}(\Phi_s, \Phi_b) = \Pi_{VH}(\Phi_1) + \Pi_{VH}(\Phi_2)$). In this regime the assumption is validated. The des Cloizeaux regime by construction (see Section 2.4) is concerned with the total monomeric content of the polymer solutions ($\phi_s + \phi_b$), not in individual polymer types and the polymerization number (N), thus making this assumption valid in this regime. Thus this assumption is quite promising in describing the free energy of a polymer mixture.

Osmotic Pressure and Chemical Potentials of the Components Once the Free Energy of Mixing of the binary mixture is known, the osmotic pressure of this solution, and the chemical potentials of the polymers are easily evaluated,

$$\frac{\mu_w}{kT} = -\frac{\bar{\nu}_w \Pi(\phi_s, \phi_b)}{kT} = \frac{\partial}{\partial n_w}\left(\frac{\Delta F}{kT}\right)\Bigg|_{n_s, n_b}, \tag{3.6}$$

$$\frac{\mu_{s,b}}{kT} = \frac{\partial}{\partial n_{s,b}}\left(\frac{\Delta F}{kT}\right)\Bigg|_{n_w, n_{b,s}}, \tag{3.7}$$

Which yields for the Osmotic Pressure,

$$\begin{aligned}\frac{\bar{\nu}_w \Pi(\phi_s, \phi_b)}{kT} &= \ln(1-\phi_s-\phi_b) + (1-\phi_s-\phi_b) - 1 + \frac{\phi_s}{N_s} + \frac{\phi_b}{N_b} \\ &\quad -\frac{1}{2}(\phi_s+\phi_b)^2 + \frac{5}{4}\tilde{\alpha}(\phi_s+\phi_b)^{9/4}.\end{aligned} \tag{3.8}$$

and for chemical potentials setting $\tilde{\mu}_{s,b} = \mu_{s,b}/kT$ and $\tilde{\alpha} = \alpha(1/2-\chi)^{3/4}$,

$$\begin{aligned}\tilde{\mu}_{s,b} &= ln\phi_{s,b} + 1 - \phi_{s,b} - \phi_w N_{s,b} - \phi_{b,s}\frac{N_{s,b}}{N_{b,s}} - \left(\chi - \frac{1}{2}\right)N_{s,b} \\ &\quad + \frac{1}{2}N_{s,b}\phi_w^2 - \frac{5}{4}\tilde{\alpha}N_{s,b}(\phi_s+\phi_b)^{9/4} + \frac{9}{4}\tilde{\alpha}N_{s,b}(\phi_s+\phi_b)^{5/4}.\end{aligned} \tag{3.9}$$

Partition Coefficients The partition coefficient of polymers is defined as the ratio of the polymer concentration in the pore (ϕ^{pore}) to that of polymer in the bulk (ϕ^{bulk}), namely $\left(p = \frac{\phi^{pore}}{\phi^{bulk}}\right)$. Once the chemical potential of each of the species is known, we can determine the partition coefficients by setting our conditions for equilibrium partitioning. Here we make two assumptions:

(i) In a binary mixture composed of two polymers, one small, one big, only the small polymer partitions into a pore.

(ii) The free energy of polymer solutions (chemical potentials) in the bulk and in the pore differ by a free energy of confinement ΔF_c. We will make further assumptions on this free energy later.

We must set the chemical potential of the solvent (water) in the bulk equal to the chemical potential of the solvent in the pore. These conditions can be expressed as,

$$\begin{aligned} \tilde{\mu}_s^{bulk}(\phi_s^{bulk}, \phi_b^{bulk}) &= \tilde{\mu}_s^{pore}(\phi_s^{pore}) + \Delta F_c \\ \tilde{\mu}_w^{bulk}(\phi_s^{bulk}, \phi_b^{bulk}) &= \tilde{\mu}_w^{pore}(\phi_s^{pore}). \end{aligned} \tag{3.10}$$

This condition can be stated in an equivalent form as,

$$\tilde{\mu}_s^{pore}(\phi_s^{pore}) - N_s\tilde{\mu}_w^{pore}(\phi_s^{pore}) + \Delta F = \tilde{\mu}_s^{bulk}(\phi_s^{bulk}, \phi_b^{bulk}) - N_s\tilde{\mu}_w^{bulk}(\phi_s^{bulk}, \phi_b^{bulk}). \tag{3.11}$$

This yields,

$$\left\{ \begin{array}{c} ln\phi_s^{pore} - N_s(ln(1-\phi_s^{pore}) + \phi_s^{pore}) \\ + N_s\frac{9}{4}\tilde{\alpha}(\phi_s^{pore})^{5/4} + \Delta F \end{array} \right\} = \left\{ \begin{array}{c} ln\phi_s^{bulk} - N_s(ln(1-(\phi_s^{bulk}+\phi_b^{bulk})) \\ -(\phi_s^{bulk}+\phi_b^{bulk})) \\ + N_s\frac{9}{4}\tilde{\alpha}(\phi_s^{bulk}+\phi_b^{bulk})^{5/4} \end{array} \right\}$$

Defining the partition coefficient as $p = \frac{\phi_s^{pore}}{\phi_s^{bulk}}$ we end up with,

$$ln(p)+\Delta F = N_s\bigg(ln(1-p\phi_s)-ln(1-\phi_s-\phi_b)+(p\phi_s-\phi_s-\phi_b)+\frac{9}{4}\tilde{\alpha}((\phi_s+\phi_b)^{5/4}-(p\phi_s)^{5/4})\bigg), \tag{3.12}$$

CHAPTER 4

ION CHANNELS

Ion Channels are pore forming proteins found in the membranes of prokaryotic and eukaryotic cells. Their main function is to facilitate transport of metabolites and ions (which in turn have their regulatory, transport or metabolic tasks) through the otherwise impermeable lipid cell membranes. Ion channels are regarded as excitable molecules [42]. They respond to membrane potential changes, chemical stimuli, and even mechanical deformations [3]. They are not static pores that simply allow metabolites and ions to pass through. Most channels are selective to metabolites and ions to some degree [42], showing different rates of conductivity for separate ions. They also show complicated gating mechanisms where portions, or the entirety of the channel closes affecting the selectivity of the channel[43][44]. Apart from gating, channels might show many conductance substates [45][46]. Our purpose in this study is to employ ion channels as nanosize pores, and only that. Fortunately there are some assumptions and studies we can refer to that allows us to circumvent the complicated behaviour and allows us to see them only as nanosize pores. In Section 4.1 we will briefly introduce the three structurally different ion channels used in this study, and in the following Section 4.2 we will briefly talk about the conductance and selectivity of ion channels and introduce certain assumptions we will be making throughout this work.

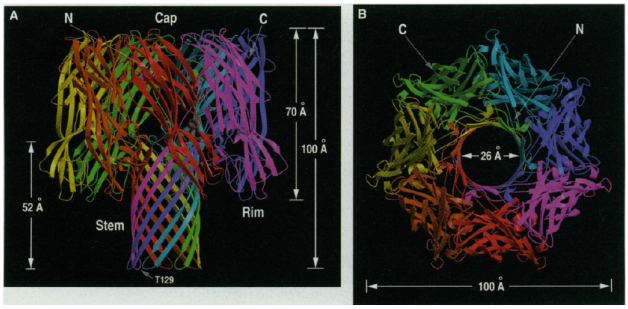

Figure 4.1: Alpha-Hemolysin[1]

4.1 Ion Channels Employed

4.1.1 Alpha-Hemolysin

Alpha-Hemolysin is a different kind of channel compared with channels commonly encountered in cells. It is a water-soluble lytic protein secreted by *Staphylococcus aureus*[47][48]. It is released from the bacteria as a 293-amino acid monomeric polypeptide with a total molecular mass of 33 kDa. It forms seven monomeric subunits that associate and create a prepore complex on cell membranes [49][50], which then penetrates further the membrane to form a lytic pore [51].

Alpha-Hemolysin is extensively studied via reconstitution on lipid bilayer membranes. Its conductance, geometric, and gating properties are investigated in many of these studies [5][13][52][53][54][55][56][57][58], some involved probing the pore with neutral polymers. Alpha-Hemolysin has recently been to perform mass spectrometry on neutral polymers [16][59]. Another application of Alpha-Hemolysin channels was to detect and identify single-stranded DNA nucleotides [60][61][62][63] while a single-stranded DNA molecule passes through the channel, as an attempt to achieve DNA sequencing using this nanopore, which has proven to be a promising but a challenging task [64].

---

[1]From Song, L., Hobaugh, M., Shustak, C., Cheley, S., Bayley, H. and Gouaux, J. (1996). Structure of Staphylococcal alpha -Hemolysin, a Heptameric Transmembrane Pore. Science, 274(5294), pp.1859-1865. Copyright (1996). Reprinted with permission from AAAS.

Figure 4.1 shows the crystal structure of this channel, determined at 2.0Å resolution [65]. The pore itself resembles a mushroom like shape consisting of three domains, the "stem", "cap" and the "rim". The cap sits outside the membrane and has a diameter of 100Å, the stem is a 14-stranded β-barrel and the part of the channel that penetrates the membrane. Its interior is hydrophilic. The diameter of the channel is $\approx$ 26Å. Two apparent constrictions exist within the channel of 9Å and $6 - 7$Å. Molecular dynamics simulations have been performed on this channel to calculate channel conductivity and the electrostatic potential along the pore [66], together with simulations to describe polymer translocation along the pore [67].

4.1.2 Voltage Dependent Anion Channel (VDAC)

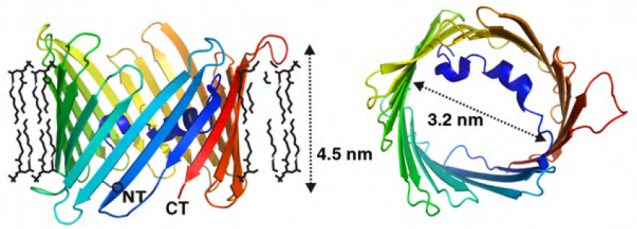

Figure 4.2: Voltage Dependent Anion Channel (VDAC)[2]

Voltage Dependent Anion Channel (VDAC) is found on the mitochondrial membrane of eukaryotic species [68]. VDAC isolated from species from all eukaryotic kingdoms has virtually the same properties of ion selectivity and voltage dependence [69]. Its primary function is to regulate the flow of metabolytes between the cell cytosol and the mitochondrial intermembrane space. Of the metabolites that translocates through the mitochondrial outer membrane, ATP and ADP are probably the most important[70][71]. This multifunctional channel has also been shown to be in-

[2]Reprinted from Trends In Biochemical Sciences. 35, S. Hiller, J. Abramson, C. Mannella, G. Wagner, K. Zeth, The 3D structures of VDAC represent a native conformation, 514-521., Copyright (2010), with permission from Elsevier.

volved in mitochondrial dependent cell death [72][71], and metabolic stresses present in cancer cells [73][74][43].

The structure of VDAC is depicted in Figure 4.2. VDAC a polypeptide of $\sim$ 30 kDa essentially forms a beta barrel channel of a diameter 32Å, and length 40Å [23]. In addition, at the N-terminus there is sequence whose polar/non-polar pattern fits that of a "sided" alpha helix. This 20 amino-acid sequence,is located within the lumen of the channel. In the refolded, non-functional structure essentially creating a constriction of about 10Å [75][23].

4.1.3 Outer Membrane Protein C (OmpC)

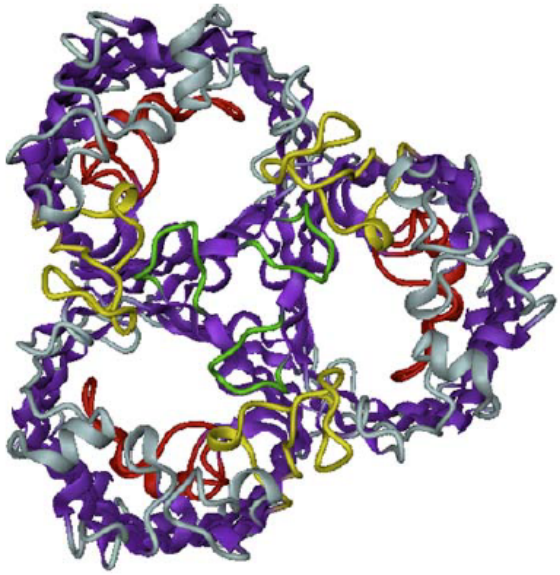

Figure 4.3: Outer Membrane Protein C (OmpC)[3]

Gram-negative bacteria characteristically are surrounded by an outer membrane, the major function of this additional membrane layer is to serve as a selective permeation barrier. OmpC belongs to a family of porins that occur on the outer membrane

[3]Reprinted from Journal Of Molecular Biology. 362, A. Basl, G. Rummel, P. Storici, J. Rosenbusch, T. Schirmer, Crystal Structure of Osmoporin OmpC from E. coli at 2.0 Å, 933-942., Copyright (2006), with permission from Elsevier.

along with OmpF and Phosphoporin PhoE. OmpF, OmpC, and PhoE are strongly similar in sequence and also in their three-dimensional structure [76], that they apparently form mixed trimers almost at random [77]. Apart from these porins others such as OmpD, OmpX, OmpW, NmpC exist on the outer membrane of gram-negative bacteria.

Studies on OmpF structure shows that porin monomers cross the lipid bilayer as a beta-barrel or a series of 16 beta-strands. The strands are tilted rather strongly in relation to the barrel axis [78]. This tilting increases the diameter of the barrel. The constriction region inside the OmpF channel called the "eyelet" is shown to be about $7 - 11$Å [76].

The crystal structure of OmpC has been determined to a 2.0Å resolution [79]. OmpC adopts the OmpF-like 16-stranded hollow beta-barrel fold with three beta-barrels associated to form a tight trimer. The pore constriction and the periplasmic outlet are very similar to OmpF with 74% of the pore lining residues being conserved. The OmpC structure suggests that not pore size, but electrostatic pore potential and particular atomic details of the pore linings are the critical parameters that physiologically distinguish OmpC from OmpF. OmpC has a radius of about 10.8Å [80].

OmpF and OmpC have been reconstituted in lipid bilayers. Antibiotic permeation [81][82] and polymer translocation experiments have been performed [83] as well as studies on residue ionization. We are interested in OmpC due to its unique structure, that it forms a trimeric pore, whereas alpha-hemolysin and VDAC forms single pores.

4.2 Working Around Ion Channel Complexities

As we have mentioned before, we want to utilize ion channels as nanosize pores. As we have seen in Section 4.1, ion channels have both complex structures and show complex behaviour, such as gating and ion selectivity. There are legitimate methods

to work around these complexities, and in certain cases we will have to make do with assumptions. In this section, we will briefly mention the Nernst relation and the diffusion potential. These are used to determine the selectivity of an ion channel. Then we will list certain effects that we are disregarding, stating the reasons and empirical evidence for doing so.

4.2.1 Basic Electrophysiology

Ion Movement in Solution

To a crude approximation, the resistivity ρ of an ionic solution is inversely proportional to the molarity n of the solution

$$\rho \propto \frac{1}{n}. \tag{4.1}$$

Assuming the simplest conditions, there are two reasons ions move in solution, one is due to diffusion, and the other is due to a potential difference. Defining the flux of ions $\phi = \frac{\text{Moles}}{\text{Area}\cdot\text{Time}}$, and the flux due to diffusion as ϕ_{Fick} (Fick's Law) and, due to the potential difference as ϕ_{Ohm} (Ohm's Law), the total flux in the solution is,

$$\phi = \phi_{Fick} + \phi_{Ohm}. \tag{4.2}$$

Fick's Law states that the flux of ions is inversely proportional to the concentration gradient inside the solution $\phi_{Fick} \propto -\frac{dn(x)}{dx}$. The proportionality constant is the diffusion coefficient $D \propto kT$, which is proportional to kT. The proportionality constant that defines diffusion coefficient is called the mobility of ions u. So for ϕ_{fick} we have,

$$\phi_{Fick} = -ukT\frac{dn(x)}{dx}. \tag{4.3}$$

The flux due to the potential difference is proportional to the electric field $\phi_{Ohm} \propto \frac{dV(x)}{dx}$, with the proportionality constants placed in,

$$\phi_{Ohm} = -zenu\frac{dV(x)}{dx}. \tag{4.4}$$

Here en is the charge density, and z is the valence of the ion. So for the total flux in solutions we get,

$$\phi = -ukT\frac{dn(x)}{dx} - zenu\frac{dV(x)}{dx}. \tag{4.5}$$

Remembering that the flux is related to the current via $I = zeA\phi$, where is A the cross-sectional area to which the field and the current is perpendicular it is easy to conclude that the resistivity is,

$$\rho = \frac{1}{z^2e^2nu}. \tag{4.6}$$

Diffusion Potential

Consider two solutions containing different concentrations of ionic solutions separated by a selective membrane (or a selective pore in our case). By imposing the condition that there is no net current,

$$\sum z_i\phi_i = 0, \tag{4.7}$$

we have,

$$z_1\left(u_1kT\frac{dn_1}{dx} + z_1en_1u_1\frac{dV}{dx}\right) + z_2\left(u_2kT\frac{dn_2}{dx} + z_2en_2u_2\frac{dV}{dx}\right) = 0. \tag{4.8}$$

Solving for the potential difference across the selective medium, imposing the condition of the neutrality of charge $n_1 = n_2 = n$, we have

$$\frac{dV}{dx} = -\frac{kt}{e}\frac{z_1u_1 + z_2u_2}{z_1^2u_1 + z_2^2u_2}\frac{dn}{n}. \tag{4.9}$$

Replacing the indices by K and Cl respectively, this yields

$$V'' - V' = -\frac{kt}{e}\frac{u_K - u_{Cl}}{u_K + u_{Cl}} ln \frac{n''}{n'}. \tag{4.10}$$

This potential difference is the diffusion potential across the membrane.

Reversal Potential and Selectivity

Note that the diffusion potential is zero if the mobilities of the ions are equal. The selectivity of an ion channel can be probed by reconstituting the channel in a membrane where it is bathed by two solutions of different concentrations. The mobilites of K^+ and Cl^- ions in free solution are similar $u_{Cl}/u_K \approx 1.03$. If, say, the ion channel is reconstituted in a membrane with a 10-fold concentration gradient and a potential difference is observed using an amplifier, then one can deduce the selectivity ratio of the channel w.r.t cations and anions.

4.2.2 Assumptions

We are going to assume that our channels are cylindrical pores, that are non-selective to ions which retain their open channel conductance state during measurements. We also assume that the presence of electrolytes does not affect the equation of state of PEGs, and does not bind to PEGs. However the presence of PEGs does affect the amount of electrolyte that move into the channel, and channel resistance is increased by access resistance, which arises due to the convergence of electric field lines towards a nanosize pore. The PEG effect on electrolytes is discussed in Section 5.1.2, and the access resistance is discussed in Section 5.1.3.3 and Appendix C.

Ion Channels Are Ohmic

An ion channel reconstituted in a membrane held at a constant potential can be simply expressed as a resistor R_{ch} in parallel with a capacitor C_m (the membrane), Figure 4.4. Any diffusion potential that could exist could be placed in series with the resistor.

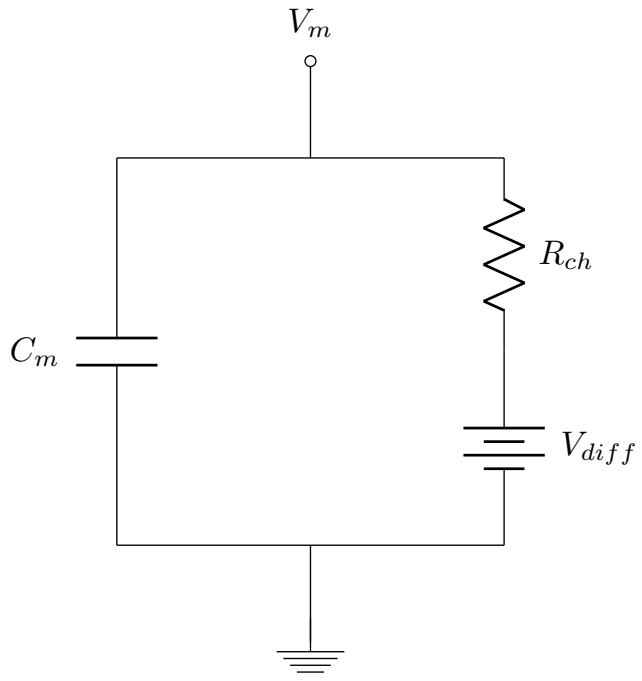

Figure 4.4: Measured Osmotic Pressures of PEG200, PEG3400 Solutions, and Their Binary Mixtures

The lipid that we use in this study, DPhPC, forms a stable bilayer on a $\approx 100\mu m$ pore on a teflon membrane of thickness $\approx 25\mu m$.The capacitance of the bilayer is $\approx 90pF$. In voltage-clamp experiments (membrane held at a constant potential) of this sort, the membrane due its low capacitance does not introduce time delayed responses and practically sustains its potential difference. Thus the experiment simply consists of passing a steady current across a resistor at a constant applied potential. Determining the channel resistance correctly under different conditions is crucial to these experiments. We need to make sure that the channel is Ohmic, that is $V \propto I$ at different conditions. This condition is satisfied by observation and measurement of the current response to potential. We see that alpha-hemolysin, OmpC and VDAC are ohmic in their responses at applied potential differences of $\pm 100mV$, $\pm 200mV$, $\pm 40mV$ respectively.

Ion Channels are non-selective

The selectivity of ion channels arises due to different mechanisms. Generally due to charged residues inside the pore lining [84] which creates a potential gradient inside the channel. The selectivity of a channel is also dependent on pH [14]. Alpha-hemolysin is known to be weakly anion selective also revealed by simulation studies determining the potential gradients inside the channel [66][85]. VDAC is an anion selective channel [68][43], and OmpC is slightly cation selective [86].

The key points that interests us in previous studies on these channels are "weakly" and "slightly" which indicates a selectivity ratio of (< 1.5), *e.g.,* 1.1 for alpha-hemolysin[66], compared with the selectivity ratio of VDAC, which is ≈ 1.75 [43]. These ratios are promising to strengthen our assumption.

However, the most important factor that makes our assumption viable is in the study performed in Ref. [87]. In this study the selectivity of VDAC practically disappears when the channel is bathed in 1.0 M KCl. This is due to the screening of the charged residues inside the channel by the high ionic strength electrolyte. This holds true for other channels [84]. Using a 1.0 M KCl solution in our studies not only allows us to work around ion selectivity of the channel, but also prevents other complexities arising due to the charged surfaces of these channels.

Ion Channels are Cylindrical

Another assumption we make in this study is that ion channels are cylindrical. VDAC is known to be an almost cylindrical channel [22]. However although alpha-hemolysin is quite cylindrical in its stem region [65], it has a strong constriction at the end of this stem region. OmpC also has its own constriction region [86].

Unfortunately there is no way to work around this fact, there are studies of polymer behavior in different geometries [88]. However ion channels do not conform to a simple geometric shape. They still best resemble cylindrical pores. One of the major reasons we employed VDAC in this study is because of its almost cylindrical shape. If VDAC agrees well with our assumptions and calculations, we will know with almost

certainty that any complexities that might arise with alpha-hemolysin and OmpC is due to channel geometry.

In fact, applying the results of this work to different geometries is possible, via analytic or computational methods. To see an example of how channel geometry might affect partitioning see the study on channel geometry performed in section 6.3.

Ion Channels are in Open State *e.g.,* **they are not gating**

Perhaps one of the simplest issues to work around is channel gating. Channels might gate due to their intrinsic mechanism [42], due to potential difference across the membrane [89], pH [90][91], and osmotic effects [3].

Selecting solution conditions carefully, 1.0 M KCl, pH 7.4 in our case, and working within the Ohmic range of the channels prevents most of the gating phenomena. At high PEG concentrations, however, channel gating is observed for all three channels used in this study. In this case one needs to monitor channel behavior carefully and unfortunately discard their data that shows properties of channel gating.

PEGs are not affected by the presence of ions in solution

There are studies on PEGs in electrolyte solutions that indicate cations bind to PEGs, where these charged PEGs are probed by ion channels [12][92][59][93]. There are also NMR and simulation studies performed to verify this claim [94][95][96][97][98].

However this effect, apart from simulations and NMR studies, is only observed in electrolyte concentrations of > 2.0 M. And there is strong evidence that at 1.0 M KCl PEG-Cation binding is non-existent [92]. We discuss these observations in detail in Appendix B.

CHAPTER 5

EXPERIMENTS ON BINARY POLYMER MIXTURES

5.1 Experimental Determination of Partition Coefficients

Determining the partition coefficient of polymers ($p = \phi_i/\phi_o$) is simply determining the polymer concentration that is inside an ion channel (ϕ_i). This quantity can only be determined indirectly by measuring channel conductance in the presence of polymer, and under several assumptions. The first assumption is that an ion channel is a cylindrical pore of a given radius (R_c) and channel proper conductance (R_p) is the integral conductivity of the solution filling this pore. Thus the reduction in channel conductance mimics the reduction in conductivity of the bulk solution. However there are certain parameters that cannot be ignored when working with ion channels of nanometer size. One of these parameters is the access resistance (R_{acc}) which arises due to the convergence of electric field lines in the vicinity of the channel opening [21]. The other parameter that could affect channel conductance is the possibility of an increase in ion activity (or "effective ion concentration") inside the pore when there is a difference in polymer concentration inside and outside the channel [12].

Thus for a proper analysis of channel conductance in the presence of polymer, effects of polymer on solution conductivity and ion activities in "Polymer Free Regions of Solution" (PFS) should be studied. Apart from these effects any attempt at a quantitative description of polymer partitioning should agree with the osmotic pressure of a solution, which is the equation of state of a polymer solution. So osmotic pressures of polymer solutions should also be determined.

In the following sections we will describe our experimental methodology for studying these effects, and how all of it comes together in determining the partition coefficients of polymers.

5.1.1 Osmotic Pressure

We chose Vapor Pressure Osmometry for the measurements of Osmotic pressures of PEGs. In the planned concentration regimes of 0%(w/w) to 40%(w/w) concentration of PEGs, Vapor Pressure Osmometry gives reliable and repeatable results given the operating range of the Osmometer. Osmotic Pressures of PEGs were measured using a Wescor Vapro 5600 Vapor Pressure Osmometer (Wescor, Inc., UT, USA). Solutions contained 5%(w/w) to 30%(w/w) PEGs in increments of 5%(w/w) for monodisperse PEG solutions. Binary mixtures contained 15%(w/w) PEG3400 and PEG200 were added up to a total concentration of 40%(w/w) total PEGs. Solutions were prepared with Millipore grade deionized water. No electrolytes (*e.g.*, KCl) were used, due to the limited range of the osmometer.

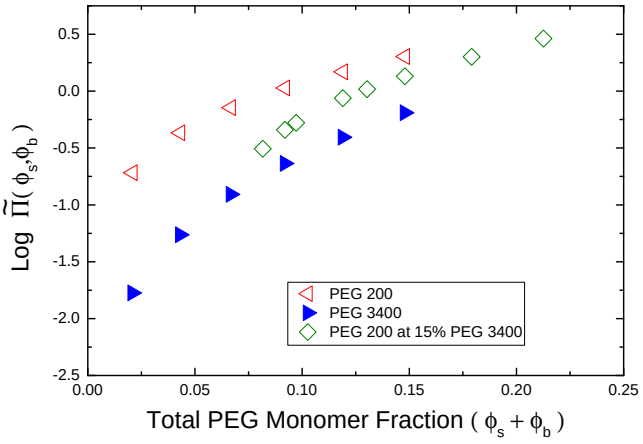

Figure 5.1: Measured Osmotic Pressures of PEG200, PEG3400 Solutions, and Their Binary Mixtures

Our results are shown in Figure 5.1. Osmotic pressures are shown in reduced units, as a function of polymer monomer fractions $\tilde{\Pi} = \frac{\bar{\nu}_w \Pi(\phi_s,\phi_b)}{kT}$, where $\bar{\nu}_w$ is the partial specific volume of water.

5.1.2 Effects of Polymer on Electrolyte Solutions

5.1.2.1 Solution Conductivity

To a first approximation in solutions containing $0.1M$ KCl, it has been observed that solution conductivity was inversely proportional to polymer concentration [12]. It was later observed in Ref [99] that polymer presence had two effects on solution conductivity. i) Polymer reduced the ion concentration in the bath by a factor $(1-\Phi)$, where Φ is the polymer volume fraction, and ii) based on self-diffusion NMR studies polymer reduced ion mobility by a factor $(e^{-k\frac{\Phi}{1-\Phi}})$, where (k) is a fitting parameter. The cumulative effect can be stated as,

$$\begin{aligned} \sigma(\Phi) &= \sigma_0(1-\Phi)e^{-k\frac{\Phi}{1-\Phi}} \quad or, \\ \sigma(c) &= \sigma_0\frac{\xi(1-c)}{c+\xi(1-c)}e^{-\frac{k}{\xi}\frac{c}{1-c}} \end{aligned} \tag{5.1}$$

Here (c) is the polymer weight fraction, and $(\xi = \frac{\bar{\nu}_w}{\bar{\nu}_{PEG}} \approx 1.13)$ is the ratio of the partial specific volume of water to that of PEG. The result of this work is summarized in Fig. 5.2.

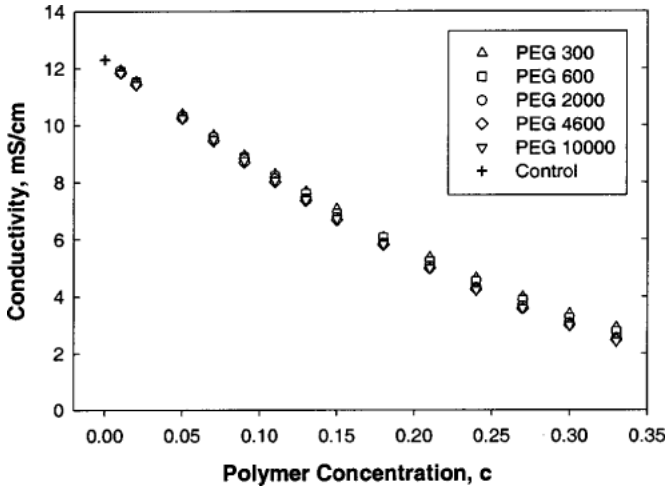

Figure 5.2: Conductivity of PEG Solutions of Different size PEGs, at 100 mM KCl[1]

It is evident from Fig. 5.2 that the effect on solution conductivity does not depend on polymer molecular weight, and only on polymer concentration (c). The experiments performed in Refs. [12, 99] were in $0.1M$ KCl solutions. We set out to test this hypothesis in $1.0M$ KCl solutions, since our experiments will be performed in $1.0M$ KCl. Performing channel conductance measurements in high salt concentrations is important for the validity of the "conducting cylindrical cuvette" assumption for ion channels. A high salt concentration screens the surface charges of ion channels, limiting possible interactions between channel walls and the conducting ions, as well as reducing the ion selectivity of the pore [87].

Fig. 5.3 sumarizes our results performed in $1.0M$ KCl solutions. Eq. 5.1 describes the data in Fig. 5.2 to a good accuracy, with fitting parameter ($k \approx 2.5 - 2.9$) for PEG molecular weights in the range $(300 - 10000)$.

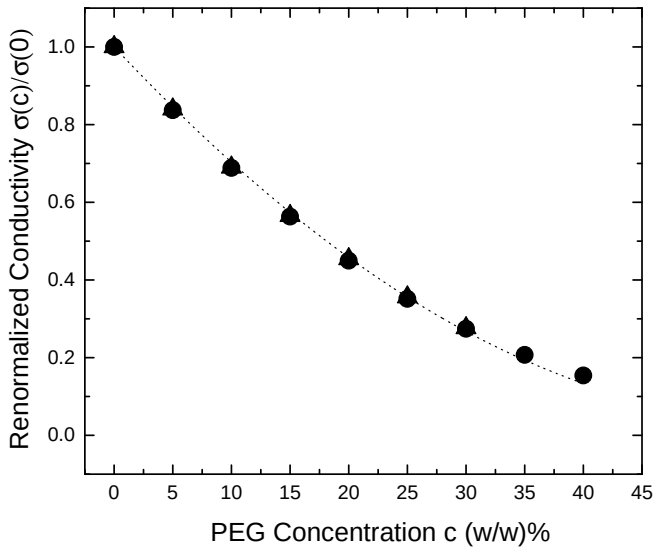

Figure 5.3: Conductivity of PEG Solutions of Different Size PEGs, at 1.0 M KCl

[1]Reprinted from Stojilkovic KS, Berezhkovskii AM, Zitserman VY, Bezrukov SM (2003) Conductivity and microviscosity of electrolyte solutions containing polyethylene glycols. J Chem Phys 119(13):69736978., with the permission of AIP Publishing

We performed experiments with PEG200, PEG3400 and their binary mixtures in $1.0M$ KCl using a Thomas Scientific 2-Cell Conductivity Probe (Thomas Scientific, NJ, USA); total PEG concentrations ranged between 0%(w/w) to 40% (w/w). As with the previous results, we observed that the polymer molecular weight had no impact on solution conductivity, and solution conductivity depended only on total polymer concentration. Our results and a fit to Eq. 5.1 are shown in Fig. 5.3. We obtained the fitting parameter $k = 2.66$.

5.1.2.2 Ion Activity in Polymer Excluded Regions

Presence of polymer in an electrolyte solution has another effect on electrolytes. It has been observed in [12], by Ion Selective Electrode (ISE) measurements and other methods (*e.g.,* ultrafiltration) that presence of polymer in an electrolyte solution increases the Ion Activity (effective ion concentration) in polymer free regions of solution (PFS). This seemingly simple observation has huge consequences on interpretation of channel conductance data, and conductance measurements.

ISEs, practically mimic channel conductance measurements with excluded polymers, since their ion selective membrane is impervious to PEGs. An immediate result of this effect is an apparent increase in channel conductance when polymers are excluded from the channel interior. This can be seen in Fig. 1.1, where PEG3400 data shows an increase in channel conductance upto 15%(w/w) polymer concentration, we also expect this factor to play an important role whenever there is a concentration difference of PEGs between the bathing solution and the pore, which has direct consequences on the interpretation and evaluation of conductance measurements.

We conducted measurements using a Thomas Scientific (K^+) ISE (Thomas Scientific, NJ, USA) in a $0.5M$ KCl solution (due to the limited range of the ISE these measurements would be unreliable if performed with $1.0M$ solutions) where PEG concentrations varied between 0%(w/w) to 40%(w/w), using PEG200, PEG3400 and

their binary mixtures. Fig. 5.4 shows a depiction of the function of ISE and our results.

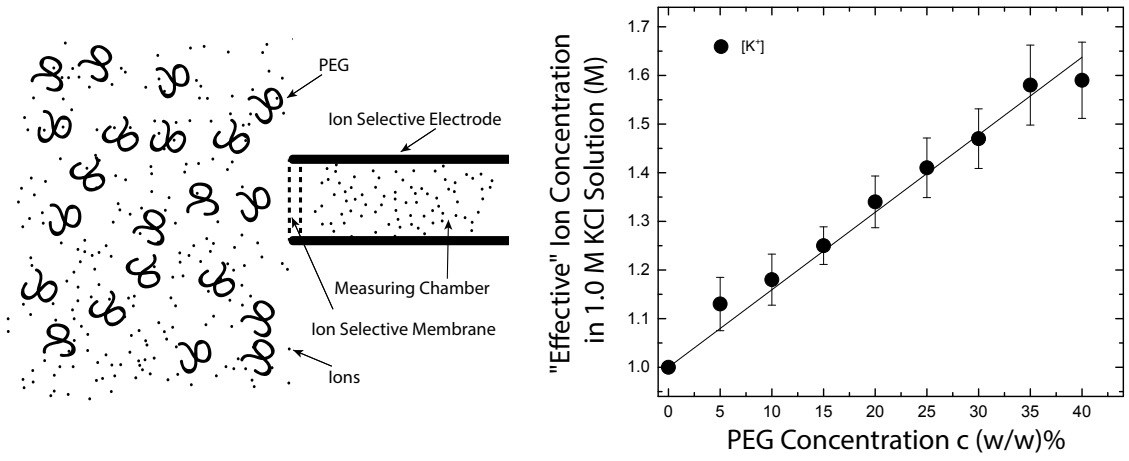

Figure 5.4: Ion Selective Electrode Function and Measurements in 0.5 M KCl with Varying PEG Concentration

We see that as polymer concentration is increased, the effective ion concentration in the measuring chamber of the electrode increases linearly with a proportionality factor β obtained from experiment. We observed that this effect does not depend on polymer molecular weight, but only to polymer concentration. The linearity of the results will allow us to describe the effective ion concentration in the pore interior as a function of the polymer concentration inside and outside the channel (c_i, c_o) as,

$$[K^+]_{eff}(c_o, c_i) = [K^+]_0(1 + \beta(c_o - c_i)). \tag{5.2}$$

Assuming that in our salt and polymer concentration regimes ($[K^+] \propto [KCl] \propto \sigma$), we can write the solution conductivity in a cavity where there is a difference in concentration of PEGs between the cavity and the bath as,

$$\sigma(c_o, c_i) = \sigma_0(1 + \beta(c_o - c_i))\frac{\xi(1 - c_i)}{c_i + \xi(1 - c_i)} e^{-\frac{k}{\xi}\frac{c_i}{1-c_i}}. \tag{5.3}$$

These preliminary investigations will allow us to infer the polymer concentration inside the channel properly, along with assisting us in determining the channel access resistance, and determination of channel radii. These calculations will be discussed in section 5.1.3.

5.1.3 Single Channel Conductance

5.1.3.1 Experimental Setup

The single-channel recording apparatus consists of a two-compartment (cis and trans) Teflon chamber ($\approx$ 3 ml each) separated by a 15 μ Teflon partition with about a 100 μm diameter aperture for membrane formation. Bathing solutions are added to both sides of the chamber. Channel current traces are recorded with Ag/AgCl electrodes in agarose bridges containing 2.0 M KCl, the *cis* side of the chamber being the virtual ground, using the Axopatch 200B (Molecular Devices, LLC., CA, USA) patch clamp amplifier in V-Clamp mode (Whole Cell $\beta = 1$) with a CV-203BU Headstage. A diagram of the recording apparatus is shown in Fig 5.5.

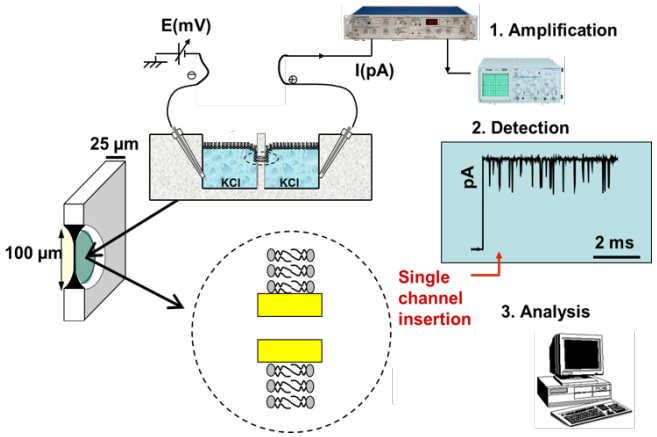

Figure 5.5: Single Channel Recording System

Channel reconstitution is achieved by adding VDAC, Alpha-Hemolysin, or OmpC to the *cis* side of the chamber in the bathing solutions at $\approx$ 1 pM concentrations from their stock solutions. Solutions are stirred until single channel reconstitution is

observed. Ion channels reconstitute in the artificial bilayer formed from DPhPC using the lipid monolayer opposition technique [100], adding $10\mu l$ of $1mg/ml$ of DPhPC in pentane (pentane is added after chloroform is fully evaporated under high purity nitrogen gas) to *cis* and *trans* sides of the chamber with the 100 μm aperture treated with 10% (v/v) hexadecane in pentane. The total capacitance after stable bilayer formation should be $\approx 90pF$.

Alpha-Hemolysin from *Staphylococcus aureus*, poly(ehtylene glycol)s PEGs of average molecular weights PEG200, PEG3400, and anhydrous pentane and hexadecane were purchased from Sigma Aldrich Chemicol Co., Inc., Milwaukee, WI. Diphytanoylphosphatidylcholine (DPhPC) 10 mg/ml in chloroform was purchased from Avanti Polar Lipids (Alabaster, AL). VDAC was isolated from frozen mitochondrial fractions of rat liver that were a generous gift of Dr. Marco Colombini (University of Maryland, College Park, USA) and purified following the standard methods [70]. OmpC was purified from *E. coli* strain AW741, a generous gift of Dr. Ann Delcour (University of Houston, Houston, USA). Cells were grown overnight in LB broth. The cells were harvested by centrifugation, resuspended in 50 mM sodium phosphate buffer, 0.1 M NaCl, 2 mM EDTA, 5% (w/v) sucrose and broken by a French press (two times, 10 MPa). Cell debris was prespun to remove non-broken cells (6000 g, 10 min) and spun down on the ultracentruifuge (100,000 g, 40 min). OmpC was extracted from the membrane fraction (pellet) by octyl-POE detergent with ultracentrifugation at 100,000 g in the buffer containing 20 mM sodium phosphate buffer and 3% octyl-POE(pH 7). Buffer solutions were prepared with 18.2 MΩ*cm Millipore grade water.

5.1.3.2 Data Collection

A single Alpha-Hemolysin, OmpC and VDAC channel conductance is measured in the absence and presence of PEGs. Experiments are performed accross the mem-

brane potential limits where channels show an ohmic response. If a second channel reconstitution is observed, or the primary channel is lost during a set of measurements the experiment is terminated.

With Alpha-Hemolysin and OmpC, channel conductances are measured in the range of -120 mV to 120 mV in steps of $\Delta V = 20$ mV and/or $\Delta V = 5$ mV. The minimum membrane potential is ± 20 mV for Alpha-Hemolysin and ± 5 mV for OmpC. Three to six single channel events were recorded at PEG concentrations of 0% to 30% for each channel. With VDAC, channel conductances are measured in the range of -40 mV to $+40$ mV in steps of $\Delta V = 2.5$ mV, minimum membrane potential being ± 2.5 mV. An entire range of PEG concentrations of a single molecular weight, from 0% to 40% (w/w) was scanned using a single reconstituted channel. Experiments are repeated for three to six single channel reconstitutions for each PEG type. Bathing solutions are collected for conductivity measurements.

Stock electrolyte solution contained 1.0 M KCl and 10 mM HEPES at pH 7.4 adjusted with 8.0N KOH. Bathing solutions containing 0% (w/w) up to 40% (w/w) PEGs were either made by adding PEGs directly to the stock electrolyte solution (for Alpha-Hemolysin and OmpC experiments) or by adding incremental amounts of PEG stock solutions (100% PEG200, 50%(w/w) PEG3400, 15%(w/w) PEG3400 and 50% PEG200) to the bathing solution containing 1.0 M KCl (for VDAC Experiments). The difference in this methodology is due to channel stability, VDAC is a very stable channel and a single channel can be maintained in the membrane for over 2 hours, however Alpha-Hemolysin and OmpC are more prone to form a secondary channel during extended time periods (≈ 30 mins).

Fig 5.6 shows two sample I-V scans peformed on VDAC, and their overlay. It is clearly seen that within the applied voltage range VDAC has an ohmic and a symmetric response. Addition of 30% (w/w) PEG reduces the conductance of the channel by $\approx$ 50%. I-V curves for all three channels obtained in this manner at

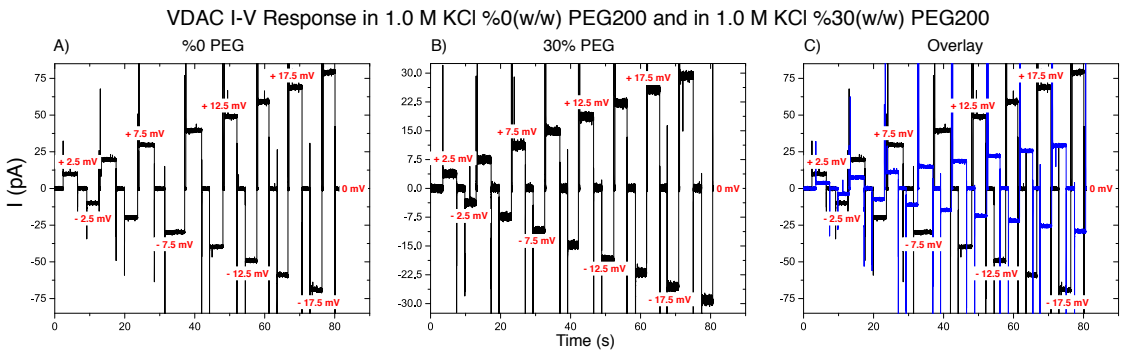

Figure 5.6: VDAC I-V Response Measurements Performed with 0%(w/w) and 30%(w/w) PEG200 in 1.0 M KCl up to 17.5mV Membrane Potential

different PEG concentrations allows us to calculate the conductance of the channels as a function of PEG concentration.

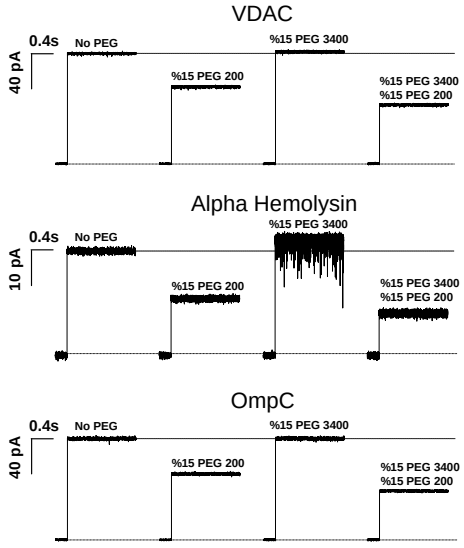

Figure 5.7: I-V Traces of Alpha-Hemolysin, VDAC and OmpC Showing the Effect of Different Size PEGs on Channel Conductance, and "Forced" Partitioning of PEG 200

Fig. 5.7 shows the effect of different polymers and binary mixtures on channels. Traces labeled "No PEG" show the current jump right after spontaneous channel formation in membrane. Addition of 15% (w/w) PEG200 causes a significant drop in single channel conductance (VDAC, 30%; Alpha-Hemolysin, 45%; OmpC, 35%).

Addition of 15% (w/w) PEG 3400, which does not penetrate the channel at this concentration, causes an apparent increase in single channel conductance (VDAC, 2%; Alpha-Hemolysin, 10%; OmpC, 2%), this effect is discussed in detail in section 5.1.3.3. Addition of 15% (w/w) PEG200 along with 15% (w/w) of PEG3400 drops the channel conductance by an extra 15% compared with the presence of only 15% (w/w) of PEG200. This extra drop is caused by additional PEG200 partitioning into the pore, being "pushed" by the PEG3400 molecules in the bathing solution. Current jumps after PEG addition correspond to the moments of trans-membrane voltage application (30 mV).

5.1.3.3 Analysis

Measured Channel Conductance After the I-V curves are determined obtaining the channel conductance is straightforward. One makes use of the I-V curves and the ohmic response to obtain channel conductance as ($G = I/V$), or one constructs G-V curves from the obtained data and extrapolates it to 0 mV. It should be noted that application of potential might impact the equilibrium partitioning of polymer [5]. Therefore data obtained at lower applied potentials are given more weight.

Fig. 5.8 shows the I-V and G-V curves for Alpha-Hemolysin in the presence of PEGs. Both approaches yield similar results, however it should be noted that G-V curves are unreliable at small applied membrane potentials ($V_{mem} < 10mV$) and I-V curves shows a deviation from the ideal ohmic behaviour at large applied membrane potentials $V_{mem} > 60mV$ therefore it is best to see both responses.

Access Resistance In reality, the measured channel conductance is the total of the channel proper conductance and the channel access resistance. Access resistence (R_{acc}), as mentioned before, arises due to the convergence of electric field lines in the vicinity of the channel opening as demonstrated in Fig 5.9.

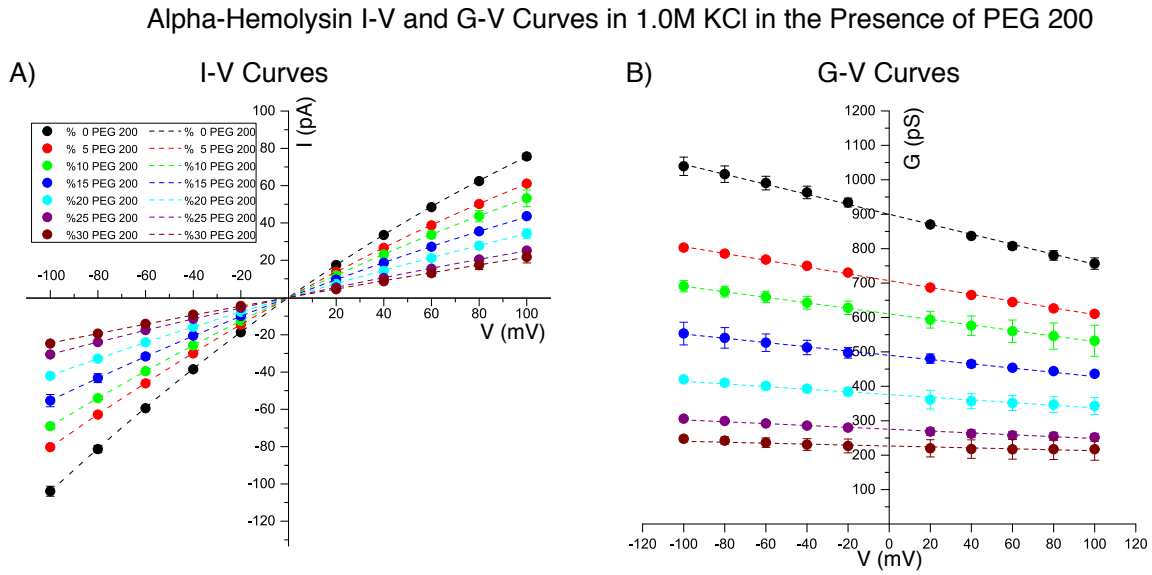

Figure 5.8: I-V and G-V Curves of Alpha-Hemolysin in the Presence PEG 200 in 1.0 M KCl

The problem of access resistance can be solved by a neat analogy of a current (I_a) passing through a disk of radius (R_c) to the capacitance C_a of a conducting disk of the same radius under the same potential difference (V_a) [101, 102], figured out in Ref. [21] in terms of the channel radius and bulk solution conductivity (σ) as,

$$R_{acc} = \frac{1}{4R_c\sigma} \tag{5.4}$$

More complicated forms of access resistance have been shown to be irrelevant at our electrolyte concentration regimes [103].

Determining Channel Proper Conductance The presence of access resistance complicates the problem by bringing in the channel radius (R_c) as an unknown parameter. However both the channel proper conductance and the channel radii can be calculated from our experiments [28]. The fact that the large polymer (PEG3400) is excluded from the channel interior up to a certain concentration (15% (w/w)) is useful in that regard. Access resistance may vary due to asymmetrical channel radii

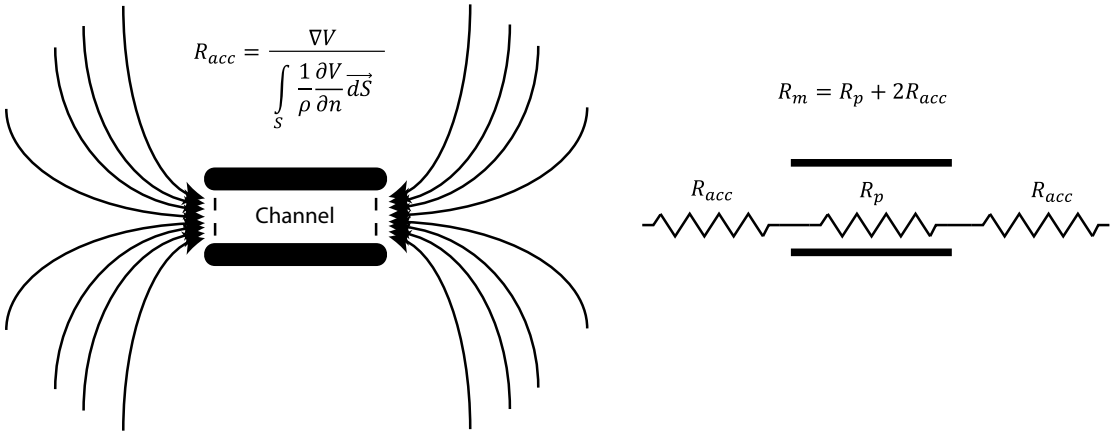

Figure 5.9: Access Resistance of an Ion Channel

at both ends of the pore. For simplicity, we take channel radii to be the same and write the total channel resistance when no polymer is present as,

$$\frac{1}{G_m(0)} = \frac{1}{G_p(0)} + \frac{1}{2\sigma(0)R_c}, \tag{5.5}$$

where G_m is the measured conductance, G_p is the channel proper conductance, and R_c is the channel radius.

Polymer addition to the bathing solution is going to affect both the channel access resistance and the conductance of the channel proper. To determine the amount of polymer partitioned into the channel, we need to obtain estimates for the channel radius in order to calculate the channel proper conductance. Using large non-partitioning polymer (PEG3400) is helpful in this respect. Up to the concentration of 15% (w/w) PEG3400 is excluded from the channel interior. In these regimes, we expect the solution conductivity to decrease according to Eq. 5.1 and the channel proper conductance to increase according to Eq. 5.2 when we take the polymer concentration inside the channel as $c_i = 0$. In this way, we arrive at

$$\frac{1}{G_m(c_o)} = \frac{1}{(1+\beta c_o)G_p(0)} + \frac{1}{2\sigma(c_o)R_c}. \tag{5.6}$$

Using Eqs. 5.5 and 5.6, eliminating $G_p(0)$, and rearranging the remainder, we derive the following form of the measured channel conductance at a given polymer concentration with β and R_c as fitting parameters

$$G_m(c_o) = \left(\frac{2\sigma(0)R_c - G_m(0)}{(1+\beta c_o)G_m(0)(2\sigma(0)R_c)} + \frac{1}{2\sigma(c_o)R_c} \right)^{-1}. \tag{5.7}$$

Using the same formulation the behavior of equi-partitioning polymers (that is partition coefficient $p(c) = 1$) can also be obtained as,

$$G_m(c_o) = G_m(0)\frac{\sigma(c_o)}{\sigma(0)}. \tag{5.8}$$

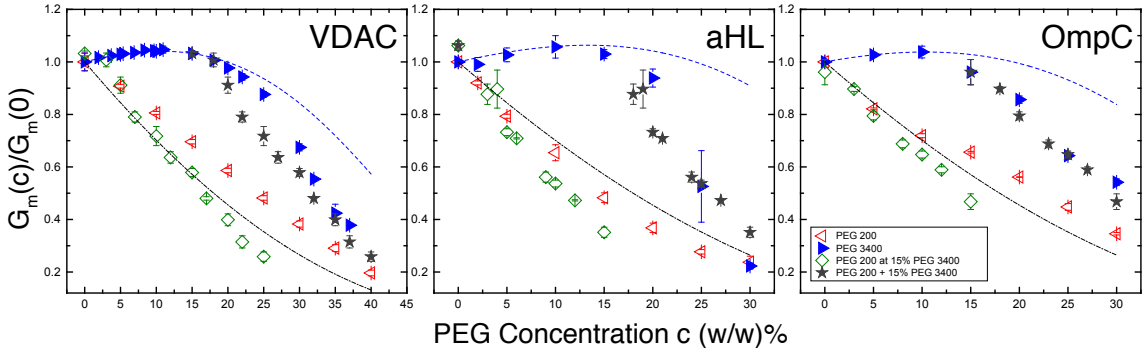

Figure 5.10: Renormalized Measured Channel Conductance of VDAC, Alpha-Hemolysin and OmpC

Fig. 5.10 shows the renormalized measured conductance of the channels ($G_m(c)/G_m(0)$) in the presence of PEGs, obtained as described at the beginning of this section. Blue dashed lines are a fit to Eq. 5.7 in the range 0% to 15% (w/w), Black dot-dashed lines show the expected channel conductance for equipartitioning polymers in accordance with Eq. 5.8. All channels show an increase in their measured conductance when PEG3400 concentrations are at or below 15% (w/w). All channels show an increased partitioning of PEG200 when 15% (w/w) PEG3400 is present in the bathing solution. The results of the fits to Eq. 5.7 are summarized in Table 5.1, showing the total resistance of the channel, access resistance of the channel and the proper resistance

of the channel ($R_t = R_p + 2R_{acc}$), as well as the β parameter obtained from these fits and the effective channel radius R_c.

Table 5.1: Derived Parameters

Channel	R_cÅ†	$R_t(M\Omega)^\ddagger$	$R_p(M\Omega)$	$R_{acc}(M\Omega)$	β^*
VDAC	11.1 ± 0.1	248 ± 6	208 ± 6	39.6 ± 0.3	1.46 ± 0.01
aHL	3.1 ± 0.13	1113 ± 11	966 ± 5	147 ± 6	1.48 ± 0.06
OmpC	7.9 ± 0.02	352 ± 2	296 ± 2	56.2 ± 0.2	1.42 ± 0.05

† Effective radius of the channel obtained from access resistance considerations by fitting PEG3400 data to Eq. 5.7.

‡ R_t, R_p, R_{acc} are the total, proper, and access resistances of the channels.

* Parameter defining the effective increase in electrolyte concentration. Obtained by fitting PEG3400 data to Eq. 5.7.

Determining Partition Coefficients Once the channel radius (R_c) is obtained, the access resistance can be taken out of our equations. The other parameter β which describes the effective increase in ion concentration inside the channel is found to be within 10% of our values obtained from our ISE measurements. Once the channel proper conductance is determined ($G_p(0)$), then the channel conductance can be written in terms of the polymer concentration outside and inside the channel as,

$$G_p(c_o)/G_p(0) = (1 + \beta(c_o - c_i))\sigma(c_i)/\sigma(0). \tag{5.9}$$

Then this equation can be solved numerically to determine c_i and c_o. Then converting these values to monomer fractions, it is trivial to determine the partition coefficient ($p = \phi_i/\phi_o$). Fig. 5.11 shows our results for the partition coefficients of polymers obtained in this manner. In the following section (Section 5.2), we test the

theories of partitioning we have discussed in Section 3.3, and how they compare with this data.

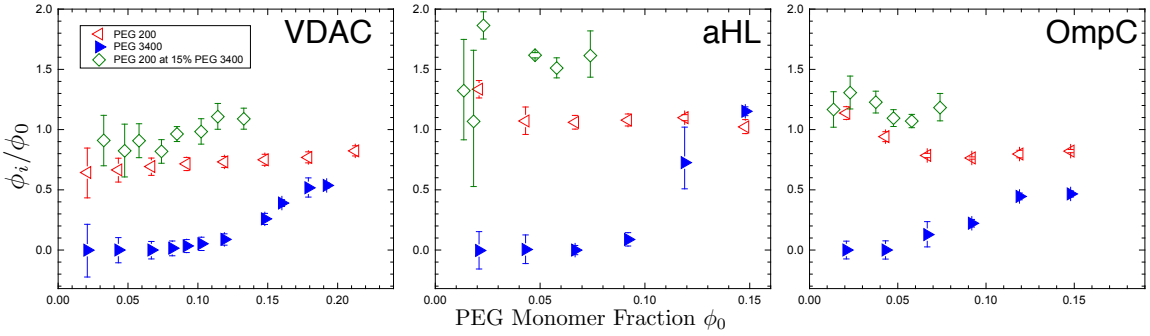

Figure 5.11: Partition Coefficients of Polymers for VDAC, Alpha-Hemolysin and OmpC

5.2 Testing Theories of Partitioning

In this section, we are going to test the theories of partitioning we have discussed in Section 3.3, and how they compare with our experimental results as outlined in Chapter 5. We are going to see that the Polymers Pushing Polymers approach successfully describes our data, with minor modifications to this theory. However, before comparing our results with the Polymers Pushing Polymers model we are going to introduce another way of determining partition coefficients (Section 5.2.1), an approach used in Ref. [5] as mentioned in section 1.2.

5.2.1 Other Approaches

Determining Partition Coefficients using a Solution Non-Ideality Term

This approach has been used in Ref. [5] as mentioned in section 1.2. Their argument is based on the fact that the Van't Hoff Osmotic Pressure $\Pi_{VH} = kTc$ only works in dilute (ideal) solutions and in solutions where $c > c^*$ (where c^* is the polymer overlap concentration) the osmotic pressure assumes the desCloizeaux form

$$\Pi_{dC} = \alpha kT \left(\frac{c}{c^*}\right)^{9/4} \tag{5.10}$$

where α is a numerical coefficient.

The assumption is that the chemical potential of a dilute polymer solution $\mu = \mu_0 + kTln(c)$ is altered by a nonideality term $kTI(c)$ to obtain

$$\mu = \mu_0 + kTln(c) + kTI(c). \tag{5.11}$$

The non-ideality term is calculated from the osmotic pressure as follows

$$\begin{aligned} \mu &= \mu_0 + kTln(c) + kTI(c) \\ d\mu(c) &= \frac{kT}{c}dc + kT\frac{dI(c)}{dc}dc \end{aligned}$$

Making use of the Gibbs-Duhem Relation and that $Np = cV$

$$\begin{aligned} N_p d\mu(c) &= V\frac{d\Pi(c)}{dc}dc \\ \frac{dI(c)}{dc}dc &= \frac{(d\Pi(c)/dc) - kT}{ckT}dc \\ P(c) &= (\Pi(c)/ckT) \\ \frac{d\Pi(c)/dc}{ckT} &= \frac{dP(c)}{dc} + \frac{P(c)}{c} \\ \frac{dI(c)}{dc}dc &= \frac{d(P)}{dc}dc + \frac{P(c)-1}{c}dc \\ \int_0^{c_b}\frac{dI(c)}{dc}dc &= \int_0^{c_b}\frac{dP(c)}{dc}dc + \frac{P(c)-1}{c}dc \\ I(c_b) &= P(c_b) - P(0) + \int_0^{c_b}\frac{P(c)-1}{c}dc \end{aligned}$$

Finally $P(0) = 1$, so one finds $I(c_b)$ at the polymer concentration c_b as,

$$I(c_b) = P(c_b) - 1 + \int_0^{c_b} \frac{P(c) - 1}{c} dc. \tag{5.12}$$

Then setting the polymer chemical potentials inside and outside the pore equal they obtain for the partition coefficient,

$$ln(p) + \frac{\Delta F}{kT} = \frac{9}{5}\alpha kT(\frac{\phi}{\phi^*})^{5/4}(1 - p^{5/4}). \tag{5.13}$$

As mentioned in section 1.2 this equation does not sufficiently describe the partitioning of PEG3400, however this equation is modified with the argument that the overlap concentrations of polymer in the pore and in the bulk are different [88, 24], that is using conventional arguments $\Phi_b^* \propto N^{-4/5}$ and $\Phi_p^* \propto (b/R_c)^{4/3}$. Here Φ_b^* and Φ_p^* are the overlap concentrations of the polymer in the bulk and in the channel respectively. When this assumption is taken into account this equation is modified as,

$$ln(p) + \Delta f = N_s \left(\frac{9}{5}\tilde{\alpha}(1 - \frac{\gamma}{\Delta f} p^{5/4})\phi_s^{5/4} \right) \tag{5.14}$$

5.2.2 Polymers Pushing Polymers Framework

Osmotic Pressures We introduced the partition coefficients obtained from the Polymers Pushing Polymers framework in Section 3.3. The first task at hand is to see if the osmotic pressure measurements agree with the predicted osmotic pressure from theory. In Section 3.3 we obtained for the osmotic pressure of a binary mixture Eq. 3.8,

$$\begin{aligned} \frac{\bar{\nu}_w \Pi(\phi_s, \phi_b)}{kT} &= \ln(1 - \phi_s - \phi_b) + (1 - \phi_s - \phi_b) - 1 + \frac{\phi_s}{N_s} + \frac{\phi_b}{N_b} \\ &\quad -\frac{1}{2}(\phi_s + \phi_b)^2 + \frac{5}{4}\tilde{\alpha}(\phi_s + \phi_b)^{9/4}. \end{aligned} \tag{5.15}$$

Now, we need to fit Eq. 5.15 to our osmotic pressure data using $\tilde{\alpha}$ and N as free parameters. We first fit this equation to PEG200 and PEG3400 data to obtain an $\tilde{\alpha}$ parameter and determine N_s and N_b separately, where N_s and N_b are the polymerization numbers of the PEG200 and PEG3400 respectively. Then we use these values to numerically fit Eq. 5.15 to the binary mixture data. The fits are shown on Figure 5.12, where $\tilde{\Pi(\phi_s}, \phi_b) = \frac{\bar{\nu}_w \Pi(\phi_s,\phi_b)}{kT}$.

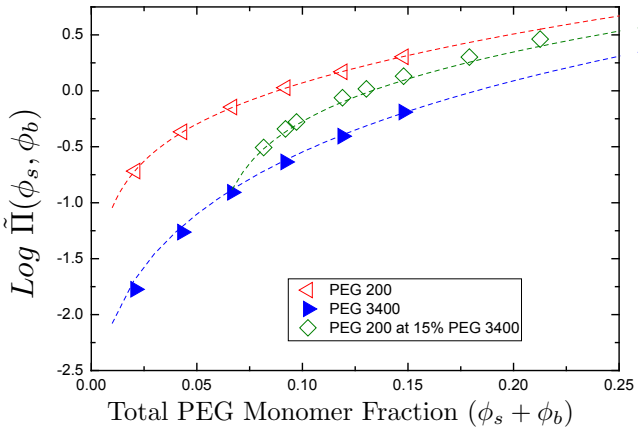

Figure 5.12: Osmotic Pressures of PEGs

The fits yield $\tilde{\alpha}_{PEG200} = 0.67$, $\tilde{\alpha}_{PEG3400} = 0.49$ and $N_{PEG200} = 6.2$, $N_{PEG3400} = 76$. We observe weak dependence of $\tilde{\alpha}$ on Ns, as noted in Ref. [104], with shorter chains in general having a higher $\tilde{\alpha}$. The difference between $\tilde{\alpha}_{PEG200}$ and $\tilde{\alpha}_{PEG3400}$ is much smaller than predicted from the finite-size effects in renormalization group theory [104]. The degrees of polymerization of PEG200 and PEG3400 obtained from the fits are excellent, $N \approx M_w^p/m_w^m$ where M_w^p and m_w^m are mass of the polymer and mass of a PEG monomer respectively we have for PEG200 $N_s \approx 4.5$ and $N_b \approx 76.5$.

Partition Coefficients Since the osmotic pressure of the binary polymer mixture is an equation of state describing the system accurately, we would expect the theory to give an accurate description of partition coefficients. First of all let us return to the equation obtained for the partition coefficients of a binary mixture Eq. 3.12,

$$ln(p)+\Delta F = N_s\bigg(ln(1-p\phi_s)-ln(1-\phi_s-\phi_b)+(p\phi_s-\phi_s-\phi_b)+\frac{9}{4}\tilde{\alpha}((\phi_s+\phi_b)^{5/4}-(p\phi_s)^{5/4})\bigg), \tag{5.16}$$

For a single type of polymer this equation reduces to,

$$ln(p)+\Delta F = N_s\bigg(\frac{ln(1-p\phi_s)}{(1-\phi_s)}+(p-1)\phi_s+\frac{9}{4}\tilde{\alpha}((\phi_s+\phi_b)^{5/4}-(p\phi_s)^{5/4})\bigg), \tag{5.17}$$

Note that the only free parameter in this equation is the free energy penalty of partitioning (the free energy of confinement). We need to fit Eq. 5.17 to our PEG200 and PEG3400 data and obtain the free energies of confinement ΔF, and then, assuming that PEG3400 does not partition into the channel in the binary mixture (see Chapter 6), we need to fit the binary mixture data to Eq. 5.16. However, we have seen that PEG3400 partitions more sharply than Eq. 5.17 predicts. We make use of two additional approaches to describe the PEG3400 partitioning:

(i) assuming that ΔF has the usual scaling form $\Delta F_c \propto (R_g/R_c)^{5/3}$ (see Section 2.4), where R_g is the radius of gyration of the polymer and R_c is the radius of the pore, we surmise that the free energy of confinement decreases with bulk polymer concentration due to a decrease in the radius of gyration of the polymer $R_g/R_{g_0} = (\Phi_s/\Phi^*)^{-1/8}$ [31]. Thus we can express the free energy penalty as $\Delta F = (\Phi_s/\Phi^*)^{(-5/24)}\Delta F_c$, where Φ^* is the polymer overlap concentration that depends on polymer monomer number N as $\Phi^* \sim N^{-4/5}$. Using the free energy penalty of this form, we are then able to successfully fit Eq. 5.17 to PEG3400 data for VDAC and OmpC.

(ii) assuming the partitioning model suggested in Section 5.2.1 we assume that the polymer overlap concentration is different in the bulk solution and in the pore. Using the equation already obtained (Eq. 5.14),

$$ln(p) + \Delta F = N_s \left(\frac{9}{5} \tilde{\alpha} (1 - \frac{\gamma}{\Delta f} p^{5/4}) \phi_s^{5/4} \right) \tag{5.18}$$

note that this equation is a limiting case of Eq. 5.17 with $\phi_s << 1$,

$$ln(p) + \Delta f = N_s \left(\tfrac{9}{4} \tilde{\alpha} (1 - p^{5/4}) \phi_s^{5/4} \right), \tag{5.19}$$

Here $\gamma/\Delta f$ is a term that arises due to the difference in overlap concentrations. γ is independent of N_s and ϕ_s. Using this form of the partition coefficient, we are then able to successfully fit Eq. (5.14) to the PEG3400 results for aHL.

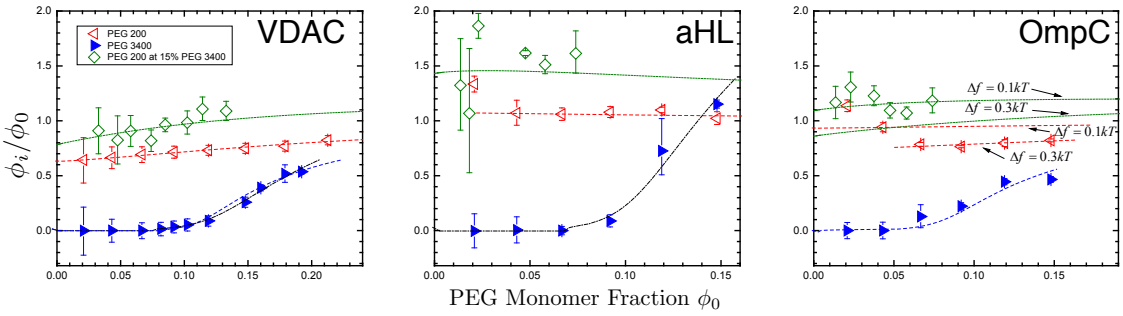

Figure 5.13: Partition Coefficients of Polymers for VDAC, Alpha-Hemolysin and OmpC

Figure 5.13 shows the partitioning coefficients calculated for different PEGs in 1.0 M KCl for VDAC, aHL, and OmpC, and fits to these data. PEG200 data are fit to Eq. 5.17, PEG3400 data are fit to Eq. 5.18 (dot-dashed line) and the modified Eq. 5.17 (dashed line) as discussed in the text, with ΔF_c as the only free parameter. The fitted values are listed in Table 5.2 and discussed in the text. Fitting to PEG mixture data (short-dashed line) was numerically calculated using Eq. 5.16 with the ΔF_c parameter obtained from the PEG200 fit.

Table 5.2: Free Energies of Confinement ΔF_c in units of kT

Polymer	VDAC	aHL	OmpC
PEG 200	0.46	-0.1	$0.1, 0.3$
PEG 3400†	12.2	-	8.5
PEG 3400‡	8.0	8.3	-

† Obtained from fitting to Eq. 5.17 as described in Fig. 5.13.

‡ Obtained from fitting to Eq. 5.18 as described in Fig. 5.13.

The ΔF_c values, Table 5.2, clearly show a marked difference between PEG200 and PEG3400, irrespective of the details of the two models. The value of ΔF_c for PEG3400 is significantly larger than PEG200. For VDAC both fits are meaningful and lead to $\sim$ 1.5 difference in the estimated value of ΔF_c. For alpha-hemolysin acceptable fits can only be obtained if one assumes the validity of model (ii), while OmpC data correspond to model (i). Of the three channels, OmpC has the most unusual behavior for partitioning profile that could be attributed to the trimeric pore structure and complexities it creates with access resistance [83].

5.2.3 Discussion of Results

In order to quantify the partitioning of PEGs into the channels, we first investigated polymer effects on electrolyte solutions. It is found that their presence both decreases solution conductivity and increases the effective ion concentration in PEG free regions, consistent with previous studies [99][26][12]. In the relevant regime of salt concentrations ($\leq$ 1 M) we do not observe any neutral vs. polyelectrolyte behavior of PEG (see Appendix B). Combining solution conductivity with the channel conductance measured in the presence of PEG3400, we estimated the mean channel radii from access resistance, Table 5.1. Structural analysis and previous estimates of channel dimensions [65][80][23] compare favorably with our findings. For VDAC the

calculated effective radius of 11Å is comparable with the radius of 16Å [23]. For the OmpC channel, the estimated effective radius is 7.9Å vs. the previously estimated ≈ 10.8Å [80]. Lastly, the effective radius of aHL of 3.1Å is comparable with the radius of the constriction, but is much smaller than the radii of the channel entrances [65].

Estimating the channel access resistance was necessary for the determination of channel proper conductance, which was used to obtain the partition coefficients. We then compared these partition coefficients with different theories of partitioning [25, 24]. Specifically, we found that the pore penetration by a single type of polymer, either PEG200 or PEG3400, is described accurately by the theory presented in Ref. [25], especially for VDAC. It yields Δf_0 values that are at least an order of magnitude larger for the bigger PEG ($\sim 8-12$kT) compared with the smaller (~ 0.5kT). Assuming a PEG monomer size $a \approx 3.5-7.2$Å [20], the energies of confinement are in agreement with the scaling argument ($\Delta F_c/kT = N(a/R)^{5/3}$) (see Section 2.4). Furthermore, if one estimates the concentration at which PEG3400 partitions into the channel by using the blob size argument [105] and that the blob size is described by $d_b = R_{g_0}(\rho/\rho^*)^{-3/4}$ (Eq. 2.29), where ρ is the polymer monomer density, we find that for the PEG3400 to reach the blob size of 22Å the polymer concentration in terms of polymer weight fraction c should reach $\approx 12\%$ (w/w). This is exactly when we start to see PEG3400 partition into VDAC.

The situation with aHL and OmpC is in this respect different. Because of the several implicit assumptions, deviations from the theoretical predictions are expected. Indeed, both approaches [24, 25] imply that (i) channel pores are circular cylinders of a constant radius, (ii) the cylinder lengths are much larger than their radii, (iii) the entropic interactions considered above are the only interactions between the polymer and the channel. From the available structural data [23, 65, 80], it follows that assumptions (i) and (ii) could be too strong and may result in oversimplification. In what concerns assumption (iii), it is known that, at least in the case of aHL, there

are significant pore-PEG attractive interactions that depend on polymer size and salt concentration [106].

Nevertheless, it appears that the Polymers Pushing Polymers hypothesis agrees with the polymer partitioning data presented and polymers that cannot penetrate nanosize pores act as agents pushing the penetrating polymers into the pore to an excess of their bath concentration. VDAC fits best the assumptions of the PPP theory, the situation is less clear-cut for aHL and OmpC. In the latter cases, one needs to invoke additional assumptions that allow for the variation of the pore penetration energy penalty with polymer concentration. We hope that these findings will lead to more refined theories that take into account structural details of the particular channels.

CHAPTER 6

NOISE ANALYSIS

As mentioned in section 5.2 we are able to successfully describe our polymer partitioning data with the approaches mentioned in the previous section. However single channel recording can also be used to provide information on dynamic properties of polymer partitioning as well as providing additional information on equilibrium partitioning. The method that provides this information is the power spectrum analysis of the signals. In this section we are going to introduce the method of power spectrum analysis. Noise analysis reveals information about conformational dynamics, blocker binding to ion channels, residue ionization of ion channels and neutral solute transport [107]. In Section 6.1.1 we are going to demonstrate what noise analysis could tell us about equilibrium partitioning, in Section 6.1.2 we are going to show how noise analysis can be employed to figure out the rates of partitioning. This type of noise analysis is used in analysis of blocker binding (*e.g,* binding of sugars to maltoporin channels)[108], residue ionization of ion channels [109, 90], and in investigations of PEG-Cation binding [92]. Studies on PEG-Cation binding are discussed in Appendix B.

But most importantly we are going to employ noise analysis to confirm one of the assumptions we have made on our study of equilibrium partitioning of polymers. As discussed in Section 3.3, one of the main assumptions of the Polymers-Pushing-Polymers framework that was used for the analysis of the forced PEG partitioning into nanopores [110] was that it was predominantly the smaller polymer, namely, PEG200 that fills the pore. In Section 6.2 we are going to demonstrate our results

on noise analysis of binary polymer mixtures partitioning into an Alpha-Hemolysin pore, and confirm that in a binary polymer mixture it is indeed the small polymer (PEG200) that predominantly partitions into the ion channel.

6.1 Noise Analysis

6.1.1 Equilibrium Properties

Apart from looking at the I-V and G-V curves of an ion channel under a potential difference V_m, there is another way to determine channel conductance, by making use of the Nyquist Fluctuation-Dissipation Theorem [111]. This theorem relates the system impedance to equilibrium current fluctuations.

$$S_I(f) = 4kTRe(1/Z(f)) \tag{6.1}$$

since channel impedance is dominated by channel conductance $1/Z(f) \propto G_m$ when the applied potential is $V_m = 0$ we can find the channel conductance by the power spectrum at $f = 0$

$$G_m(0) = S_I(0)/4kT \tag{6.2}$$

Fig. 6.1 shows this analysis performed on Alpha-Hemolysin with PEG2000 when 13 channels were present in the membrane in Ref. [5], and our analysis with a single channel present with PEG200. The downside of using this method is that power spectrum reveals more information when there are multiple channels present and that our setup has more low frequency interference from the environment.

6.1.2 Dynamic Properties

The power spectrum of the noise can be used to investigate blocker binding to ion channels (namely polymer in and out rates k_{on}, k_{off}), and residue ionization of ion channels. This information is obtainable when complete channel blockages are

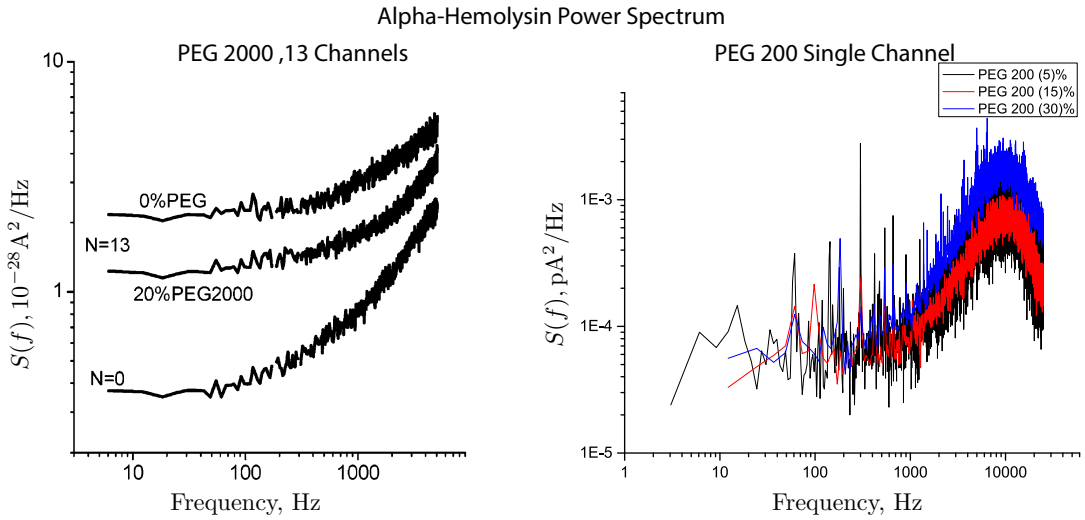

Figure 6.1: Power Spectral Analysis of Alpha-Hemolysin at $V_m = 0$, with PEG 2000 and PEG 200

observed, and is extremely useful. Alpha-Hemolysin is a useful channel in that regard, having a constriction zone of about 3Å [65] complete blockages are observed when large polymers are utilized, as apparent in 5.7.

Polymer in and out rates can be expressed as a two-state independent markov process, where "on" and "off" states are two independent events with decay lengths τ_{on}, τ_{off}.

$$P(t)_{on\to off} = e^{t/\tau_{on}}$$

$$P(t)_{off\to on} = e^{t/\tau_{off}}$$

The relation of such a process to its power spectrum is worked out for noise in semiconductors in Ref. [112]. The power spectrum of such a process is Lorentzian

$$S(f) = \frac{S(0)}{1 + (f/f_c)^2} \tag{6.3}$$

Here f_c is $f_c = \left(\frac{\tau_{on}\tau_{off}}{\tau_{on}+\tau_{off}}\right)^{-1}$ is the cut-off frequency of the Lorentzian spectrum. The two lifetimes can be obtained by determining the cut-off frequency of the signal

f_c, and obtaining the channel open probability P_{open} from the signal. Channel open probability is calculated by measuring ratio of the total time the channel is open (higher conductance state) to the total time the channel spends in blocked states (lower conductance state).

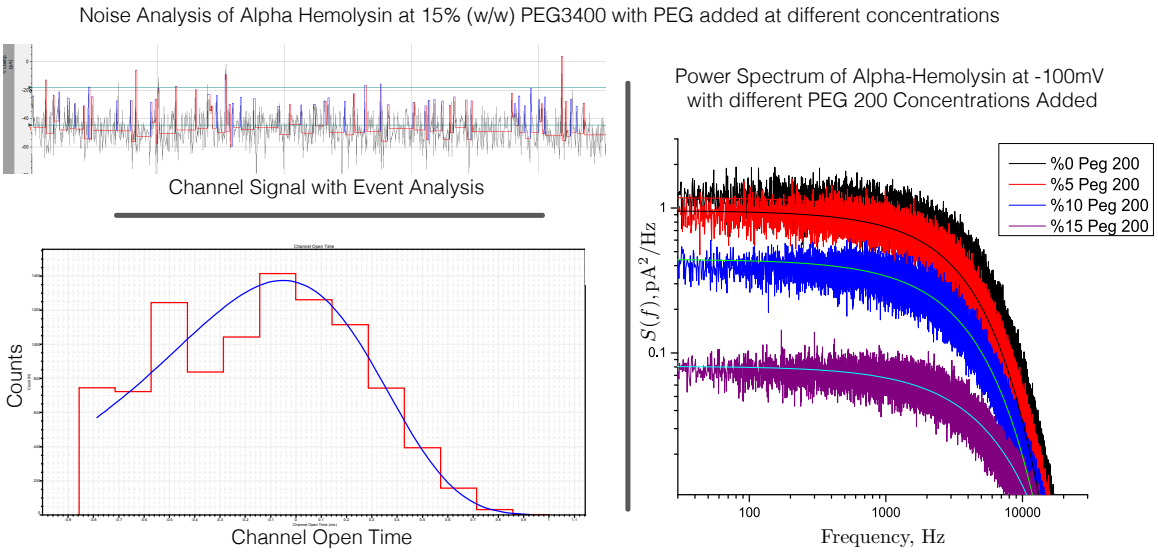

Figure 6.2: An Example of Power Spectral Analysis of Alpha-Hemolysin for Determining Partitioning Dynamics

Fig. 6.2 shows examples of analysis done on the Alpha-Hemolysin channel. Unfortunately careful analysis of such signals requires a relatively noiseless setup, such that resolvable single channel blockage events are observed. The rates of polymer blockages are also dependent on the salt concentration in the bathing solution [93][59][16][92]. The reason for this salt dependency is attributed to PEG-Cation binding [59] which is apparent in Chlorides of Na^+, K^+, Rb^+ and Cs^+ [93], which causes PEG to "bind" to charged residues inside the ion channel. We discuss the observations of PEG-Cation binding in Appendix B.

6.2 Noise Analysis of Partitioning of Binary Polymer Mixtures

6.2.1 Materials and Methods

Single channel recording and membrane formation is performed on the same setup as described in Section 5.1.3. Stock electrolyte solution contained 1.0 M KCl and 10 mM HEPES at pH 7.4 adjusted with 8.0 N KOH. Bathing solutions were binary mixtures of PEG3400 and PEG200 containing 30% (w/w) total PEGs. They were made by adding PEGs directly to the stock electrolyte solution. Individual concentrations of PEGs in bathing solutions varied by $\Delta 5\%$ (w/w). Measurements are performed on a single reconstituted Alpha-Hemolysin channel, at membrane potentials $0, \pm 50$ and ± 100 mV. 3 - 4 single channel measurements are performed per PEG concentration. Bathing Solutions are collected for conductivity measurements.

Signals are collected at a sampling frequency of 50 kHz, signals are filtered with a software Bessel low-pass filter at 15 kHz (pClamp Software, Molecular Devices, LLC., CA, USA) and an analog 8-Pole Butterworth low-pass filter at 10 kHz (Molecular Devices, LLC., CA, USA). Power Spectra are measured using a Fast Fourier Transform (FFT) algorithm (ClampFit Software Molecular Devices, LLC., CA, USA).

6.2.2 Results

If we first look at the raw data of samples of currents through the channels before and after additions of different PEG mixtures (Figure 6.3), we observe two effects of PEG on the current. As expected, PEG addition to the membrane bathing solution reduces channel conductance and increases the noise in the channel. Both these effects are PEG-size dependent, that is the increase in channel noise is significantly higher in the case of PEG3400.

Figure 6.4 shows the relative channel conductance in PEG200 and PEG3400 mixtures of different composition, in which monomeric PEG concentration is held con-

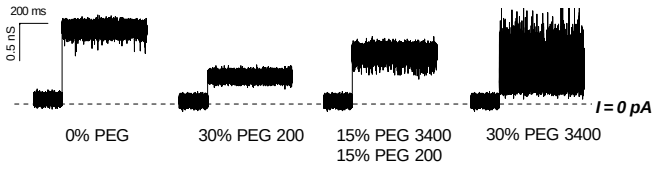

Figure 6.3: Current Noise in Binary Mixtures of PEGs

stant at the 30% (w/w). As expected from our results in partitioning, channel conductance displays a non-monotonic dependence on the mixture composition. It first increases with the increasing fraction of the larger PEG in the mixture, but then, after this fraction reaches 2/3 (corresponds to 20% (w/w) in the graph), it starts to decrease. Using the language of partitioning [110], this means the following. Substitution of smaller PEG200 by larger PEG3400 first leads to a decrease in partitioning due to the extra entropic penalty of moving larger polymer into the nanopore, but then, with the fraction of the larger polymer increasing, the partitioning increases again.

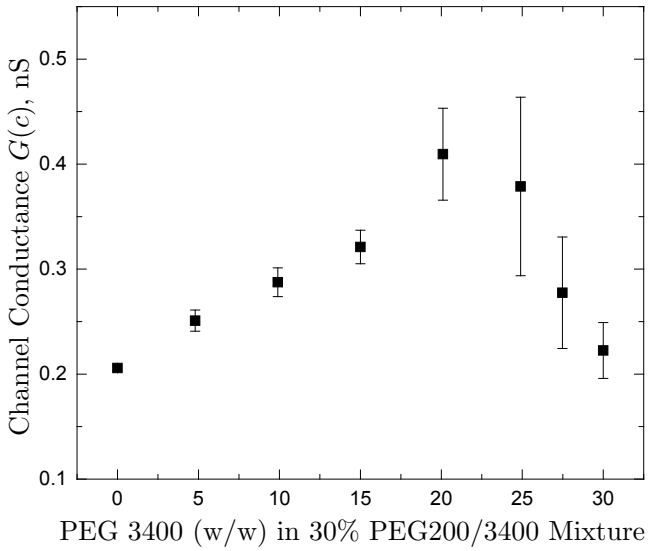

Figure 6.4: Relative Channel Conductance at 30% Total PEGs

Figure 6.5 shows the results of the spectral analysis of fluctuations in the currents through the Alpha-Hemolysin nanopore in the polymer-free solutions and in the presence of the PEG200 and PEG3400 mixtures of different compositions. It is immediately seen that while for the solutions enriched with PEG200 the noise is barely different from that of the nanopore in the absence of polymers, for the ones enriched with PEG3400 the polymer-induced noise is quite significant. The larger polymer produces a lot of current fluctuations, the smaller one does not. Visual examination of the data suggest that at PEG200 relative concentrations not greater than $\frac{1}{2}$ (corresponding to 15% (w/w) PEG3400 in the figure) the contribution of PEG3400 to the partitioning is negligible. Indeed, the low-frequency spectral density of current fluctuations at 15% (w/w) PEG 3400 is three orders of magnitude lower than it is at 30% (w/w) PEG3400. Assuming that this spectral parameter reports on the presence of PEG3400 in the nanopore, one may immediately conclude that this larger polymer is practically excluded from the pore.

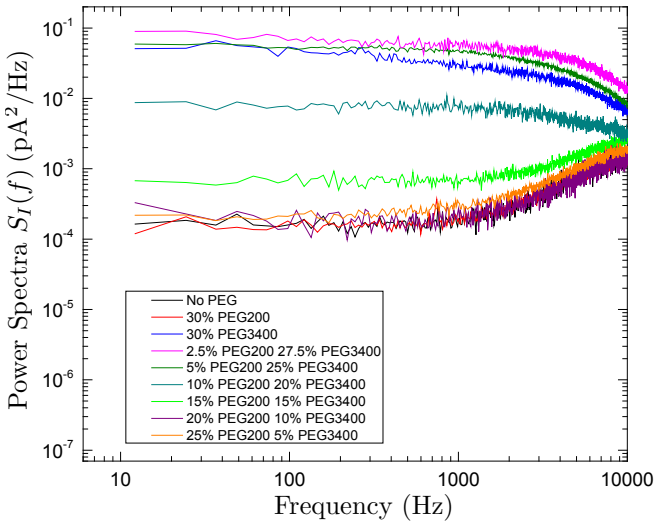

Figure 6.5: Power Spectrum Analysis of Alpha-Hemolysin at 30% Total PEGs

6.2.3 Discussion

In order to obtain quantitative estimates, we need to use the available analytical approaches. One of them, deemed to be most appropriate in our case, is based on the diffusion model of channel-facilitated transport [113]. For the fluctuations, which are induced by equilibrium exchange of non-conductive particles between the pore and the bulk, it gives the following expression for the spectral density of current noise $S_I(f)$as a function of frequency f :

$$S_I(f) = \langle N \rangle (\Delta G)^2 V^2 S(f) \tag{6.4}$$

where $\langle N \rangle$ is the average number of particles in the channel, ΔG is the reduction in pore conductance due to the entrance of one particle, V is the applied potential, and $S(f)$ is the spectral density obtained from the normalized correlation function of the number of particles in the channel $C(t)$:

$$S(f) = 4 \int_0^\infty C(t) cos(2\pi f t) dt \tag{6.5}$$

Solutions for $C(t)$ demonstrate that the spectral density may have a quite complex frequency behavior [114] which is defined by many parameters of the pore and pore-particle interactions. However, for the low-frequency spectral limit, $S(0)$, and particle diffusional dynamics, the expression is simplified to,

$$S(0) = \frac{L^2}{3D} \left(1 + \frac{3\pi}{2} \frac{D R_c}{D_b L} \right), \tag{6.6}$$

where, L is the channel length, R_c is the channel radius, D is the particle diffusivity in the channel, and D_b is the particle diffusivity in the bulk. For alpha-hemoysin $L \gg R_c$ [65] and $D_b \gg D$ [13], the last term in the brackets can be omitted, and we obtain the following form for the low-frequency spectral density:

$$S_I(0) = \langle N \rangle \frac{L^2}{3D} (\Delta G)^2 V^2. \tag{6.7}$$

It is convenient to introduce the normalized spectra by the following expression:

$$S_{rel} \equiv \frac{S_I(f)}{\langle G \rangle^2 V^2} \tag{6.8}$$

where $\langle G \rangle$ is the average conductance of the nanopore. Finally we have for the normalized low frequency spectra:

$$S_{rel}(0) = \langle N \rangle \frac{L^2}{3D} \left(\frac{\Delta G}{\langle G \rangle} \right)^2. \tag{6.9}$$

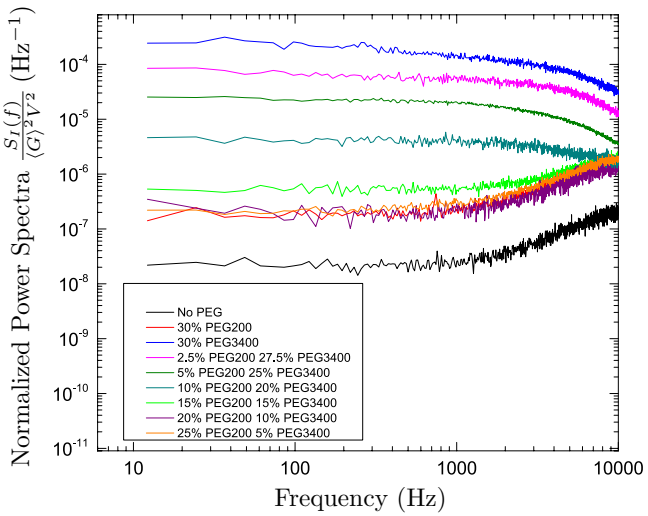

Figure 6.6: Normalized Power Spectra at 30% Total PEGs

Experimentally obtained spectra transformed according to Eq. 6.8 are shown in Figure 6.6. The values of $S_{rel}(0)$ for different polymer mixtures are presented in Figure 6.7. Now, these data and Eq. 6.9 allows us to quantify the relative population of PEG3400 in the nanopore. Assuming that $\Delta G/\langle G \rangle$, the normalized change in conductance due to the entrance of one PEG3400 molecule, does not vary greatly for the studied mixtures, we can estimate the average number of PEG3400 molecules in

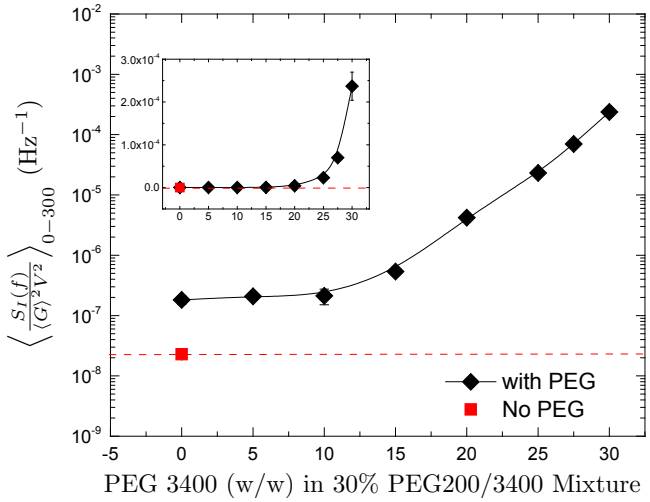

Figure 6.7: Low Frequency Normalized Power Spectra at 30% Total PEGs

the channel at 15% (w/w) PEG3400 in the mixture ($\langle N_{15\%}\rangle$) through their relative number at 30% (w/w) ($\langle N_{30\%}\rangle$) as:

$$\frac{\langle N_{15\%}\rangle}{\langle N_{30\%}\rangle} \simeq \frac{S_{rel}(0)_{15\%}}{S_{rel}(0)_{30\%}} \frac{D_{15\%}}{D_{30\%}}, \tag{6.10}$$

Where $S_{rel}(0)_{15\%}$ and $S_{rel}(0)_{30\%}$ are the low-frequency spectral densities of PEG3400 induced fluctuations at 15% and 30% (w/w) respectively and $D_{15\%}/D_{30\%}$ is the ratio of PEG3400 diffusivities at these concentrations. To find this ratio, we interpolate results of a study on the viscosity and microviscosity of PEG solutions [99]. It follows from this interpolation that the diffusivity ratio is approximately $D_{15\%}/D_{30\%} \approx 8$. As for the spectral densities in question, from the data in Figure 6.7 we have $S_{rel}(0)_{15\%} \simeq 3.7 \cdot 10^{-7} s^{-1}$ and $S_{rel}(0)_{30\%} \simeq 2.5 \cdot 10^{-4} s^{-1}$. These values substituted into Eq. 6.9 gives the following estimate: $\langle N_{15\%}\rangle/\langle N_{30\%}\rangle \simeq 0.012$. That is the polymeric content of the channel, bathed by the $1:1$ ratio of PEG mixtures (15% each) is mostly that of PEG200.

6.3 Channel Geometry and Other Considerations

Channel geometry is another important factor that could be taken into account, as mentioned in section 5.1 the channels are assumed to be of cylindrical pores of a given radius (R_c). However ion channels are rarely found as perfect cylinders. One of the most important results that cannot be ignored is that most often the channel conductance that is measured when no polymer is present usually does not conform to the cylindrical assumption (*e.g* VDAC conductance is $G_p \approx 4nS$ however at a radius of $R_c = 11$Å at a length of $l_c = 40$Å and given that $1.0M$ KCl has the conductivity of $\sigma_{KCl} = 1.11nS/$Å it should have a conductance of $10nS$.) [23].

A simple approach to this problem is to introduce a tapered channel, and using Eq. 5.1 finding the radius of the constriction of the taper such that the resistivity integral over the tapered channel matches the measured resistance of the channel.

$$G_p^{-1} = 2 \cdot \int_{R_c}^{R_t} \frac{\sigma(r)^{-1}}{\pi r^2} dr \tag{6.11}$$

Once a channel taper is determined in this form partitioning to a tapered channel can be tested. One simple approach is to assume a model for partitioning where the free energy of confinement is the only free parameter (as in our tested theories in section 5.2). Since free energies of confinement depends on the channel radius, one can attempt to numerically calculate the polymer concentration as a function of channel radii $\phi(r)$. Then equation 5.1 can be integrated along the channel taper inserting $\phi(r)$ as a parameter and it could be tested whether the measured conductance agrees with the form of partitioning.

We have tested this approach with a simple form of partitioning [31] using our data for VDAC and PEG200.

Fig. 6.8 shows the calculations done on VDAC as a tapered channel. It was found that at a length of $l_c = 40$Å VDAC should have had a radius of $R_t = 5$Å at the constriction to satisfy the measured conductance of $\approx 4nS$. Details of the calculation

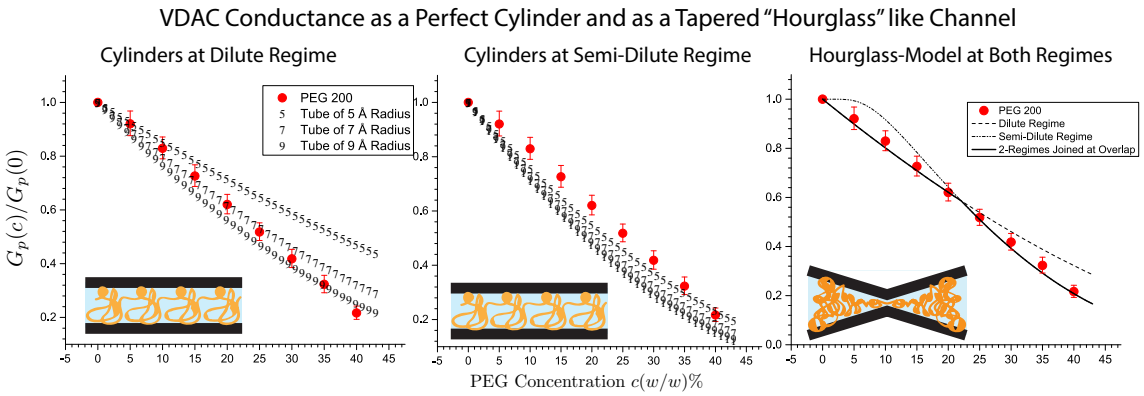

Figure 6.8: Proper Channel Conductance of VDAC with PEG 200 with Cylindrical and Hourglass Shaped Channel Models

for the partitioning is not discussed here, however the important fact here is that while a cylindrical channel cannot satisfy the measured conductance properly (*e.g* a cyclinder with a 7Å radius satisfies the data at dilute regimes, but does not agree with the data at semi-dilute regimes) an hourglass shaped channel successfully describes the data.

APPENDIX A

POLYMER SOLUTION CONCENTRATIONS

Table A.1: Polymer Concentration Types

ϕ = Monomer Fraction	Φ = Volume Fraction
c_w = Weight(Mass) Fraction	p = Monomer Density #(Monomer) /V
c_m = Weight(Mass)Density (M/V) usually g/ml	c = Polymer Density #(Polymer) /V

Table A.2: Polymer Concentration Types in Functional Form

$\phi = \frac{n_p N_p}{n_p N_p + n_w}$	$\Phi = \frac{n_p N_p m_p \bar{\nu}_p}{n_p N_p m_p \bar{\nu}_p + n_w m_w \bar{\nu}_w}$
$c_w = \frac{n_p N_p m_p}{n_p N_p m_p + n_w m_w}$	$p = \frac{n_p N_p}{n_p N_p m_p \bar{\nu}_p + n_w m_w \bar{\nu}_w}$
$c_m = \frac{n_p N_p m_p}{n_p N_p m_p \bar{\nu}_p + n_w m_w \bar{\nu}_w}$	$c = \frac{n_p}{n_p N_p m_p \bar{\nu}_p + n_w m_w \bar{\nu}_w}$

Define

$$\gamma = \frac{m_p \bar{\nu}_p}{m_w \bar{\nu}_w} \quad \kappa = \frac{\bar{\nu}_p}{\bar{\nu}_w} \quad \theta = \frac{m_p}{m_w}$$

Values of $m_p, m_w, \bar{\nu}_p, \bar{\nu}_w$ for PEG and Water

$m_p = 44.44\ amu$	$m_w = 18\ amu$	$\bar{\nu}_p = 0.885\ {}^{ml}/_{g}$	$\bar{\nu}_w = 1.0\ {}^{ml}/_{g}$
$= 44.44 \cdot 1.66 * 10^{-24}\ g$	$= 18 \cdot 1.66 * 10^{-24}\ g$	$= 0.885 \cdot 1.0 * 10^{-24}\ \text{Å}^3/_{g}$	$= 1.0 \cdot 1.0 * 10^{-24}\ \text{Å}^3/_{g}$
$\approx 7.37 * 10^{-23}\ g$	$\approx 2.99 * 10^{-23}\ g$	$\approx 0.885 * 10^{-24}\ \text{Å}^3/_{g}$	$\approx 1.0 * 10^{-24}\ \text{Å}^3/_{g}$

Table A.3: Polymer Concentration Conversion Table

	ϕ	c_w	Φ	c_m	p	c
ϕ	1	$\frac{c_w}{c_w+\theta(1-c_w)}$	$\frac{\Phi}{\Phi+\gamma(1-\Phi)}$	$\frac{c_m}{c_m+\gamma(\frac{1}{\bar{\nu}_p}-c_m)}$	$\frac{p}{p+\gamma(\frac{1}{m_p\bar{\nu}_p}-p)}$	$\frac{c}{c+\gamma(\frac{1}{N_pm_p\bar{\nu}_p}-c)}$
c_w	$\frac{\theta\phi}{1+\phi(\theta-1)}$	1	$\frac{\Phi}{\Phi+\kappa(1-\Phi)}$	$\frac{c_m}{c_m+\kappa(\frac{1}{\bar{\nu}_p}-c_m)}$	$\frac{p}{p+\kappa(\frac{1}{m_p\bar{\nu}_p}-p)}$	$\frac{c}{c+\kappa(\frac{1}{N_pm_p\bar{\nu}_p}-c)}$
Φ	$\frac{\gamma\phi}{1+\phi(\gamma-1)}$	$\frac{\kappa c_w}{1+c_w(\kappa-1)}$	1	$c_m\cdot\bar{\nu}_p$	$p\cdot m_p\bar{\nu}_p$	$c\cdot N_pm_p\bar{\nu}_p$
c_m	$\left(\frac{1}{\bar{\nu}_p}\right)\cdot\frac{\gamma\phi}{1+\phi(\gamma-1)}$	$\left(\frac{1}{\bar{\nu}_p}\right)\cdot\frac{\kappa c_w}{1+c_w(\kappa-1)}$	$\Phi\Big/\bar{\nu}_p$	1	$p\cdot m_p$	$c\cdot N_pm_p$
p	$\left(\frac{1}{m_p\bar{\nu}_p}\right)\cdot\frac{\gamma\phi}{1+\phi(\gamma-1)}$	$\left(\frac{1}{m_p\bar{\nu}_p}\right)\cdot\frac{\kappa c_w}{1+c_w(\kappa-1)}$	$\Phi\Big/m_p\bar{\nu}_p$	$c_m\Big/m_p$	1	$c\cdot N_p$
c	$\left(\frac{1}{N_pm_p\bar{\nu}_p}\right)\cdot\frac{\gamma\phi}{1+\phi(\gamma-1)}$	$\left(\frac{1}{N_pm_p\bar{\nu}_p}\right)\cdot\frac{\kappa c_w}{1+c_w(\kappa-1)}$	$\Phi\Big/N_pm_p\bar{\nu}_p$	$c_m\Big/N_pm_p$	$p\Big/N_p$	1

$$\gamma = \frac{m_p\bar{\nu}_p}{m_w\bar{\nu}_w} \approx 2.18$$
$$\kappa = \frac{\bar{\nu}_p}{\bar{\nu}_w} \approx 0.885$$
$$\theta = \frac{m_p}{m_w} \approx 2.47$$

APPENDIX B

PEG CATION BINDING

In this Appendix we are going to discuss the phenomena of PEG-Cation binding, first mentioned in Section 4.1. The references in this section indicate strong evidence for PEG-Cation binding, which, at first sight, seems to contradict with our measurements with Ion Selective Electrodes that gives a sense of "Volume Exclusion" (Section 5.1.2). Here we are going to investigate two questions, (i) Do our ISE measurements indicate that cations are excluded from PEG and PEG-Water complex? (ii) Are Cations Bound to PEG in KCl Solutions?.

B.1 Do our ISE measurements indicate that cations are excluded from PEG and PEG-Water complex?

In our measurements performed with (K^+) Ion Selective Electrodes (ISE), performed on PEG-KCl solutions where PEG concentration is varied between 0%(w/w) - 40%(w/w) and electrolyte solution contained 1.0M KCl, we see an increased "Effective Ion Concentration" in PEG excluded part of the solution which is the measuring chamber of the electrode. The same effect has been observed in Ref. [13] with NaCl solutions, and in Ref. [12] performed in "constant volume" experiments, using ISEs, ultrafiltration and single channel recording. Our findings indicate that there is a linear correlation between the effective ion concentration and polymer weight percent (c). The results of our measurements and performed in Ref. [13] are shown in Fig. B.1.

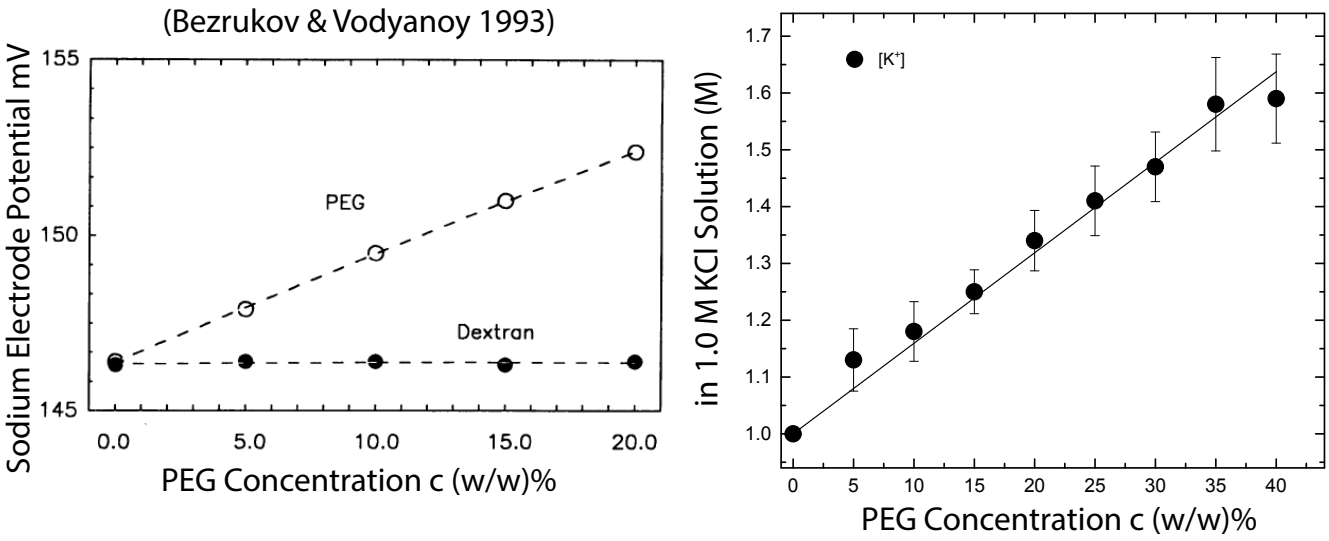

Figure B.1: Increase in Effective Ion Concentration in NaCl and KCl Solution in the presence of PEGs[1]

Is this effect necessarily related to KCl being excluded from PEG or PEG-Water complex? The answer is most probably no, in Ref. [12] it is clearly stated that there is no indication of significant "salt" exclusion. A very simple calculation for total salt exclusion from the Hydrated-PEG molecule shows that in that case we would see an increase in KCl concentration, in terms of (c w/w%), as:

$$[KCL] = \left(1 - \frac{1}{\bar{\nu_p} m_p}(\frac{c}{1-c})V_h\right)[KCL]_0 \tag{B.1}$$

(V_h) being hydration volume per monomer and ($\bar{\nu_p}, m_p$) are specific volumes and monomer mass of PEG. This is clearly not the case, we see a linear correlation.

[1]Reprinted from Biophysical Journal 64, Bezrukov SM, Vodyanoy I, Probing alamethicin channels with water-soluble polymers Effect on conductance of channel states. 16-25., Copyright (1993), with permission from Elsevier.

B.2 Are Cations Bound to PEG in KCl Solutions?

The clear indications of PEG-Cation binding are listed in Section 4.2. However, the study of these references reveals some information. Ref. [95] presents a simulation that uses only (K^+) ions in solution, there are no anions. NMR studies performed in Refs. [94] and [96] uses methanol as the solvent, in fact in Ref. [96] it is specifically stated that no cation binding is observed when the solvent used was water. Refs. [98] and [97] uses highly modified PEG molecules and the main result in Ref. [97] is an observation on the increase of viscosity, which is also stated in Ref. [99] that we use to describe the decrease in the conductivity of the solution, an does not directly indicate PEG-Cation binding.

Perhaps the strongest indicators of PEG-Cation binding is in Ref. [92] and [93]. In Ref. [93] all alkali metal ion-chloride salts have been studied and a voltage dependent channel-PEG event binding has been observed in all of them barring (Li^+), however all salt concentrations used were 2.0 M.

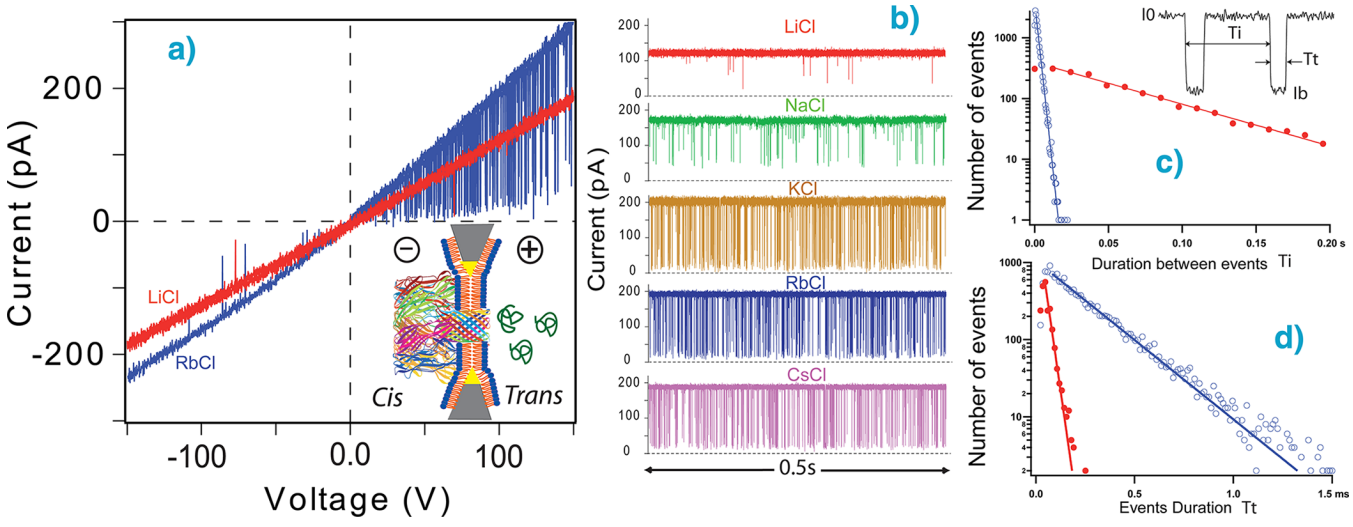

Figure B.2: Cation Binding to PEG in Alkali metal-Chloride Salts[2]

This effect is seen in Fig. B.2. This study follows the example of Ref. [92] where similar work is performed in KCl solutions of various molarities. In the study performed in Ref. [92] there is undeniable evidence of PEG-Cation binding, however not in 1.0 M KCl. The strongest indicator of binding is the (k_{on}) and (k_{off}) rates describing polymer-channel association constants. These constants vary with cation concentration, but also are voltage dependent. The results are seen in Fig. B.3

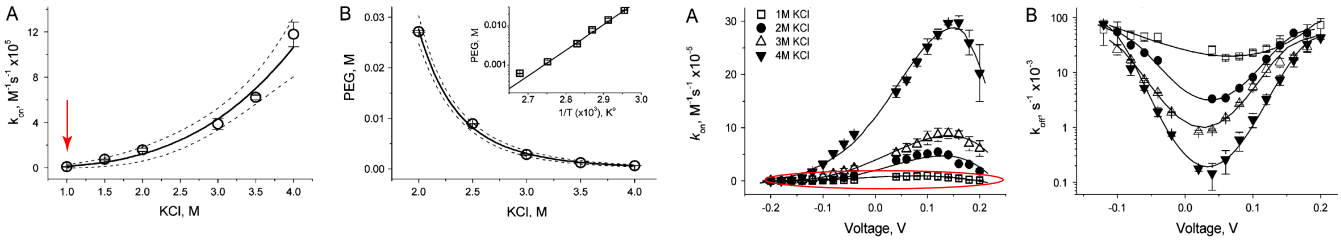

Figure B.3: PEG-Cation interactions in different KCl concentrations[3]

However, (k_{on}) rate is almost 0 at 1.0 M KCl, and the voltage dependence of the (k_{on}) and (k_{off}) rates are negligible at 1.0 M KCl. Our conclusion is that Cation-PEG binding exists, but this phenomnena is not present at 1.0 M KCl, even if it does it should be negligible to take into account in our study. Thus any sort of PEG-Cation complexities can be safely disregarded in this work. We attribute the effect of the increase in the concentration of ions inside the channel when PEGs are present to the complex issue of water structuring or Hofmeister effects.

[2]Reprinted with permission from 1. Breton MF, et al. (2013) Exploration of neutral versus polyelectrolyte behavior of poly(ethylene glycol)s in alkali ion solutions using single-nanopore recording. J Phys Chem Lett 4(13):22022208. Copyright (2013) American Chemical Society.

[3]Reprinted from Biophysical Journal 95(11), Rodrigues CG, Machado DC, Chevtchenko SF, Krasilnikov O V, Mechanism of KCl enhancement in detection of nonionic polymers by nanopore sensors, 51865192., Copyright (2008), with permission from Elsevier.

APPENDIX C

ACCESS RESISTANCE OF A CIRCULAR PORE

The access resistance, is the additional we need to take into account when dealing with small pores. Access Resistance occurs due to the convergence of electric field lines from the bulk to the mouth of the pore. This is demonstrated in Figures 5.9 and C.1. Using a simple assumption one can find the access resistance easily by calculating the integral resistance from infinity to a hemispherical shell of radius equal to the pore radius, ignoring the resistance that occurs within the hemisphere. This is an easy calculation, however calculating the access resistance towards the disk-like mouth of the pore turns out to be an interesting and a beautiful problem that involves a symmetry relation between resistance and capacitance, finding the charge distribution on a conducting disk and calculating the capacitance of a disk. Digging through these problems, one can see that some concepts we take for granted (like the charge distribution on a conducting disk) are not so straightforward at all. The calculation of the access resistance was realized by James E. Hall [21] and the credit for methods used goes to William R. Smythe [101]. First we will perform the hemisphere calculation, then we will proceed with the calculation of the access resistance of a circular pore.

C.1 Hemisphere Approximation

This calculation is straightforward. We assume a uniform current density ($J(\vec{r})$), and we assume that the electric field is aligned with the current density, giving a

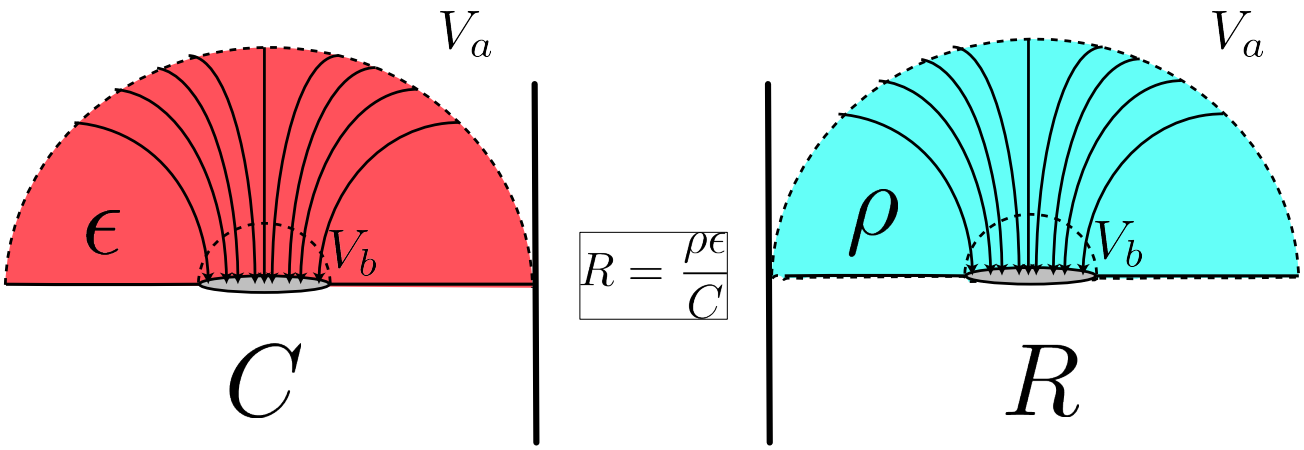

Figure C.1: Relation of The Resistance of a Circular Pore to the Conductance of a Disk in the Same Geometry

constant resistivity $\rho = \frac{\vec{E}(\vec{r})}{\vec{J}(\vec{r})}$. Given that the current is $I = \vec{J}(\vec{r})\vec{A}(\vec{r})$, where $\vec{A}(\vec{r})$ is the cross sectional area the total resistance along the path is:

$$R_{acc}^{hs} = \frac{\Delta V}{I} = \frac{\int_{\infty}^{R_{hs}} \vec{E}(\vec{r})d\vec{r}}{\int_{\infty}^{R_{hs}} \vec{J}(\vec{r})\vec{A}(\vec{r})d\vec{r}} = \int_{\infty}^{R_{hs}} \frac{\rho}{\vec{A}(\vec{r})} \tag{C.1}$$

Where R_{hs} is the radius of the hemisphere. Since $A(r) = 2\pi r^2$ this integral yields $R_{acc}^{hs} = \frac{\rho}{2\pi r}$

C.2 Access Resistance for a Circular Disk

Symmetry Argument of the Resistance of a Pore to the Capacitance of a Conducting Disk

Direct integration of the field lines to a disk difficult [42], but the problem could be easily solved by a symmetry relation between the resistance of a pore and the capacitance of a disk. Imagine a circular pore of radius R_p held at a potential difference $V_a - V_b$ w.r.t the potential at infinity and the space is filled with a medium of uniform resistivity ρ. Now Imagine a circular conducting disk of radius R_p held at a potential

difference $V_a - V_b$ w.r.t the potential at infinity and the space is filled with a medium of uniform dielectric constant ϵ. These two systems are illustrated in Figure C.1.

In both of these cases, the equation to be solved that describes the potential is the Laplace Equation:

$$\nabla^2 V = 0 \tag{C.2}$$

With boundary conditions

$$\begin{aligned} V &= V_b, \quad Q_b = -\int_S \frac{1}{\epsilon}\frac{\partial V}{\partial n} dS \\ V &= V_b, \quad R_b = -\int_S \frac{1}{\rho}\frac{\partial V}{\partial n} dS \end{aligned} \tag{C.3}$$

The equipotential surfaces in both of these problems are identical, which allows us to relate the Resistance of the pore to that of the Capacitance of a disk, via:

$$R = \frac{|V_a - V_b|}{|I_b|} = \rho\epsilon\frac{|V_a - V_b|}{|Q_b|} = \frac{\rho\epsilon}{C} \tag{C.4}$$

All we need to do is to find the capacitance of a conducting disk (at half space), and we can easily obtain the access resistance of a pore.

The surface charge density of a conducting disk is first calculated by William Thompson (Lord Kelvin) [115] using a geometrical argument. William Smythe gives a more general and a more modern solution to this problem, calculating both the capacitance and the surface charge density of a conducting disk [101].

Condition for a Set of Surfaces forming Equi-potentials

We will follow through Smythe's approach here skipping certain steps through the calculation. Smythe, first finds out if a set of surfaces can be equi-potentials, then proceeds to calculate the potentials for a general set of ellipsoids, which then yields the capacitance and the surface charge density of a conducting disk.

We start with a general set of surfaces

$$F(x, y, z) = \psi \tag{C.5}$$

Note that each value of ψ corresponds to a different surface. If these surfaces forms a set of equi-potentials then each value of ψ must correspond to a single potential, that is $V = f(\psi)$, where each V must satisfy the Laplace equation $\nabla^2 V = 0$. Note that,

$$\frac{\partial V}{\partial x} = \frac{\partial f(\psi)}{\partial \psi}\frac{\partial \psi}{\partial x} \tag{C.6}$$

Calculating the Laplacian in this manner yields to,

$$\frac{\nabla^2 \psi}{(\nabla \psi)^2} = -\frac{f''(\psi)}{f'(\psi)} = \Phi(\psi) \tag{C.7}$$

So for a set of surfaces given by the equation $F(x, y, z) = \psi$ to be equipotentials, the necessary condition is for $\frac{\nabla^2 \psi}{(\nabla \psi)^2}$ to be a function of ψ only. From here on, one can calculate the potential via integration, noting that $\frac{f''(\psi)}{f'(\psi)} = \frac{d(lnf'(\psi))}{d\psi}$ integrating twice, one has,

$$V = f(\psi) = A \int e^{-\int \Phi(\psi) d\psi} d\psi + B \tag{C.8}$$

Solution for General Ellipsoids

We can represent the general equation for ellipsoids as,

$$\frac{x}{a^2 + \psi} + \frac{y}{b^2 + \psi} + \frac{z}{c^2 + \psi} = 1 \tag{C.9}$$

For $-a^2 < \psi < \infty$ and $a < b < c$ we have an ellipsiod. When $\psi = \infty$ we have a sphere of infinite radius, and when $\psi = -a^2$ and $b = c$ we a circular disk. Showing that these sets of surfaces forms equi-potential surfaces requires calculating $\frac{\nabla^2 \psi}{(\nabla \psi)^2}$. This is easily performed by introducing two auxiliary functions,

$$
\begin{aligned}
M_n &= \frac{x}{(a^2+\psi)^n} + \frac{y}{(b^2+\psi)^n} + \frac{z}{(b^2+\psi)^n} \\
N &= \frac{1}{a^2+\psi} + \frac{1}{b^2+\psi} + \frac{1}{c^2+\psi}
\end{aligned}
\tag{C.10}
$$

And one ends up with,

$$
\begin{aligned}
\frac{\nabla^2\psi}{(\nabla\psi)^2} &= \frac{N}{2} \\
\Phi(\psi) &= \frac{1}{2}\left(\frac{1}{a^2+\psi} + \frac{1}{b^2+\psi} + \frac{1}{c^2+\psi}\right)
\end{aligned}
\tag{C.11}
$$

Satisfying the necessary condition for forming equi-potential surfaces. The potential due to these surfaces is then, via Eq. C.8

$$
V(\psi) = A\int^{\psi} \left((a^2+\psi')(b^2+\psi')(c^2+\psi')\right)^{-1/2} d\psi' + B \tag{C.12}
$$

Finding the Capacitance and the Surface Charge Density

Now, setting the potential at infinity to zero $V_\infty = 0$ when $\psi \to \infty$ we have

$$
0 = \left[A\int^{\psi} \left((a^2+\psi')(b^2+\psi')(c^2+\psi')\right)^{-1/2} d\psi'\right]_{\psi=\infty} + B \tag{C.13}
$$

Giving us the value of B. Setting the potential to V_a when $\psi = 0$. We have

$$
V_a = \left[A\int^{\psi} \left((a^2+\psi')(b^2+\psi')(c^2+\psi')\right)^{-1/2} d\psi'\right]_{\psi=0} - \left[A\int^{\psi} \left((a^2+\psi')(b^2+\psi')(c^2+\psi')\right)^{-1/2} d\psi'\right]_{\psi=\infty} \tag{C.14}
$$

Which yields for V_a

$$V_a = -A \int_0^\infty \left((a^2+\psi')(b^2+\psi')(c^2+\psi')\right)^{-1/2} d\psi' \tag{C.15}$$

Now, remembering that at infinity, the electric field $\vec{E}(r)|_{r\to\infty}$ due to this ellipsoid, given that the total charge on the ellipsoid is Q_a is going to be $\frac{Q_a}{4\pi\epsilon r^2}$, where r is the radius of the ellipsoid. We can obtain the capacitance. The electric field at infinity is,

$$\frac{\partial V}{\partial r}\Big|_{r\to\infty} = \frac{\partial V}{\partial \psi}\frac{\partial \psi}{\partial r}\Big|_{r\to\infty}. \tag{C.16}$$

Note that as $\psi \to \infty$, $r^2 \to \infty$. That is at infinity $\frac{\partial \psi}{\partial r} = 2r$. And $\frac{\partial V}{\partial \psi} = \frac{A}{r^3}$ from Eq. C.12.This yields,

$$\frac{2A}{r^2} = -\frac{Q_a}{4\pi\epsilon r^2} \tag{C.17}$$

And finally the capacitance of the ellipsoid is from Eq. C.15

$$C = \frac{Q_a}{V_a} = -\frac{8\pi\epsilon A}{V_a} = \left[\int_0^\infty \left((a^2+\psi')(b^2+\psi')(c^2+\psi')\right)^{-1/2} d\psi'\right]^{-1} \tag{C.18}$$

And the surface charge density σ is

$$\sigma = -\epsilon(\nabla V)_{\psi=0} = -\epsilon\left(\frac{\partial V}{\partial \psi}|\nabla\psi|\right)_{\psi=0} \tag{C.19}$$

Now, $\left(\frac{\partial V}{\partial \psi}\right)_{\psi=0} = \frac{A}{abc}$ and $|\nabla\psi| = 2M_2^{-1/2}$ and the surface charge density is then

$$\sigma = \frac{Q_a}{4\pi abc}\left(\frac{x^2}{a^4}+\frac{y^2}{b^4}+\frac{z^2}{c^4}\right)^{-1/2} \tag{C.20}$$

Capacitance of the Disk and the Access Resistance

Using Eqs. C.19 and C.20 and setting $a = 0$, and $b = c = R$, noting that $x^2 + y^2 = r^2$ we can obtain the Capacitance and the surface charge density of a conducting disk. Where the Capacitance is,

$$C = 8\pi\epsilon \left[\int_0^\infty \psi^{-\frac{1}{2}} (R^2 + \psi)^{-1} d\psi \right]^{-1} = 8\epsilon R \tag{C.21}$$

And the surface charge density is

$$\sigma = \frac{Q_a}{4\pi R (R^2 - r^2)^{1/2}} \tag{C.22}$$

And finally we can obtain the access resistance of the pore using Eqs. C.4 and C.21, paying attention that Eq. C.21 gives the capacitance of the whole space and we only need the capacitance in the half space, for the access resistance we end up with

$$R_{acc} = \frac{\rho}{4R} = \frac{1}{4\sigma R} \tag{C.23}$$

Here, R_{acc} is the access resistance, R is the radius of the pore, and $\sigma = 1/\rho$ is the conductivity, not to be confused with the surface charge density.

BIBLIOGRAPHY

[1] Zimmerman, S. B. and A. P. Minton, 1993. Macromolecular Crowding: Biochemical, Biophysical, and Physiological Consequences. *Annu Rev Biophys Biomol Struct* 22:27–65.

[2] Ellis, R. J., 2001. Macromolecular crowding: Obvious but underappreciated. *Trends Biochem Sci* 26:597–604.

[3] Zimmerberg, J. and V. A. Parsegian, 1986. Polymer inaccessible volume changes during opening and closing of a voltage-dependent ionic channel. *Nature* 323:36–9.

[4] Vodyanoy, I., S. M. Bezrukov, and V. A. Parsegian, 1993. Probing alamethicin channels with water-soluble polymers. Size-modulated osmotic action. *Biophys. J.* 65:2097–2105.

[5] Krasilnikov, O. V. and S. M. Bezrukov, 2004. Polymer Partitioning from Non-ideal Solutions into Protein Voids. *Macromolecules.* 37:2650–2657.

[6] Muthukumar, M., 2011. Polymer translocation. Taylor & Francis.

[7] Bezrukov, S. M., I. Vodyanoy, and V. A. Parsegian, 1994. Counting polymers moving through a single ion channel.

[8] Gu, L. Q., O. Braha, S. Conlan, S. Cheley, and H. Bayley, 1999. Stochastic sensing of organic analytes by a pore-forming protein containing a molecular adapter. *Nature* 398:686–690.

[9] Bezrukov, S. M., 2000. Ion channels as molecular coulter counters to probe metabolite transport. *J. Membr. Biol.* 174:1–13.

[10] Kasianowicz, J. J., J. W. F. Robertson, E. R. Chan, J. E. Reiner, and V. M. Stanford, 2008. Nanoscopic porous sensors. *Annu. Rev. Anal. Chem.* 1:737–766.

[11] Krasilnikov, O., R. Sabirov, V. Ternovsky, P. Merzliak, and J. Muratkhodjaev, 1992. A simple method for the determination of the pore radius of ion channels in planar lipid bilayer membranes. *FEMS Microbiology Letters* 105:93 – 100.

[12] Sabirov, R. Z., O. V. Krasilnikov, V. I. Ternovsky, and P. G. Merzliak, 1993. Relation between ionic channel conductance and conductivity of media containing different nonelectrolytes. A novel method of pore size determination. *Gen Physiol Biophys* 12:95–111.

[13] Bezrukov, S. M., I. Vodyanoy, R. A. Brutyan, and J. J. Kasianowicz, 1996. Dynamics and free energy of polymers partitioning into a nanoscale pore. *Macromolecules.* 29:8517–8522.

[14] Bezrukov, S. M. and J. J. Kasianowicz, 1997. The charge state of an ion channel controls neutral polymer entry into its pore. *Eur. Biophys. J.* 26:471–476.

[15] Movileanu, L., S. Cheley, and H. Bayley, 2003. Partitioning of individual flexible polymers into a nanoscopic protein pore. *Biophys. J.* 85:897–910.

[16] Robertson, J. W. F., C. G. Rodrigues, V. M. Stanford, K. A. Rubinson, O. V. Krasilnikov, and J. J. Kasianowicz, 2007. Single-molecule mass spectrometry in solution using a solitary nanopore. *Proc. Natl. Acad. Sci. U.S.A.* 104:8207–11.

[17] Baaken, G., I. Halimeh, L. Bacri, J. Pelta, A. Oukhaled, and J. C. Behrends, 2015. High-Resolution Size-Discrimination of Single Nonionic Synthetic Polymers with a Highly Charged Biological Nanopore. *ACS Nano.* 9:6443–6449.

[18] Prinsen, P., L. T. Fang, A. M. Yoffe, C. M. Knoblerx, and W. M. Gelbart, 2009. The force acting on a polymer partially confined in a tube. *J. Phys. Chem. B.* 113:3873–3879.

[19] Nurmemmedov, E., M. Castelnovo, C. E. Catalano, and A. Evilevitch, 2007. Biophysics of viral infectivity: matching genome length with capsid size. *Quarterly Reviews of Biophysics* 40:327–356.

[20] Cohen, J. A., R. Podgornik, P. L. Hansen, and V. A. Parsegian, 2009. A phenomenological one-parameter equation of state for osmotic pressures of PEG and other neutral flexible polymers in good solvents. *J. Phys. Chem. B.* 113:3709–3714.

[21] Hall, J. E., 1975. Access resistance of a small circular pore. *J. Gen. Physiol.* 66:531–2.

[22] Carneiro, C. M., O. V. Krasilnikov, L. N. Yuldasheva, A. C. Campos de Carvalho, and R. A. Nogueira, 1997. Is the mammalian porin channel, VDAC, a perfect cylinder in the high conductance state? *FEBS Lett* 416:187–189.

[23] Hiller, S., J. Abramson, C. Mannella, G. Wagner, and K. Zeth, 2010. The 3D structures of VDAC represent a native conformation. *Trends Biochem. Sci.* 35:514–21.

[24] Zitserman, V. Y., A. M. Berezhkovskii, V. A. Parsegian, and S. M. Bezrukov, 2005. Nonideality of polymer solutions in the pore and concentration-dependent partitioning. *J. Chem. Phys.* 123:146101.

[25] Podgornik, R., J. Hopkins, V. A. Parsegian, and M. Muthukumar, 2012. Polymers pushing Polymers: Polymer Mixtures in Thermodynamic Equilibrium with a Pore. *Macromolecules.* 45:8921–8928.

[26] Bezrukov, S. M. and I. Vodyanoy, 1993. Probing alamethicin channels with water-soluble polymers. Effect on conductance of channel states. *Biophys. J.* 64:16–25.

[27] Bezrukov, S. M. and J. J. Kasianowicz, 2001. Neutral polymers in the nanopores of alamethicin and alpha-hemolysin. *Biol. Membr.* 18:453–457.

[28] Vodyanoy, I. and S. M. Bezrukov, 1992. Sizing of an ion pore by access resistance measurements. *Biophys. J.* 62:10–1.

[29] Flory, P. J., 1953. Principles of polymer chemistry. Cornell University Press.

[30] Des Cloizeaux, G., JacquesJannink, 1990. Polymers in solution. Clarendon Press.

[31] Teraoka, I., 2002. Polymer solutions. Wiley.

[32] Flory, P. J., 1941. Thermodynamics of high polymer solutions. *The Journal of Chemical Physics* 9:660.

[33] Huggins, M. L., 1941. Solutions of long chain compounds. *The Journal of Chemical Physics* 9:440.

[34] Muthukumar, M., 1986. Thermodynamics of polymer solutions. *J. Chem. Phys.* 85:4722.

[35] Dobashi, T., M. Nakata, and M. Kaneko, 1984. Coexistence curve of polystyrene in methylcyclohexane. iii. asymptotic behavior of ternary system near the plait point. *The Journal of Chemical Physics* 80:948.

[36] Shinozaki, K., T. van Tan, Y. Saito, and T. Nose, 1982. Interfacial tension of demixed polymer solutions near the critical temperature: polystyrene + methylcyclohexane. *Polymer* 23:728–734.

[37] Sanchez, I. C., 1985. A universal coexistence curve for polymer solutions. *Journal of Applied Physics* 58:2871.

[38] Izumi, Y., YoshinobuMiyake, 1984. Universality of the coexistence curves in a polymer solution. *The Journal of Chemical Physics* 81:1501.

[39] Kumar, A., H. Krishnamurthy, and E. Gopal, 1983. Equilibrium critical phenomena in binary liquid mixtures. *Physics Reports* 98:57–143.

[40] Landau, E. M., L. DLifshitz, 1958. Statistical physics. Pergamon Press.

[41] Edwards, S. F., 1966. The theory of polymer solutions at intermediate concentration. *Proceedings of the Physical Society* 88:265.

[42] Hille, B., 2001. Ion channels of excitable membranes. Sinauer.

[43] Choudhary, O. P., R. Ujwal, W. Kowallis, R. Coalson, J. Abramson, and M. Grabe, 2010. The electrostatics of VDAC: implications for selectivity and gating. *J Mol Biol* 396:580–92.

[44] Gurnev, P. a., T. K. Rostovtseva, and S. M. Bezrukov, 2011. Tubulin-blocked state of VDAC studied by polymer and ATP partitioning. *FEBS Lett* 585:2363–6.

[45] Bezrukov, S. M., R. P. Rand, I. Vodyanoy, and V. a. Parsegian, 1998. Lipid packing stress and polypeptide aggregation: alamethicin channel probed by proton titration of lipid charge. *Faraday Discuss* :173–83; discussion 225–46.

[46] Braha, O., B. Walker, S. Cheley, J. J. Kasianowicz, L. Song, J. E. Gouaux, and H. Bayley, 1997. Designed protein pores as components for biosensors. *Chem Biol* 4:497–505.

[47] Bernheimer, A. W., J. P. Arbuthnott, and J. H. Freer, 1967. Physical states of staphylococcal alpha toxin. *Japanese Journal of Microbiology* 11:356–357.

[48] Bhakdi, S., R. Fussle, and J. Tranum-Jensen, 1981. Staphylococcal alpha-toxin: oligomerization of hydrophilic monomers to form amphiphilic hexamers induced through contact with deoxycholate detergent micelles. *Proceedings of the National Academy of Sciences* 78:5475–5479.

[49] Valeva, A., 2006. Evidence that clustered phosphocholine head groups serve as sites for binding and assembly of an oligomeric protein pore. *Journal of Biological Chemistry* 281:26014–26021.

[50] Wilke, J. B., G. A.Wardenburg, 2010. Role of a disintegrin and metalloprotease 10 in staphylococcus aureus -hemolysin-mediated cellular injury. *Proceedings of the National Academy of Sciences* 107:13473–13478.

[51] Fussle, R., 1981. On the mechanism of membrane damage by staphylococcus aureus alpha- toxin. *The Journal of Cell Biology* 91:83–94.

[52] Belmonte, G., L. Cescatti, B. Ferrari, T. Nicolussi, M. Ropele, and G. Menestrina, 1987. Pore formation by staphylococcus aureus alpha-toxin in lipid bilayers. *European Biophysics Journal* 14.

[53] Korchev, Y., G. Alder, A. Bakhramov, C. Bashford, B. Joomun, E. Sviderskaya, P. Usherwood, and C. Pasternak, 1995. Staphylococcus aureus alpha-toxin-induced pores: Channel-like behavior in lipid bilayers and patch clamped cells. *The Journal of Membrane Biology* 143.

[54] Merzlyak, P. G., L. N. Yuldasheva, C. G. Rodrigues, C. M. Carneiro, O. V. Krasilnikov, and S. M. Bezrukov, 1999. Polymeric nonelectrolytes to probe pore geometry: application to the alpha-toxin transmembrane channel. *Biophys J* 77:3023–3033.

[55] Krasilnikov, O. V., P. G. Merzlyak, L. N. Yuldasheva, C. G. Rodrigues, S. Bhakdi, and A. Valeva, 2000. Electrophysiological evidence for heptameric stoichiometry of ion channels formed by staphylococcus aureus alpha-toxin in planar lipid bilayers. *Molecular Microbiology* 37:1372–1378.

[56] Gu, H., Li-QunBayley, 2000. Interaction of the noncovalent molecular adapter, -cyclodextrin, with the staphylococcal a-hemolysin pore. *Biophysical Journal* 79:1967–1975.

[57] Menestrina, G., M. Dalla Serra, M. Comai, M. Coraiola, G. Viero, S. Werner, D. Colin, H. Monteil, and G. Prvost, 2003. Ion channels and bacterial infection: the case of -barrel pore-forming protein toxins of staphylococcus aureus. *FEBS Letters* 552:54–60.

[58] Gurnev, P. a., D. Harries, V. A. Parsegian, and S. M. Bezrukov, 2009. The dynamic side of the hofmeister effect: A single-molecule nanopore study of specific complex formation. *ChemPhysChem* 10:1445–1449.

[59] Reiner, J. E., J. J. Kasianowicz, B. J. Nablo, and J. W. F. Robertson, 2010. Theory for polymer analysis using nanopore-based single-molecule mass spectrometry. *Proc. Natl. Acad. Sci. U.S.A.* 107:6–11.

[60] Deamer, D. W. and D. Branton, 2002. Characterization of nucleic acids by nanopore analysis. *Acc Chem Res* 35:817–825.

[61] Ashkenasy, N., J. Sánchez-Quesada, H. Bayley, and M. R. Ghadiri, 2005. Recognizing a single base in an individual DNA strand: A step toward DNA sequencing in nanopores. *Angew Chem Int Ed* 44:1401–1404.

[62] Maglia, G., M. R. Restrepo, E. Mikhailova, and H. Bayley, 2008. Enhanced translocation of single DNA molecules through alpha-hemolysin nanopores by manipulation of internal charge. *Proc. Natl. Acad. Sci. U.S.A.* 105:19720–5.

[63] Clarke, J., H.-C. Wu, L. Jayasinghe, A. Patel, S. Reid, and H. Bayley, 2009. Continuous base identification for single-molecule nanopore DNA sequencing. *Nat Nanotechnol* 4:265–270.

[64] Branton, D., D. W. Deamer, A. Marziali, H. Bayley, S. A. Benner, T. Butler, M. Di Ventra, S. Garaj, A. Hibbs, X. Huang, S. B. Jovanovich, P. S. Krstic, S. Lindsay, X. S. Ling, C. H. Mastrangelo, A. Meller, J. S. Oliver, Y. V. Pershin, J. M. Ramsey, R. Riehn, G. V. Soni, V. Tabard-Cossa, M. Wanunu, M. Wiggin, and J. A. Schloss, 2008. The potential and challenges of nanopore sequencing. *Nat Biotechnol* 26:1146–1153.

[65] Song, L., M. R. Hobaugh, C. Shustak, S. Cheley, H. Bayley, and J. E. Gouaux, 1996. Structure of staphylococcal alpha-hemolysin, a heptameric transmembrane pore. *Science.* 274:1859–66.

[66] Aksimentiev, A. and K. Schulten, 2005. Imaging α-Hemolysin with Molecular Dynamics: Ionic Conductance, Osmotic Permeability, and the Electrostatic Potential Map. *Biophys J* 88:3745–3761.

[67] Muthukumar, M. and C. Y. Kong, 2006. Simulation of polymer translocation through protein channels. *Proc. Natl. Acad. Sci. U.S.A.* 103:5273–5278.

[68] Colombini, M., 2012. Vdac structure, selectivity, and dynamics. *Biochimica et Biophysica Acta (BBA) - Biomembranes* 1818:1457–1465.

[69] Colombini, M., 1989. Voltage gating in the mitochondrial channel, vdac. *The Journal of Membrane Biology* 111:103–111.

[70] Rostovtseva, T. and M. Colombini, 1996. ATP flux is controlled by a voltage-gated channel from the mitochondrial outer membrane. *J Biol Chem* 271:28006–28008.

[71] Rostovtseva, T. K., K. L. Sheldon, E. Hassanzadeh, C. Monge, V. Saks, S. M. Bezrukov, and D. L. Sackett, 2008. Tubulin binding blocks mitochondrial voltage-dependent anion channel and regulates respiration. *Proc. Natl. Acad. Sci. U.S.A.* 105:18746–18751.

[72] McCommis, C. P., Kyle S.Baines, 2012. The role of vdac in cell death: Friend or foe? *Biochimica et Biophysica Acta (BBA) - Biomembranes* 1818:1444–1450.

[73] Shimizu, S., M. Narita, and Y. Tsujimoto, 1999. Bcl-2 family proteins regulate the release of apoptogenic cytochrome c by the mitochondrial channel VDAC. *Nature* 399:483–487.

[74] Galluzzi, L., O. Kepp, N. Tajeddine, and G. Kroemer, 2008. Disruption of the hexokinasevdac complex for tumor therapy. *Oncogene* 27:4633–4635.

[75] Ujwal, R., D. Cascio, J.-P. Colletier, S. Faham, J. Zhang, L. Toro, P. Ping, and J. Abramson, 2008. The crystal structure of mouse VDAC1 at 2.3 A resolution reveals mechanistic insights into metabolite gating. *Proc. Natl. Acad. Sci. U.S.A.* 105:17742–7.

[76] Cowan, S. W., T. Schirmer, G. Rummel, M. Steiert, R. Ghosh, R. A. Pauptit, J. N. Jansonius, and J. P. Rosenbusch, 1992. Crystal structures explain functional properties of two e. coli porins. *Nature* 358:727–733.

[77] Gehring, K. B. and H. Nikaido, 1989. Existence and purification of porin heterotrimers of Escherichia coli K12 OmpC, OmpF, and PhoE proteins. *J. Biol. Chem.* 264:2810–2815.

[78] Nabedryk, E., R. Garavito, and J. Breton, 1988. The orientation of beta-sheets in porin. a polarized fourier transform infrared spectroscopic investigation. *Biophysical Journal* 53:671–676.

[79] Baslé, A., G. Rummel, P. Storici, J. P. Rosenbusch, and T. Schirmer, 2006. Crystal Structure of Osmoporin OmpC from E. coli at 2.0Å. *J Mol Biol* 362:933–942.

[80] Seltmann, O., GuntramHolst, 2001. The bacterial cell wall. Springer.

[81] Nestorovich, E. M., C. Danelon, M. Winterhalter, and S. M. Bezrukov, 2002. Designed to penetrate: time-resolved interaction of single antibiotic molecules with bacterial pores. *Proc. Natl. Acad. Sci. U.S.A.* 99:9789–9794.

[82] Mahendran, K. R., M. Kreir, H. Weingart, N. Fertig, and M. Winterhalter, 2010. Permeation of Antibiotics through Escherichia coli OmpF and OmpC Porins: Screening for Influx on a Single-Molecule Level. *J Biomol Screen* 15:302–307.

[83] Rostovtseva, T. K., E. M. Nestorovich, and S. M. Bezrukov, 2002. Partitioning of differently sized poly(ethylene glycol)s into OmpF porin. *Biophys J* 82:160–9.

[84] Gurnev, E., PhilipNestorovich, 2014. Channel-forming bacterial toxins in biosensing and macromolecule delivery. *Toxins* 6:2483–2540.

[85] Noskov, S. Y., W. Im, and B. Roux, 2004. Ion permeation through the a-hemolysin channel: Theoretical studies based on brownian dynamics and poisson-nernst-plank electrodiffusion theory. *Biophysical Journal* 87:2299–2309.

[86] Nikaido, H., 2003. Molecular basis of bacterial outer membrane permeability revisited. *Microbiology and Molecular Biology Reviews* 67:593–656.

[87] Zambrowicz, E. B. and M. Colombini, 1993. Zero-current potentials in a large membrane channel: a simple theory accounts for complex behavior. *Biophys J* 65:1093–1100.

[88] Daoudil, S. and F. Brochard, 1978. Flexible Polymer Solutions in Pores. *Macromolecules* 11:751.

[89] Finkelstein, A., 1985. The ubiquitous presence of channels with wide lumens and their gating by voltagea. *Annals of the New York Academy of Sciences* 456:26–32.

[90] Kasianowicz, J. J. and S. M. Bezrukov, 1995. Protonation dynamics of the alpha-toxin ion channel from spectral analysis of pH-dependent current fluctuations. *Biophys J* 69:94–105.

[91] Mobasheri, H. and E. J. Lea, 2002. Biophysics of gating phenomena in voltage-dependent OmpC mutant porin channels (R74C and R37C) of Escherichia coli outer membranes. *Eur Biophys J* 31:389–399.

[92] Rodrigues, C. G., D. C. Machado, S. F. Chevtchenko, and O. V. Krasilnikov, 2008. Mechanism of KCl enhancement in detection of nonionic polymers by nanopore sensors. *Biophys J* 95:5186–5192.

[93] Breton, M. F., F. Discala, L. Bacri, D. Foster, J. Pelta, and A. Oukhaled, 2013. Exploration of neutral versus polyelectrolyte behavior of poly(ethylene glycol)s in alkali ion solutions using single-nanopore recording. *J Phys Chem Lett* 4:2202–2208.

[94] Liu, K.-J., 1968. Numclear Magnetic Resonance Studies of Polymer Solutions. V. Cooperative Effects in the Ion-Dipole Interaction between Potassium Iodide and Poly(ethylene oxide). *Macromolecules* 1:308–311.

[95] Tasaki, K., 1999. Poly (oxyethylene) cation interactions in aqueous solution : a molecular dynamics study. *Comput Theor Polym Sci* 9:271–284.

[96] Hakem, I. and J. Lal, 2002. Evidence of solvent-dependent complexation in non-ionic polymer salt 533:531–533.

[97] Park, J. H., J. H. Yum, S. Y. Kim, M. S. Kang, Y. G. Lee, S. S. Lee, and Y. S. Kang, 2008. Influence of salts on ionic diffusion in oligomer electrolytes and its implication in dye-sensitized solar cells. *J Photochem Photobiol A Chem* 194:148–151.

[98] Heeb, R., S. Lee, N. V. Venkataraman, and N. D. Spencer, 2009. Influence of salt on the aqueous lubrication properties of end-grafted, ethylene glycol-based self-assembled monolayers. *ACS Appl Mater Interfaces* 1:1105–1112.

[99] Stojilkovic, K. S., A. M. Berezhkovskii, V. Y. Zitserman, and S. M. Bezrukov, 2003. Conductivity and microviscosity of electrolyte solutions containing polyethylene glycols. *J. Chem. Phys.* 119:6973.

[100] Montal, M. and P. Mueller, 1972. Formation of bimolecular membranes from lipid monolayers and a study of their electrical properties. *Proc. Natl. Acad. Sci.* 69:3561–3566.

[101] Smythe, W. R., 1967. Static and dynamic electricity. McGraw-Hill.

[102] Jackson, J. D., 1962. Classical electrodynamics. Wiley.

[103] Levadny, V., V. M. Aguilella, and M. Belaya, 1998. Access resistance of a single conducting membrane channel. *Biochim. Biophys. Acta - Biomembr.* 1368:338–342.

[104] Cohen, J. A., R. Podgornik, and V. A. Parsegian, 2012. Finite length effects for osmotic pressures of {PEG} polymers. *Biophysical Journal.* 102:400a.

[105] Oukhaled, A. G., A. L. Biance, J. Pelta, L. Auvray, and L. Bacri, 2012. Transport of long neutral polymers in the semidilute regime through a protein nanopore. *Phys Rev Lett* 108:1–4.

[106] Krasilnikov, O. V., C. G. Rodrigues, and S. M. Bezrukov, 2006. Single polymer molecules in a protein nanopore in the limit of a strong polymer-pore attraction. *Phys Rev Lett* 97:1–4.

[107] Bezrukov, S. M., 2004. Noise analysis in studies of protein dynamics and molecular transport. *Fluct. Noise Lett.* 04:L23–L31.

[108] Gurnev, P. a., D. Harries, V. A. Parsegian, and S. M. Bezrukov, 2010. Osmotic stress regulates the strength and kinetics of sugar binding to the maltoporin channel. *J Phys Condens Matter* 22:454110.

[109] Nestorovich, E. M., T. K. Rostovtseva, and S. M. Bezrukov, 2003. Residue ionization and ion transport through OmpF channels. *Biophys J* 85:3718–29.

[110] Aksoyoglu, M. A., R. Podgornik, S. M. Bezrukov, P. A. Gurnev, M. Muthukumar, and V. A. Parsegian, 2016. Size-dependent forced PEG partitioning into channels: VDAC, OmpC, and α-hemolysin. *Proc. Natl. Acad. Sci. U.S.A.* 113:9003–9008.

[111] Nyquist, H., 1928. Thermal Agitation of Electric Charge In Conductors. *Phys Rev* 32:110–113.

[112] Machlup, S., 1954. Noise in semiconductors: Spectrum of a two-parameter random signal. *J Appl Phys* 25:341–343.

[113] Bezrukov, S., A. Berezhkovskii, M. Pustovoit, and A. Szabo, 2000. Particle number fluctuations in a membrane channel. *J Chem Phys* 113:8206–8211.

[114] Berezhkovskii, A. M., M. a. Pustovoit, and S. M. Bezrukov, 2002. Effect of binding on particle number fluctuations in a membrane channel. *J Chem Phys* 116:6216–6220.

[115] Kelvin, W. T., 1884. Reprint of papers on electrostatics and magnetism. Macmillan & Co.